POLSKA AKADEMIA NAUK
INSTYTUT FIZYKI

ACTA PHYSICA POLONICA

DWUMIESIĘCZNIK

Vol. XIX — Fasc. 3

WARSZAWA 1960

First reprint by PWN — Polish Scientific Publishers 1969

SUR UNE MÉTHODE D'ÉVALUATION DE L'ANHARMONICITÉ DES MOLÉCULES POLYATOMIQUES

PAR M. RYTEL

Chaire de Physique de l'École Supérieure de l'Agronomie, Szczecin

(Reçu le 14 Juillet 1959)

On sait [1] que la solution formelle du problème de l'anharmonicité des molécules polyatomiques consiste à la présentation du terme d'énergie sous la forme de série, où on rencontre les fréquences harmoniques ω_i et les constantes anharmoniques x_{ik} (en négligeant les termes suivants). En principe, elles sont diverses pour des molécules isotopiques de la même combinaison. Comme leur désignation exige la connaissance de beaucoup de fréquences du spectre de vibration, les fréquences harmoniques sont déterminées avec assez d'assurance pour un petit nombre de molécules triatomiques.

A cause de la difficulté du calcul des fréquences harmoniques des molécules polyatomiques, divers auteurs emploient des méthodes approximatives, qui se réduisent à deux sortes:

a) introduction de „la masse spectroscopique" des atomes et

b) emploi de diverses formules, qu'on peut amener à la formule de la fréquence fondamentale de la molécule diatomique

$$\nu = \omega\,(1+\eta\omega) \tag{1}$$

Les méthodes de la première sorte sont des méthodes pas trop exactes et peuvent servir en premier lieu pour tenir compte de plus grandes anharmonicités liées avec les vibrations de valence C—H et C—D (bien que Maïantz [2] a montré que ces méthodes usées conformément sont de même importance que les méthodes de la deuxième sorte; mais à cause des calcules trop compliqués elles ne sont pas commodes). Les méthodes du deuxième genre, employées conséquemment pour toutes les vibrations exigent l'introduction de trop de constantes d'anharmonicité et peuvent être appliquées seulement pour les molécules de la même symétrie.

Maïantz [2] a proposé aussi la formule (1), mais il a fait une certaine essentielle supposition supplémentaire. La constante d'anharmonicité η est, chez lui, commune pas seulement pour les fréquences des molécules isotopiques de même symétrie, mais pour toutes les fréquences, qui sont attribuées en sens approximatif à des mêmes coordonnées naturelles sans égard pour la symétrie d'oscillation et pour la symétrie

de la molécule isotopique. Le nombre des constantes d'anharmonicité n'est pas alors grand et leur addition comme inconnues ne complique pas le calcul des constantes de force fait à base des fréquences expérimentales de molécules isotopiques. P. e. Maïantz dans son travail [2] désigne 5 constantes de force et 2 constantes d'anharmonicité (η_q pour oscillations de valence C—H et C—D et η_γ pour oscillations de déformation) de la molécule du méthane et de ses dérivés deuterées à base de 26 fréquences en appliquant la méthode des plus petits carrés. C'est dommage qu'on ne connait pas les fréquences harmoniques du méthane et à cause de celà on ne peut faire une assez certaine conclusion sur la possibilité de la calculation des fréquences harmoniques.

L'auteur de cette notice croyait qu'il était indispensable de faire un calcul analogique d'une molécule avec les fréquences harmoniques connues de l'analyse d'un vaste spectre d'oscillation.

Les résultats du calcul des constantes de force et des constantes d'anharmonicité fait pour l'eau et ses dérivés deutérées après la supposition de Maïantz par la méthode des plus petits carrés à base des fréquences fondamentales présentées par Benedict, Gailar et Plyler [4] sont placés dans les tableaux 1 et 2. Dans le tableau 1 nous voyons les constantes de force et d'anharmonicité avec des erreurs statistiques et par com-

Tableau 1

Constante	Calcul actuel	Après Darling et Dennison [7]
K_q	$(8{,}441 \pm 0{,}022) \cdot 10^5$ dynes/cm	$8{,}428 \cdot 10^5$ dynes/cm
K_γ	$(0{,}7028 \pm 0{,}0056) \cdot 10^5$ erg/rad^2	$0{,}7044_8 \cdot 10^5$ erg/rad^2
h	$-(0{,}0981 \pm 0{,}0033) \cdot 10^5$ dynes/cm	$-0{,}1051 \cdot 10^5$ dynes/cm
a	$(0{,}2422 \pm 0{,}0434) \cdot 10^5$ dynes/rad	$0{,}2415_1 \cdot 10^5$ dynes/rad
η_q	$-(0{,}01183 \pm 0{,}00032) \cdot 10^{-3}$ cm	
η_γ	$-(0{,}02120 \pm 0{,}00277) \cdot 10^{-3}$ cm	

Tableau 2

		Calcul actuel	Après Darling et Dennison [7]	Après Benedict, Gailar et Plyler [4]	Après Khatchkuruzow [6]
H_2O	ω^1	$3829{,}9 \pm 5{,}1$	3825,32	3832,17	3835,37
	ω_2	$1651{,}4 \pm 8{,}1$	1653,91	1648,47	1647,59
	ω_3	$3939{,}1 \pm 5{,}4$	3935,59	3942,53	3938,74
D_2O	ω_1	$2761{,}4 \pm 2{,}6$	2758,06	2783,80*	———
	ω_2	$1208{,}3 \pm 4{,}2$	1210,25	1206,39	———
	ω_3	$2886{,}2 \pm 2{,}8$	2883,79	2888,78	———
HDO	ω_1	$2821{,}7 \pm 2{,}6$	2820,3	2824,32	———
	ω_2	$1447{,}2 \pm 6{,}2$	1449,4	1440,21	———
	ω_3	$3886{,}8 \pm 5{,}3$	3883,8	3889,84	———

paraison les constantes de force de Darling et Dennison [7] (les symboles après Eliachévitch [3]). Dans le tableau.2 on voit les comparaisons des fréquences harmoniques calculées (avec des erreurs statistiques) et des fréquences harmoniques obtenues par d'autres auteurs à base d'analyse du spectre d'oscillation. Le seul plus grand désaccord, dans le lieu marqué d'étoile, est, évidemment, une faute d'imprimerie dans le travail [4] (les auteurs écrivent, que leurs fréquences réalisent la règle du produit parfaitement, mais la substitution des fréquences montre un désaccord de 2 %). On a calculé aussi les fréquences harmoniques et prévu les fréquences fondamentales pour molécules avec tritium en obtenant un résultat conforme aux expériences de Staats, Morgan et Goldstein [5] (tableau 3).

Tableau 3

		Fréquences harmoniques	Fréquences fondamentales calculées	Fréquences fondamentales observées
HTO	ω_1	2367,1	2300,8±1,8	———
	ω_2	1372,5	1332,6±5,2	1324
	ω_3	3885,7	3707,1±4,8	3720±10
DTO	ω_1	2359,4	2293,5±1,8	———
	ω_2	1116,8	1090,3±3,5	———
	ω_3	2832,7	2737,8±2,5	2735±5
T_2O	ω_1	2299,3	2236,7±1,7	———
	ω_2	1016,8	994,9±2,9	995,5
	ω_3	2437,1	2366,8±1,9	2370±5

Il est difficile d'admettre le calcul ci-joint, malgré ses résultats, comme preuve de raison de la supposition de Maïantz. C'est seulement la vérification faite sur un exemple; son succès fait cette supposition vraisemblable à certain degré. C'est important à cause de l'éventuelle possibilité de désigner plus exactement les constantes de force des molécules polyatomiques et d'apprécier leur fréquences harmoniques, ce qui d'autre côté peut faciliter l'interprétation des fréquences composées.

L'auteur désire d'exprimez sa reconaissance à M. Thomas Daca pour des nombreuses et précieuses discussions.

BIBLIOGRAPHIE

1 Herzberg G., Molecular Spectra and Molecular Structure. II. *Infrared and Raman Spectra of Polyatomic Molecules* — New York, 1945.

2 Maiantz L. S., *Trudy Fiz. Inst. A. N.* S.S.S.R. **5**, 63 (1950).

3 Volkenchtein M. W., Eliachevitch M. A., Stepanow B. I., — *Kolebanija Molekuł* — Moscou, 1949.

4 Benedict W. S., Gailar N., Plyler E. K., *J. chem. Phys.*, **24**, 1139 (1956).

5 Staats P. A., Morgan H. W., Goldstein, J. H., *J. chem. Phys.*, **24**, 916 (1956).

6 Khatchkuruzow G. A., *Optika i Spektroskopia*, **6**, 463 (1959).

7 Darling B. T., Dennison D. M., *Phys. Rev.*, **57**, 128 (1940).

DETERMINATION OF THE MASS OF THE Λ^0 HYPERON

By J. Bogdanowicz, M. Danysz, A. Filipkowski, E. Marquit, E. Skrzypczak A. Wróblewski and J. Zakrzewski

Institute of Physics, Warsaw University
and
Institute of Nuclear Research, Warsaw

(Received August 10, 1959)

An analysis of 53 $\Lambda^0 \to p + \pi^-$ decays found in a stack of emulsion exposed to a beam of K^- mesons gives $Q_\Lambda = (37.58 \pm 0.18)$ MeV and $M_\Lambda = (1115.42 \pm 0.19)$ MeV. From an analysis of the results of other laboratories on the standard range of protons from the decay of Σ_p^+ hyperons at rest and the results obtained in the calibration of the emulsion used in the present work one obtains as the best estimates the value $R_{st} = (1678.6 \pm 3.2)\,\mu$, which corresponds to $M_{\Sigma^+} = (1189.43 \pm 0.31)$ MeV.

I. Experimental part and scanning

The energy of the decay $\Lambda^0 \to p + \pi^-$ has been measured in recent years by several groups of investigators using chamber and emulsion technique. Results obtained by the various groups show discrepancies which in some cases are large in comparison with the error quoted. Using nuclear emulsion, one might expect to get in this case an accuracy somewhat better than 0.2 MeV. Such an accuracy is of interest, e. g. in evaluating the binding energies of the Λ^0 hyperons in hyperfragments, especially in the lightest ones. It was thus felt that further efforts in determining the mass of the Λ^0 based on larger statistics would be justified.

As a source of Λ^0 hyperons we chose interactions of K^- mesons in nuclear emulsion. We used in this work a stack of 180 plates 10×10 cm $\times 600\mu$ of Ilford G5 emulsion exposed to the enriched K^- beam (~ 300 MeV/c) from the Berkeley bevatron. We expected to find there a rather large number of Λ^0 decays with a relatively low background of pseudo $\Lambda^0 \to p + \pi^-$ events.

Eighty pellicles from the central part of the stack were available to us for this analysis. A strip 2.5 cm wide in which most of the kaons were expected to stop was area-scanned for σ_{π^-} and σ_{K^-} stars. An average of about 62 σ_{K^-} stars and about 105 σ_{π^-} stars per plate were found in the scanned area. An additional scanning for purposes of calibration provided us with 22 Σ_p^+ decays at rest.

In order to find the Λ^0 decays the tracks of light mesons ending in a σ star were followed back for a distance up to about 20 mm. Of the 680 tracks traced back in this way 54.5 % were abandoned after about 20 mm, 2.7% originated from stars with one prong, 1.9 %were due to π^- mesons emitted from σ_K stars, 11.3 % originated from stars with three or more prongs, 10.4 % traversed the emulsion prior to or after exposure of the stack (no prolongation in the neighbouring plate), 10.5 % were abandoned before the range of 20 mm was reached, as they originated outside our part of the stack, came from a region of high distortion, or were lost during the prolongation; the remaining 59 tracks[1] originated in the two-prong stars. In all but three of the cases the second prong ended in our part of the stack. Assuming that these two prong stars were the products of decay of a neutral particle into a proton and a π^- meson, we determined the energy of the decay of each of the 56 such particles (see Table I). In 54 cases the values of energy of decay are concentrated in a narrow region.

II. Calibration

The two quantities to be determined here are the shrinkage factor and the stopping power of our emulsion. The ranges of 22 protons from the decays at rest were measured all in one day on two Koristka MS2 microscopes fitted with Zeiss Optimeters. In order to permit the emulsion to attain a state of approximate equilibrium, an effort was made to maintain constant conditions of humidity and temperature in the measuring room for about 40 hours preceding the measurement and also during the time of the measurement (about 15 hours)[2]. These conditions were taken as standard conditions to which all measurements of this work were reduced (see § *III*).

In order to avoid coarse errors the results of the proton range measurements made on the "standard" day were compared with measurements made by another observer and at other periods. Applying to the set of 22 measured proton ranges the method developed by Fry and White [2], we obtained for the average value of the shrinkage factor:

$$s_1 = 2.20 \pm 0.033$$

and for the mean value of the ranges of the secondary protons

$$R_p = (1676.2 \pm 7.3)\,\mu\,.$$

The shrinkage factor was also determined by another independent method based on the analysis of the set of values $Q(s_1)$ calculated by taking the preliminary value s_1 as a first approximation (see § *IV*, page 281). This procedure gave

$$s_2 = 2.23 \pm 0.045.$$

[1] This is less then the number given in an earlier report on this work [1]. In two cases previously reported as background, after reexamination, a third track was found.

[2] See footnote page 281.

The weighted mean of these two independent estimates of the shrinkage factor s_1 and s_2:

$$2.21 \pm 0.027$$

was used in further calculations.

As communicated to us by Dr. E. J. Lofgren the density of our emulsion was contained between 3.809 and 3.853 g/cm³. Using this information (see [3]) and combining it with the ratio of the mean range of protons from Σ_p^+ decays available from other work[3] to our value of R_p given above, we obtained the stopping power of our emulsion:

$$\frac{R_{st}}{R} = 1.002 \pm 0.003.$$

This value was used in further calculations.

III. Measurements

All measurements for each decay were made under high magnification independently by two observers on different days, the mean of the two measurements being taken for the calculations. In the range measurements of the secondary particles the track was divided into segments which could be approximated by straight lines.

The measurements of the horizontal projections of the tracks were generally made on Zeiss Lumipan miroscopes adapted for emulsion work. The movement of the microscope stage could be read on a micrometer screw. In the event that the last grain of a track was not in focus with the upper or lower surface of the emulsion we made a correction Δl estimated from the slope of the track and the distance Δh of the last grain from the surface.

All vertical projections were measured on a Zeiss Optimeter coupled to a Koristka MS2 microscope. The measurements were corrected by the formula

$$h_0 = h_x \frac{a_0}{a_x}, \qquad (1)$$

where a_0 denotes the "standard depth", i. e. a previously selected difference in depth ($\sim 200\ \mu$ of processed emulsion); a_x is the same depth recorded the day h_x was measured.

The projected angles between the decay prongs were measured on a goniometer attached to the eye-piece of the microscope.

The dip angles of the tracks were measured on a Koristka MS2 microscope. In each case the mean dip was determined from a series of measurements of the depth h on a base l:

$$\text{arc tan}\left(\frac{h_0}{l}\, s\right)$$

[3] See Appendix.

where the value of l ranged from several to several hundred microns, depending on the character of the track. It was found that the variation in thickness of different layers of the emulsion as a result of variation of humidity and temperature were not strictly proportional. Therefore in the measurement of the dip angles the standardization (1) was made by means of "partial standards." Three such standards, each of a thickness of about 100 μ of processed emulsion, were chosen in the vicinity of the main "standard." These standards were used in the dip measurements.

In order to avoid systematic errors in the ranges owing to the linearization of tracks during the measurements, a constant length-correction was added to the measured ranges to account for the increased scattering of the track near the final part of its range. This correction was determined from measurements of several pion and proton tracks, the tracks in question being divided into a large number of small segments. The mean value of the correction for pions obtained in this way was 10 μ, while for protons the correction was negligible.

An investigation was made to determine whether a small thickness of emulsion may have been removed from the upper surface during the processing; this would result in loss of part of track. To determine the gap between the upper surface of one pellicle and the lower surface of the neighbouring one, measurements were made on both surfaces of the distance between prongs from stars located near the surface. A number of such measurements indicated that the gap due to air or missing emulsion did not exceed 2 μ. In the case of an air gap this factor can be neglected, but in the case of missing emulsion it would affect the mean range of steep tracks. A comparison of ranges of flat and steep protons from the decays of Σ_p^+ did not indicate the existence of such a difference.

IV. Evaluation of error.

On the basis of measurements of the angles and ranges and assuming that the secondary particles are protons and pions, we calculated the Q value for each event from the formula:

$$Q_\Lambda = M_\Lambda - (m_p + m_{\pi^-}),$$

where

$$M_\Lambda = \sqrt{(W_p + W_{\pi^-})^2 - (\bar{p}_p + \bar{p}_{\pi^-})^2};$$

W_p and W_{π^-} are the total energies and $\bar{p}_p$ and $\bar{p}_{\pi^-}$ are the momenta of the proton and pion respectively. In the evaluation of the random errors for the individual Q values the folloving sources of errors for were taken into account:

a) Angular measurements.

The accuracy of the goniometer for measuring the projected angles was taken as 0.5°. In each case comparison was made between this value and the error which could be determined from the difference between independent measurements by

two observers[4]. The larger of the two values was taken as the error of the projected angle. This procedure takes into account both the instrument error and the subjective error of the observer. In 26 of the 54 cases the error was greater than 0.5°. A similar procedure was used in evaluating the error in the dip angles. The random errors of space angles were in 8 cases $> 2°$, in 3 cases $> 3°$.

b) Range measurements and straggling.

To determine the error in range it was neccesary to determine the error in the projected vertical and horizontal segment of the track in each plate. The projected length errors were calculated from the differences in the results of two observers, separately for mesons and protons; the tracks were divided into classes of large and small dip.

The error in the measurement of the vertical projection was evaluated in a similar way (about 5 μ per processed plate)[5].

For each track the range straggling error (from [4]) was combined with the measurement errors.

The error in each Q value resulting from the above errors in ranges and angles will henceforth be referred to as the random error ($\sigma_r\{Q\}$).

In the evaluation of the systematic error for individual Q values the following sources of error were considered:

a) Shrinkage factor.

The shrinkage factor first used for the calculations was $s_1 = 2.20 \pm 0.033$. Since the separation of the Λ^0 decays from the background leaves little room for doubt (see § V) it was possible to determine the shrinkage factor independently under the assumption that all the observed Qs refer to a single value. To do this we plotted the individual values of Q (s_1) as a function of $\frac{\partial Q}{\partial s}$ $\left(\frac{\partial Q}{\partial s}\right.$ is the partial derivative taken at the point $s_1 = 2.20\Big)$. In the first-order approximation this dependence should be a linear one. From the slope of the straight line drawn through these points (weighted with respect to the random errors) we found $s_2 = 2.23 \pm 0.045$. Finally,

---

[4] We calculated the mean error of two measurements by employing Student's distribution

$$\{\bar{x}\} = 1.8 \frac{|x_1 - x_2|}{2}$$

[5] It turned out that the difference between measurements of thickness of the same emulsion at the same place in the plate made under different laboratory conditions of temperature and humidity exceeded the expected error of measurement. In seeking the cause for this, several series of measurements were made of the emulsion thickness. A number of these measurements were made under different laboratory conditions and were standardized according to (1). From the analysis of the measurements one may conclude that the "standardizing" procedure does not guarantee reproducibility of the measurements performed under greatly varied conditions of humidity and temperature. This introduces a source of error considerably larger than the instrument error, the latter in our case being about 1 μ.

for each case $Q(s)$ and the error $\sigma_s\{Q\}$ associated with the uncertainty of the shrinkage factor was calculated by using the weighted value of the shrinkage factor $s = 2.21 \pm \pm 0.027$.

b) Stopping power.

For all the ranges reduced to the standard emulsion the errors resulting from the uncertainty of the stopping power (see § *II*) and the corresponding error for the individual Q values ($\sigma_R\ \{Q\}$) were calculated.

c) Range-energy relation.

Assuming an uncertainty of 0.5 percent[6] in the range-energy relation [6], we calculated the corresponding errors for individual Q values ($\sigma_B\ \{Q\}$).

d) Mass values.

The mass values used in the calculations were [7]

$$m_p = (938.213 \pm 0.01)\ \text{Mev},$$
$$m_{\pi^-} = (139.63 \pm 0.06)\ \text{Mev}.$$

The coresponding errors in the Q values could be neglected; however in the calculation of the Λ° mass value this source of error was taken into account.

V. Results and discussion.

The Q values and their errors for the 56 events mentioned in § *I* are listed in Table I. The distribution of these Q values is shown in Fig. 1. The Q values of 54

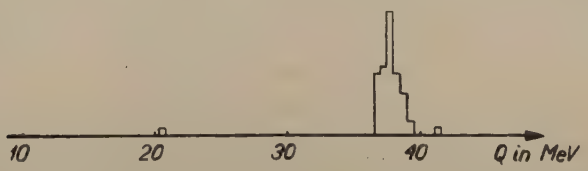

Fig. 1

of our two-prong stars are concentrated in the region 36.5 — 39.5 MeV. In one of these events inelastic scattering of the pion with a change of grain density was observed. Calculations based on the angle between the prongs, the range of the proton and the ionization of the pion gave $Q = (39 \pm 7)$ MeV. The remaining two cases quite distinctly lie outside the region 36.5 — 39.5 Mev. The event with $Q = 41$ MeV occurred 2 mm from the edge of the emulsion in a strongly distorted region, where measurements of the angles and ranges are not reliable. The point of decay of anotherone ($Q = 20.5$ Mev) is situated on the very surface of the emulsion or perharps between the plates, and consequently could not be carefully examined for the presence of other prongs.

[6] Private communication from W. H. Barkas; see also [5]

Table 1

No.	Q_Λ	$\sigma_r\{Q\}$	$\sigma_s\{Q\}$	$\sigma_R\{Q\}$	$\sigma_B\{Q\}$
1	36.83	0.66	0.27	0.06	0.11
2	36.85	0.52	0.11	0.07	0.11
3	37.01	0.44	0.21	0.06	0.10
4	36.75	0.57	0.20	0.07	0.11
5	38.36	0.81	0.11	0.07	0.12
7	38.14	0.62	0.13	0.07	0.11
8	41.2				
9	37.85	1.24	−0.21	0.07	0.12
10	37.05	1.00	0.24	0.06	0.11
11	37.33	0.51	0.03	0.07	0.11
12	36.76	0.58	−0.03	0.06	0.11
13	37.53	0.46	0.16	0.06	0.11
14	38.83	0.99	0.30	0.07	0.11
15	39.22	0.64	0.04	0.07	0.12
16	37.63	0.51	−0.02	0.07	0.11
17	39 ± 7				
18	37.55	0.67	0.04	0.07	0.11
19	38.42	0.76	0.25	0.07	0.12
20	37.99	0.82	0.16	0.07	0.11
21	38.74	0.56	0.12	0.07	0.11
22	36.94	0.59	0.02	0.07	0.11
23	38.61	1.02	0.22	0.07	0.11
24	20.5				
25	37.45	0.39	0.23	0.07	0.11
26	37.91	0.71	0.06	0.07	0.12
27	38.10	0.78	0.02	0.07	0.12
28	36.63	0.86	−0.08	0.07	0.11
29	37.87	0.65	0.14	0.07	0.12
30	37.41	0.62	0.07	0.07	0.11
31	38.88	0.70	0.07	0.07	0.12
32	38.20	0.71	0.04	0.07	0.12
33	37.10	0.50	0.16	0.07	0.11
34	37.61	0.51	0.08	0.07	0.11
35	37.08	0.59	0.03	0.07	0.11
36	37.88	0.47	0.01	0.07	0.11
37	37.98	0.62	0.07	0.07	0.11
38	37.60	0.70	0.05	0.07	0.11
39	37.57	0.52	0.11	0.07	0.11
40	36.95	0.66	0.28	0.07	0.11
43	38.36	0.60	0.05	0.07	0.12
44	37.52	2.14	0.40	0.07	0.11
45	37.56	0.57	0.06	0.07	0.11
46	38.80	1.13	0.10	0.07	0.12
47	38.18	0.61	0.01	0.07	0.11
48	37.96	0.93	0.23	0.07	0.12

Table 1 continued

No.	Q_Λ	$\{\sigma_r Q\}$	$\{\sigma_s Q\}$	$\{\sigma_R Q\}$	$\{\sigma_B Q\}$
49	37.49	0.69	0.08	0.06	0.11
50	37.88	0.53	0.10	0.07	0.11
51	37.68	0.56	0.02	0.07	0.11
52	36.76	0.52	0.11	0.07	0.11
54	37.12	0.45	0.15	0.07	0.11
55	38.65	0.54	0.05	0.07	0.11
56	37.86	0.53	0.03	0.07	0.11
57	37.20	0.43	—0.02	0.07	0.11
58	37.02	0.68	0.13	0.07	0.11
60	36.50	0.59	0.04	0.07	0.11
61	37.88	0.58	—0.02	0.06	0.11

We therefore conclude that no more than 3 events of our sample are to be regarded as background, while the remining 53 correspond to the decay of the Λ^0 hyperon. The mean of those 53 individual Q values, weighted according to their random errors is:

$$Q_\Lambda = (37.58 \pm 0.18) \text{ MeV}.$$

The external and internal random errors of the mean are in good agreement: 0.084 MeV and 0.082 MeV respectively. The final error of the mean includes all the random and systematic errors described above namely:

$$\sigma_r \{Q\} = 0.08 \text{ MeV},$$
$$\sigma_s \{Q\} = 0.09 \text{ MeV},$$
$$\sigma_R \{Q\} = 0.07 \text{ MeV},$$
$$\sigma_B \{Q\} = 0.11 \text{ MeV}.$$

A constant area histogram based on the Q values and random errors is shown in Fig. 2.

For the mass of the Λ^0 hyperon we obtain:

$$M_\Lambda = (1115.42 \pm 0.19) \text{ MeV},$$

where in the final error the uncertainty in the pion and proton masses are also included ($\sigma \{M_\Lambda\} = 0.06$ MeV). Two possible sources of error were not discussed: the influence of distortion and the possibility of some undetected inelastic scattering of the secondary pions. The agreement between the external nad internal errors indicates that influence of distortion is small. As regards inelastic scattering of the pions, we note that even if one takes the geometric cross section for such interactions (in reality, it is probably less [8]), we would expect ~ 2 cases of such scattering in our sample. One case of inelastic scattering was found (see § V). If we discard even the five lowest Q values the mean value of Q_Λ changes by less than 0.1 MeV.

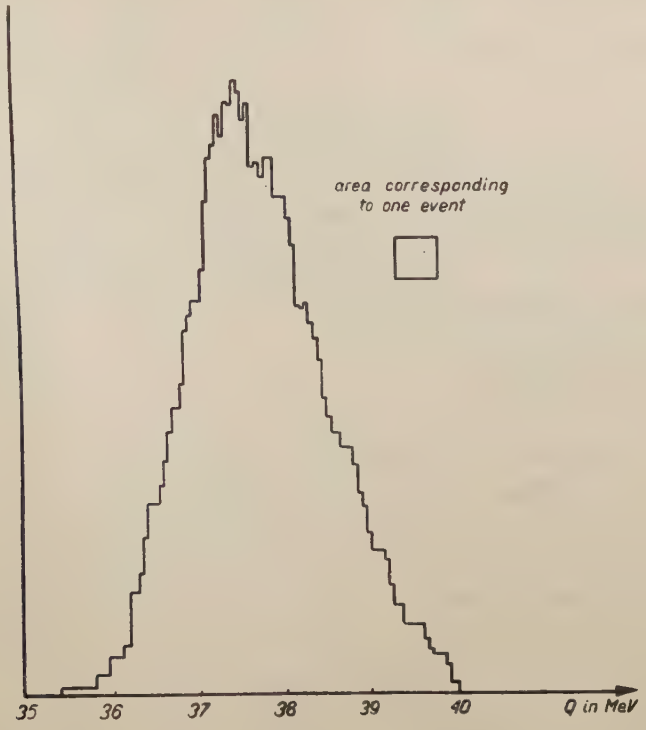

Fig. 2

The evaluation of the Λ^0 mass presented by Alvarez at the Kiev Conference on HighEnergy Physics 1959 and based on recent experimental results (which includes our value) yields:

$$Q_\Lambda = (37.61 \pm 0.12) \text{ MeV}.$$

Appendix

The table below lists data obtained by several laboratories, on the proton range from $\Sigma^+ \rightarrow p^+ + \pi^0$ decays at rest. All the values are reduced to ranges in standard emulsion; the present Warsaw value was based on the density of the emulsion as communicated by Dr. E. J. Lofgren. The table gives the total random and systematic error.

Table 2

Authors	R_p normalised	$\sigma\{R_p\}$	Number of events	Reference
Glasser et al.	1658.0	8.4	20	[9]
Gilbert et al.	1709	12.0	8	[10]
Swami	1686.5	6.0	29	[11]
Barkas et al.	1674.2	4.5	31	[5]
Warsaw Group	1694.0	33.0	8	[12]
Warsaw Group	1681.7	10.5	22	present work

The weighted-mean value of the proton ranges according to the data in the table above is:

$$R_{st} = (1678.6 \pm 3.2)\ \mu.$$

Taking into consideration the proton and π^0 meson masses

$$m_p = 938.213 \text{ MeV},$$
$$m_{\pi^0} = 135.04 \text{ MeV},$$

and the sources of systematic errors:

A) $\sigma\{m_p\} = 0.01$ MeV,

B) $\sigma\{m_{\pi^0}\} = 0.16$ MeV,

C) 0.5 % uncertainty in range-energy relation,

we obtain the mean value of the mass of the Σ^+ hyperon

$$M_{\Sigma^+} = (1189.43 \pm 0.31) \text{ MeV}.$$

It is worth mentioning that the systematic errors due primarily to (*C*) exceed the statistical error connected with the number of measured decays.

$$\sigma_{m_p}\ \{M_\Sigma\} = 0.01 \text{ MeV} \quad (A)$$
$$\sigma_{m_{\pi^0}}\ \{M_\Sigma\} = 0.09 \text{ MeV} \quad (B)$$
$$\sigma_B\ \{M_\Sigma\} = 0.27 \text{ MeV} \quad (C)$$

Thus at present the lower limit of the attainable accuracy in the estimation of the Σ^+ hyperon mass by means of the emulsion technique is 0.29 MeV.

Acknowledgements

We are greatly indebted to Dr. E. Segrè for making the stack available, to Dr. E. J. Lofgren for exposure of the stack and to Dr. S. Goldhaber for processing the emulsion. We wish thank Drs. C. Dilworth and G. Occhialini for their helpful discussion. We also would like to express our appreciation to the scanning staff of our laboratory: Mrs. K. Bobińska, Mr. R. Dąbrowski, Mrs. M. Pazdanowska, Miss W. Saniewska for their careful work, and especially Mrs. I. Przypkowska for her efficient help in scanning, measurements, and calculations.

REFERENCES

[1] Bogdanowicz, J., Danysz, M., Filipkowski, A., Marquit, E., Skrzypczak, E., Wróblewski, A. and Zakrzewski, J., *Nuovo Cimento*, **11**, 727 (1959).

[2] Fry, W. F. and White, G. R., *Phys. Rev.*, **90**, 207 (1953).

[3] Barkas, W. H., Barret, F. H., Cüer, P., Heckman, H., Smith, F. H., and Ticho, N. K., *Nuovo Cimento*, **8**, 185 (1958).

[4] Barkas, W. H., and Young, D. M., UCRL — 2579 (1954).
[5] Barkas, W. H., Giles, P. C., Heckman, H. H., Inman, F. W., Mason, C. J., and Smith, F. M., *Padua-Venice Conference* (1957).
[6] Barkas, W. H., *Nuovo Cimento*, **8**, 201 (1958).
[7] Barkas, W. H., and Rosenfeld, A. H., UCRL — 8030 (1958).
[8] Minguzzi, A., Puppi, G., Ranzi, A., *Nuovo Cimento*, II, 697 (1954). Silin, V. P., Fainberg, V. Ya., *Uspekhi Fiz. Nauk*, **50**, 326 (1953).
[9] Glasser, R. G., Seeman, N., and Snow, G., *Padua-Venice Conference* (1957).
[10] Gilbert, F. C., Violet, C. E., and White, R. S., *Phys. Rev.*, **101**, 228 (1957).
[11] Swami, M. S., *Phys. Rev. Letters*, **1**, 308 (1958).
[12] Filipkowski, A., Skrzypczak, E., Somogyi, A., and Wróblewski, A., *Nuclear Physics*, **7**, 643 (1958).

ON THE STATISTICS OF SPIN WAVES BY THE BETHE METHOD

By Bogdan Fechner

Institute of Theoretical Physics, A. Mickiewicz University, Poznań

(Received August 22, 1959)

The exact solution of Slater-Bloch's secular equations by the Bethe method without any additional conditions is considered. The bearing of the results upon the question of statistics of spin waves is discussed. It is shown, that there exists an ambiguity which cannot be overcome without additional assumption.

I. Introduction

The starting point in the Bloch's spin waves theory is the Heisenberg model of a ferromagnetic crystal, where the interactions between electrons are considered as perturbation. Using the perturbation theory with such a model, one gets in first approximation the system of Slater-Bloch's secular equations

$$J \sum_{m'_1 \ldots m'_r} \{a_{m_1 \ldots m_r} - a_{m'_1 \ldots m'_r}\} = E_r a_{m_1 \ldots m_r}. \tag{1}$$

The summation is extended over all pairs of contiguous electrons having opposite spins, for the indices m_i, m_i the spins in the pair are interchanged, J is the exchange integral between nearest neighbour sites, $a_{m_1 \ldots m_r}$ stands for the amplitude of the state in which two reversed spins occupy the $m_1 \ldots m_r$ sites and E_r is the energy of r reversed spin states.

The discussion of this system is simplest for a linear chain. For this case Bethe (1931) has proposed a treatment in order to obtain a rigorous solution. Basing on this treatment Frank (1956) has discussed the symmetry properties of the a amplitudes for interchange of k and has arrived the conclusion that for the spin waves the Fermi--Dirac statistics is more apposite than that of Bose-Einstein. Svirskii-Ishmukhametov (1957) and Vonsovsky-Svirskii (1959) call in question this conclusion. They point out, the Frank results rest on an artificial introduction of additional equations, which requires an extension of the definition of the a amplitudes on the case $m_i = m_j$.

In the present paper this problem will be examined once more without making use of any subsidiary equations.

II. Solution of the secular equations for a linear chain

The method used in this paper is the same as that of Bethe, i. e. one introduces some additional coefficients choosing them in such a way, that the secular equations should be rigorously satisfied. The easiest to investigate is the case when there are only two spins reversed from the ground state ($r = 2$). Taking into account the distribution of the reversed spins in a linear chain, one can divide the system (1) into two groups. In the case when the two reversed spins are not located at the nearest neighbour sites the secular equations take the form:

$$J\{4a_{m,n} - a_{m-1,n} - a_{m+1,n} - a_{m,n-1} - a_{m,n+1}\} = E_2\, a_{m,n}. \tag{2a}$$

On the other hand, when the two reversed spins are nearest neighbours, we get

$$J\{2a_{m,m+1} - a_{m,m+2} - a_{m-1,m+1}\} = E_2\, a_{m,m+1}. \tag{2b}$$

As is well known, the equations ($2a$) can be satisfied by the substitution

$$a_{m,n}(k_1, k_2) = c_1\, e^{id(k_1 m + k_2 n)} + c_2\, e^{id(k_1 n + k_2 m)} \tag{3}$$

which gives

$$E_2 = 2J\{2 - \cos k_1 d - \cos k_2 d\} \tag{4}$$

where d is the lattice spacing, and the k_1, k_2 one sets from the Born-Karman condition. The coefficients c_1 and c_2 can be freely chosen. One can, however, choose them in such a way that (3) will be also a solution of equation ($2b$). For this purpose we substitute (3) and (4) into ($2b$). After a simple calculation, we arrive at the condition which the coefficients c must satisfy for (3) to be a solution of the whole system ($2a$) and ($2b$). This condition has the form:

$$\frac{c_1(k_1, k_2)}{c_2(k_1, k_2)} = -\frac{\cos\dfrac{(k_1 + k_2)\,d}{2} - e^{id\frac{k_1 - k_2}{2}}}{\cos\dfrac{(k_1 + k_2)\,d}{2} - e^{id\frac{k_1 - k_2}{2}}}. \tag{5}$$

We make now the substitution

$$c_1(k_1, k_2) = c_2^*(k_1, k_2)$$

whence we obtain

$$c_1(k, k) = -\,c_2(k, k) \quad \text{for} \quad k \neq 0$$

$$c_1(k_1, k_2) = \pm\, c_2(k_2, k_1).$$

Introducing this into equation (3) we get (dropping the subscripts)

$$a_{m,n}(k_1, k_2) = c(k_1, k_2)\, e^{id(k_1 m + k_2 n)} \pm c(k_2, k_1)\, e^{id(k_2 m + k_1 n)} \qquad k_1 \neq k_2, \tag{6a}$$

$$a_{m,n}(k, k) = 0 \qquad k \neq 0. \tag{6b}$$

However, for $k_1 = k_2 = 0$ we obtain from (5)

$$\lim_{k_1 \to 0} \lim_{k_2 \to 0} \frac{c_1(k_1, k_2)}{c_2(k_1, k_2)} = 1.$$

Taking this into account in (3) one gets

$$a_{m,n}(0,0) \neq 0. \tag{6c}$$

These results can be easily generalized to the case $r > 2$. When no reversed spins are nearest neighbours, the secular equations have the form:

$$J \sum_{g=1}^{r} \{2a_{m_1 \ldots m_g \ldots m_r} - a_{m_1 \ldots m_g - 1 \ldots m_r} - a_{m_1 \ldots m_g + 1 \ldots m_r}\} = E_r \, a_{m_1 \ldots m_g \ldots m_r}. \tag{7a}$$

On the other hand, when two of the reversed spins are nearest neighbours

$$J\{2a_{m_1 \ldots m_f, m_f+1 \ldots m_g \ldots m_r} - a_{m_1 \ldots m_f - 1, m_f+1 \ldots m_g \ldots m_r} - a_{m_1 \ldots m_f, m_f+2 \ldots m_g \ldots m_r}\} +$$

$$+ J \sum_{g \neq f, f+1}^{r-2} \{2a_{m_1 \ldots m_f, m_f+1 \ldots m_g \ldots m_r} - a_{m_1 \ldots m_f, m_f+1 \ldots m_g - 1 \ldots m_r} - a_{m_1 \ldots m_f, m_f+1 \ldots m_g + 1 \ldots m_r}\} =$$

$$= E_r \, a_{m_1 \ldots m_f, m_f+1 \ldots m_g \ldots m_r}. \tag{7b}$$

(We do not get anything new taking into account more than two neighbouring reversed spins). One can satisfy the equations (7a) by the substitutution

$$a_{m_1 \ldots m_r}(k_1 \ldots k_r) = \sum_{P}^{r!} c_P(k_1 \ldots k_r) \, e^{id \sum_{j=1}^{r} k_{Pj} m_j} \tag{8}$$

with

$$E_r = 2J \sum_{s=1}^{r} (1 - \cos k_s d).$$

In the same manner as in the case $r = 2$ we look for the condition which must be satisfied by the c_P if (8) is to be a solution of (7a) and (7b). Substituting (8) and (9) into (7b) we get the expression

$$\sum_{P}^{r!} c_P \, e^{id \sum_{j=1}^{r} k_{Pj} m_j} \{2e^{idk_{P(f+1)}} + e^{id(k_{P(f+1)} - k_{Pf})} + e^{2idk_{P(f+1)}} + \sum_{g \neq f, f+1}^{r-2} e^{id(k_{P(f+1)} - k_{Pg})} +$$

$$+ \sum_{g \neq f, f+1}^{r-2} e^{id(k_{P(f+1)} + k_{Pg})} - \sum_{s=1}^{r} e^{id(k_s + k_{P(f+1)})} - \sum_{s=1}^{r} e^{id(k_{P(f+1)} - k_s)}\} = 0 \tag{10}$$

From all permutations P one can form $\frac{r!}{2}$ pairs of permutations $P_\mu P_\nu$ which satisfy the relations

$$\begin{aligned} &P_\mu(f) = P_\nu(f+1), \\ &P_\mu(f+1) = P_\nu(f), \\ &P_\mu(g) = P_\nu(g) \quad \text{for all} \quad g \neq f, f+1. \end{aligned} \tag{11}$$

This means, that we can group all the elements in $\sum_P$ into pairs, which differ only in the transpositions of k in the points m_f and m_f+1. Performing such a grouping in (10) we obtain for all pairs

$$\frac{c_{P\mu}}{c_{P\nu}} = -\frac{\cos k - e^{i\delta}}{\cos k - e^{-i\delta}} \tag{12}$$

where

$$k = \frac{(k_{P\mu f} + k_{P\mu(f+1)})\, d}{2} \qquad \delta = \frac{(k_{P\mu(f+1)} - k_{P\mu f})\, d}{2}.$$

Following Bethe and Frank we make the substitution

$$c_P = \prod_{i<j} (\pm 1)^p\, c(k_{Pi}, k_{Pj}) \quad \text{for all } P \tag{13}$$

where the $+$ sign corresponds to the symmetrical and the $-$ sign to the antisymmetrical a amplitudes and $p = 0,1$ depending on whether the permutation P is even or odd. Taking the above considerations into account, we get

$$\frac{c\,(k_{P\mu f},\, k_{P\mu(f+1)})}{c\,(k_{P\mu(f+1)},\, k_{P\mu f})} = \pm \frac{\cos k - e^{i\delta}}{\cos k - e^{-i\delta}}. \tag{14}$$

Since always one can pick out P_μ and f in such a way that $P_\mu f$ and $P_\mu(f+1)$ would be any two given numbers from the sequence $1, 2 \ldots r$, the relation holds for all pairs of wave numbers $k_1 \ldots k_r$. These $\binom{r}{2}$ relations are the conditions under which (8) is a solution of the system (7a) and (7b).

III. Conclusions

The relations (5) and (14) are deduced directly from the secular equations without introducing any additional equations and without extending the definition of the a amplitudes. These relations are equivalent to those of Bethe and Frank[1]. Thus it can be seen that the objection of Svirskii-Ishmukhametov and Vonsowsky-Svirskii according to whom Frank results stem from the baseless additional equations, is not valid. However, the correct results of Frank do not yet prove the reality of his conclusions. The above results are, however, not single valued. In (6a) and in (8) taken together with (13) there are namely allowed two signs and the calculations do not answer the question which of them is the right one. Since the choice of the sign determines

[1] These relations can be obtained by the substitution:

for Bethe $c(k_1, k_2) = e^{i\varphi(k_1,k_2)/2}$
for Frank $c(k_1, k_2) = e^{i\varphi(k_1,k_2)}$

the symmetry of the a amplitudes for interchage of k, it follows, that the symmetric as well as the antisymmetric amplitudes fulfil the system of secular equations. Which of them, however, correctly describes the spin waves, cannot be decided without any additional assumption.

This reminds to some degree the situation which occurs in elementary quantum mechanics dealing with system containing many particles of the same type. As is well known, in this case both the symmetrical and antisymmetrical functions are physical admissible solutions of the Schrödinger equation and there is no a priori way of deciding which one of the two solutions is preferable. This ambiguity is suppressed by the exclusion principle.

The application of this principle to the spin waves requires the knowledge which is the value of the spin of the quasiparticles corresponding to the spin waves. However, this question has not yet been exactly discussed. Generally it is assumed that this value is 1; this would lead to the symmetric function.

Frank picks out the minus sign in (6a) explaining that it is distinguished by the equation (6b) and that for this sign one gets the right number of states in the real k space. This argumentation, however, is not convincing because, the equation (6c) distinguishes the plus sign. On the other hand, the equation (6b) taken alone does not yet mean that the a amplitudes are antisymmetrical. Some light would be thrown upon the question by the generalization of the method of this paper for the case $s > 1/2$ and consideration of three dimensional lattices. This, however, cannot be performed in a simple manner. With more powerful methods this was done by Dyson (1956) who came to the conclusion that the quasiparticles of spin waves can be considered as a Bose gas, subject to no exclusion principle. The investigation on the neutron scattering, performed by Riste, Blinowski and Janik (1959) seems to support this conclusion.

I am indebted to Prof. S. Szczeniowski for his continuous interest and encouragement during this work as well as for reading and discussing the text. I wish alsa to thank Dr. H. Cofta for discussion on some points.

REFERENCES

Bethe, H., *Z. Phys.*, **71**, 205 (1931).
Dyson, F. J., *Phys. Rev.*, **102**, 1217 (1956).
Frank, D., *Z. Phys.*, **146**, 615 (1956).
Riste, T., Blinowski, J. and Janik, J., *J. Phys. Chem. Solids*, **9**, 153 (1959).
Svirskii, M. S. and Ishmukhametov, B. Kh., *Fiz. Metallov i Metallovedenie*, **5**, 548 (1959).
Vonsovsky, S. V. and Svirskii, M. S., *Zh. eksper. teor. Fiz.*, **35**, 1447 (1958).

EFFECTIVE MASS METHOD IN THE CASE OF NON-QUADRATIC DISPERSION FORMULA

By Zbigniew Kopeć

Institute of Physics, Polish Academy of Sciencies, Warsaw

(Received August 22, 1959)

The case of a non-parabolic energy band in a semiconductor has been analyzed and the necessary modification of the usual effective mass method has been found. It turns out that to describe the motion of single electrons, one must introduce instead of the coefficient m_{ef} several coefficients, called the differential effective masses. It has been shown that in the above case the phenomena of electrical transport can be described by the same expressions as in the parabolic case with the only difference that m_{ef} has to be replaced by a characteristic quantity for the given phenomenon, the so-called integral effective mass, being a mean of the differential effective masses. Making use of E. O. Kane's dispersion formula some integral effective masses for In-Sb — n have been calculated, as well as some scattering coefficients appearing in the Hall and Seebeck effect.

The theoretical description of transport phenomena in semi-conductors is usually based in the so-called effective mass method wherein the carriers in the semi-conductor are assumed to possess the properties of free electrons the mass of which, however, has undergone modification. It is this modified value of the mass (effective mass, m_{ef}) that accounts for interactions between the lattice and the carrier.

Thus, the effective mass method represents a problem of mass renormalisation. The method itself was developed on two tacit assumptions, namely:

I.

The assumption of spherical structure of the conductivity band and of the fundamental band, as expressed by the condition $\varepsilon(\vec{k}) = \varepsilon(k)$, with ε denoting the energy of the electron, and $\vec{k}$ its wave vector. Until recently (up to the date of discovery of the cyclotron effect in Ge) it was considered to be justified in the case of all crystals of the regular system. As a great many semi-conductors and, first among these, those that can be obtained to a very high degree of purity, crystalize in the regular system, the assumption was thought to be fully justified.

II.

Moreover, the electrons (holes) were assumed to occupe only levels sufficiently close to the bottom of the conductivity band (top of the fundamental band) for ε to be given by the first term in the Taylor expansion of $\varepsilon(k)$ in powers of k. Clearly, at the extremities of the band, the Taylor expansion of the energy begins from the quadratic term; thus by assumption (I):

$$\varepsilon = \frac{1}{2}\left(\frac{\partial^2 \varepsilon}{\partial k^2}\right)_{k=0} k^2 + \text{higher order terms} \tag{1}$$

or, denoting

$$\frac{1}{\hbar^2}\left(\frac{\partial^2 \varepsilon}{\partial k^2}\right)_{k=0} = \frac{1}{m_{ef}}$$

and with $\hbar\vec{k} = \vec{p}$, wherein $\hbar = \frac{h}{2\pi}$, $h =$ Plancks constant

$$\varepsilon = \frac{p^2}{2m_{ef}} \tag{2}$$

Assumption (II) was based on the fact that the free carriers usually occupied a very small part of the band in semi-conductors (i. e. substances wherein the permitted bands are separated by energies of the order of 1 eV). Even at medium concentrations of the order of 10^{16} cm^{-3} only one millionth percent of the free states is occupied. Hence, in a great number of cases, this may be a region wherein the quadratic approximation is really sufficiently accurate.

With the foregoing assumptions, the behaviour of the electrons in the crystal when subjected to an external force $\vec{F}$ is described, according to Bloch's general theorem (1929), by the classical law of motion:

$$m_{ef}\frac{d\vec{v}}{dt} = \vec{F} \tag{3}$$

(with $\vec{v}$ denoting the mean velocity of the electron in the crystal), the only difference consisting in the fact that instead of the rest mass of the electron, eq. (3) contains the effective mass of eq. (2).

On the other hand, eq. (2) yields a simple expression for the density of electron states (the number of electron states per unit energy interval):

$$D(\varepsilon) = \frac{4\pi}{h^3}(2m_{ef})^{3/2}\sqrt{\varepsilon} \tag{4}$$

The simple effective mass method based on assumptions (I) and (II) will be here termed the "classical" method, with respect to its close bearing on the classical theory of electron motion and the part played by it in the development of semi-conductor physics.

It will be subsequently proved that the inverse is also exact, namely: the assumption of constant carrier mass leads to the conclusion that assupmtions (I) and (II) must be fulfilled simultaneously. Thus, "classical" effective carrier mass implies a highly specialized (simple) energy structure model of the semi-conductor. Inversely, a substance for which Assumption (I) or (II) is not fulfilled is not accounted for by the "classical" concept of effective mass.

Renouncement of Assumption of Sphericality

Investigation of the cyclotron effect in Ge and Si carried out in 1954-1955 (A. F. Kipp, C. Kittel 1955) clearly proved that Assumption (I) (that of sphericality) was not justified in the case of these crystals. Experiments showed the conductivity band to be given by a dispersion formula, $\varepsilon(\vec{k})$, corresponding to surfaces of equal energy having the shape of greatly elongated rotational ellipsoids whose principal axis had the direction of [111] (Ge) or [100] (Si). Here, minimum energy does not coincide with $\vec{k} = 0$, but with several crystallographically equivalent points $\vec{k}^i \neq 0$ wherein $i = 1, 1, \ldots N$, and N denotes the number of minima of $\varepsilon(k)$.

Hence, this represents a model that is not only non-spherical, but is at the some time one possessing several minima points (multi-valey model). In the neighbourhood of each minimum in point $\vec{k}^i$, the dispersion formula is of the shape

$$\varepsilon^i(\vec{k}) = \frac{\hbar^2}{2}\left\{\frac{(k_1 - k_1^i)^2}{m'} + \frac{(k_2 - k_2^i)^2 + (k_3 - k_3^i)^2}{m''}\right\} \qquad (5)$$

In eq. (5), the principal axes of the i-th ellipsoid have been chosen as coordinate axes. Clearly, the coefficients m' and m'' have the dimension of mass and replace the effective mass of earlier formulas. (see eq. (2)); the quantities m' and m'' are usually termed the longitudinal and transversal effective mass, respectively.

Eq. (5) can be rewritten to become formally identical with eq. (2) viz.:

$$\varepsilon^i = \frac{p_i^2}{2m^*} \qquad \text{wherein } \vec{p}_i = \hbar(\vec{k} - \vec{k}^i) \qquad (2°)$$

The constant quantity m_{ef} of eq. (2) is now replaced by one that is, generally, variable: $m^* = m^*(\vec{k})$. Considering eq. (5) to represent the specialized dispersion formula, it is readily seen that m^* depends solely on the angle subtended by the vector $\vec{k}$ and the rotation axes of the ellipsoid; thus, on changing from the rectangular coordinates k_1, k_2, k_3 to the spherical coordinates k, ϑ, φ, the quantity m^* is a function of the polar angle ϑ, thus: $m^* = m^*(\vartheta)$. The dispertion formula is clearly seen to conserve the quadratic form analytically, i. e. notwithstanding the fact that the first condition of the former model has been removed, the second condition is still fulfilled. The clasical equation (3) will be replaced by the law of motion for a Bloch wave packet in the presence of external forces, in tensor form (F. Bloch 1929).

Thus, in place of eq. (3), we have now

$$\frac{1}{M} \cdot \vec{F} = \frac{d\vec{v}}{dt} \tag{3°}$$

wherein the tensor $\frac{1}{M}$ (in the system of principal axes of the ellipsoid (5), as above) is given simply in the form

$$\frac{1}{M} = \begin{vmatrix} \frac{1}{m'} & 0 & 0 \\ 0 & \frac{1}{m''} & 0 \\ 0 & 0 & \frac{1}{m''} \end{vmatrix} \tag{6}$$

Thus, eqs. (2^0) and (3^0) replace eqs. (2) and (3) of the common effective mass theory in the case under consideration. Eqs. (2^0) and (3^0) still retain the form of dynamic laws and can be used for investigating electron motion in a crystal by classical methods (common diffrential equations). The present case, however, introduces a more profound modification into the laws of motion of the electron than that implied by the effective mass theory in its "classical" form.

In the present case, both fundamental laws of motion (2^0) and (3^0) no longer contain one and the same effecive mass, but two distinct "mass coefficients" namely: the energy formula contains the quantity $m^* = m^*(m', m''; \vartheta)$, whereas the force-acceleration relation contains no less than 9 tensor elements which are yet other functions of the same coefficients m', m'' and ϑ. Characteristically for the case under consideration, both m^* and the tensor $\frac{1}{M}$ are independent of the absolute value of the wave vector $\vec{k}$ but depend solely on the angle subtended by $\vec{k}$ and the rotation axis of the ellipsoid. The foregoing fact, which is a consequence of the quadratic form of eq. (5) implies quite generally, in the expressions accounting for various electronic processes, that the structural factors related to the quantities m^* and $\frac{1}{M}$ are independent of the degree of ivestment of the band (and, hence, are concentration and temperature independent).

The foregoing relatively simple example of failure of the former concept of effective mass has been dealt with at length in order to show, that — if the formalism is appropriately modified — the motion of the carriers, and, thus, a specialized transport phenomenon can still be described by a method that is, in principal, classical. On the other hand, the computations required in the case under consideration as given by eq. (5) for the electronic effects hitherto accounted for by the "classical" method of constant effective mass are, as yet, a highly involved problem and one whose greater part still awaits solution. It is not the present author's intention to

give a detailed account of the computations, wich will be reproduced here in their general outline only. Thus, eqs. (2⁰) and (3⁰) should be completed by an expression accounting for the density of states, formally idencitcal with eq. (4), but such that m^*_{ef} is therein replaced by the quantity $m_{d.s.}$ being yet another, though well-defined function of the coefficients by eq. (5), namely

$$m_{d.s} = N^{\frac{2}{3}} m'^{\frac{1}{3}} m''^{\frac{2}{3}} \qquad (4^0)$$

To replace (2), (3) and (4), the quantities (2⁰), (3⁰) and (4⁰), respectively, should be substituted in the expressions for the various electric effects in semi-conductors. Hence, expressions with m^*, $\frac{1}{M}$ and $m_{d.s.}$ will appear in the respective sums and intergrals resulting from integration of the momenta or energies over all the electrons. This means that the formulas for the transport phenomena retain, in the case of Ge, their previous formal character, with various new structural expressions (related to the form of $\varepsilon(\vec{k})$) to replace in the various formulas. The generally different structural expressions will be jointly termed mass coefficients or effective masses, each of these being additionally denoted according to the kind of phenomenon under consideration. In this manner, the universal effective mass of the simple model is now replaced by a set of different masses. All mass coefficients are obtained from the three fundamental masses m^*, $\frac{1}{M}$, $m_{d.s.}$, and can be ultimately and univocally derived from the dispersion formula by the procedure already outlined. Here, as exemplified by the ellipsoidal modification of the band, a consistent procedure has been put to effect making it possible to correct the theory. This requires, in general, that all three fundamental formulas defining the effective mass be modified.

In a paper on germanium (Z. Kopeć 1956), the formula accounting for the thermoelectric force and mobility has been corrected along lines corresponding to the modified theory already mentioned. The corrected expressions have served to remove certain experimental "anomalies" existing in this field of research and have made it possible to relate quantitatively the various electronic phenomena in germanium, thus assembling them into one consistent group. In particular, the (by "classical" standards) anomalously high thermoelectric force in Ge — n as compared with Ge — p found its explanation; similarly, the source of the discrepancy between the effective mass values from electron mobility, on the one hand, and thermoelectric force, on the other, was clarified (the respective values had differed by 150—200 %). Within the framework of the corrected theory, the foregoing "anomaly" served to corroborate the discovery of band anisotropy.

In the analysis of carrier effective mass in Ge as proposed at the time, the author based on eq. (5). It has been already mentioned that this is equivalent to retaining Assumption (II) of the previous concept of mass.

Sufficiently far from the bottom of the band, however, there should be divergence from the quadratic law for $\varepsilon = f(k)$, leading to temperature and concentration depend-

ence of the effecitve mass. The experimental results obtained with Ge — n samples of a very high degree of purity are in agreement with computations based on the quadratic approximation. On the other hand, in samples of medium and high carrier concentrations, numerous measurements lead to disagreement with theoretical results based on this approximation (Z. Kopeć 1956), which points to the probability of a divergence of the kind discussed. However, at the present stage of our knowledge of band structure in Ge — n, no quantitative expression of this divergence could be given.

In InSb—n, the state of affairs is one of still much more drastic desagreement. In this case the effective mass of electron state density is by over one order lower than in Ge. Hence, levels that are far remote from the extremity of the band are occupied already at relatively low concentrations. Thus, we are now entitled to expect especially grave results of the divergence from the quadratic dispersion formula. Indeed, such divergences were shown to exist from our experiments on the thermoelectric force in InSb and from the optical experiments by Fan and Spitzer on infrared absoption in strongly doped InSb samples (H. J. Fan, W. G. Spitzer 1955).

Renouncement of Assumption of Quadraticity

To generalize the effective mass method to include non-quadratic structures ($\varepsilon \neq ak^2$), a quite general problem will now be discussed. No assumptions whatsoever will be made as to the form of the dependence of the energy of the electron on the set of quantum numbers accounting for its state. For a dependence of quite general form it will be the author's aim to derive laws of motion formally analogous to the entirely classical formulas, and expressions for the density of states formally identical with that of the "classical" theory of effective mass discussed in the Introductory chapter.

In the equations describing the motion of the carrier in external fields and in the fields of various perturbations of the ideal crystal lattice (to which energy band structure relates) different effective masses will appear which in general, can be functions of all the quantum numbers accouting for the state of the electron. Th us each electron will in general, be described by several distinct masses: the energy mass, state density and dynamic masses. Each of these quantities can be different for the various electrons within one and the same semi-conductor.

By summation (statistics) of elementary processes, it is possible, as previously, to achieve description of phenomena involving great numbers of electrons (transport and other electronic processes). The structural factors appearing in this description will already be highly complex. In following we find namely the form of these coefficients in nonparabolical case.

All mass coefficients can be classified in one of the following two groups: that of differential and that of integral mass coefficients.

Differential and Integral Effective Masses

Quantities accounting for a separate electron in the band will be termed differential quantities. Three fundamental effective masses will be distinguished, in accordance with the following three definitions:

$$\varepsilon = \frac{p^2}{2m^*} \tag{2^I}$$

$$\frac{1}{M_{ij}} F_j = \frac{dv_i}{dt} \tag{3^I}$$

$$D(\varepsilon) = \frac{4\pi}{h^3} (2m_{d.s.})^{3/2} \sqrt{\varepsilon} \tag{4^I}$$

The quantities m^* and $\frac{1}{M}$ account for the properties of motion of the electrons in the semi-conductors in a field of external forces; on the other hand, $m_{d.s.}$ describes the electron state density $D(\varepsilon)$ whose knowledge is indispensable for summation over all occupied electron states in the band in the procedure of computing transport processes.

Eqs. (2^I), (3^I) and (4^I) can be considered to arise from (2), (3) and (4) by replacing m_{ef} therein by m^*, M and $m_{d.s.}$, respectively.

To conserve the previous form of the expressions describing transport phenomena, integral effective masses, being certain combinations of the differential masses, will be introduced.

In the general case, any electron transport phenomenon was accounted for in the classical effective mass method by relation (a):

(a) $z = z$ (semi-conductor parameters, external conditions, m_{ef}.); in the present case, in accordance with the generalized fundamental equations (2^I), (3^I) and (4^I) the expression for z will be appropriately modified. This is carried out as follows. In a great number of cases, the expression corresponding to the phenomenon under consideration will be able to be put in the form

(a') $\bar{z} = \bar{z}$ (semi-conductor parameters, external conditions m_{ph}); identical with the "classical" form, but one wherein m_{ph} has replaced the previous universal effecitve mass m_{ef}. For a given phenomenon, m_{ph} will be expressed by a specific mean value of the differential effective masses, to be termed the integral effective mass of the electron phenomenon under consideration (index: *ph*).

In some cases, a structure-independent expression can correspond "classicaly" to an electron process:

(b) $z' = z'$ (semi-conductor parameters, external conditions).

On the other hand, within the framework of the generalized effective mass method, this kind of structural dependence can occur, then assuming the form

(b') $\bar{z}' = \bar{z}'$ (semi-conductor parameters, external conditions; a_{ph}), wherein a_{ph} represents a structural coefficient being an integral function of the same differential massess.

The possibility of the foregoing simple generalization of the "classical" effective mass method results from the fact that the "classical" quantities (2), (3) and (4) are replaced by the three fundamental equations (2^{I}), (3^{I}) and (4^{I}).

The set of mass coefficients play a role similar to that of the effective mass of the simple theory and lend profounder significance to the intuitions inherent in the "classical" method of effective mass.

We shall now proceed to compute the differential and, subsequently, some of the integral mass coefficients for an InSb crystal.

Differential Effective Masses in InSb—n

Using the wave vector as quantum index of the state of the electron (perfect periodicity), the equations can be written as follows (see Appendix):

$$\varepsilon = \frac{\hbar^2 k^2}{2m^*} \tag{2^{II}}$$

$$\frac{1}{M_{ij}} = \frac{1}{\hbar^2} \frac{\partial^2 \varepsilon}{\partial k_i \partial k_j} \tag{3^{II}}$$

$$m_{d.s.} = \frac{1}{2}\left[\frac{h^3}{4\pi\sqrt{\varepsilon}} \frac{D(k_1, k_2, k_3)}{D(\varepsilon, \vartheta, \varphi)}\, d\vartheta\, d\varphi\right]^{2/3} \tag{4^{II}}$$

It should be noted that eqs. (2^{II}) (3^{II}) and (4^{II}) define the fundamental differential effective masses in accordance with the scheme assumed for a perfect crystal (description in terms of the wave vector). However, eqs. (2^{I}), (3^{I}) and (4^{I}) are of a much more general form. Eqs. (2^{II}), (3^{II}) and (4^{II}) result from definitions (2^{I}), (3^{I}) and (4^{I}) as applied to the Brillouin band (description in terms of the wave vector $\vec{k}$). However, various experimentally known facts speaking in favour of a qualitative analogy between phenomena in periodical and amorphous structures (vitrous semi-conductors) seem to indicate that the possibilities of a semi-classical description of the dynamic properties of the electron in solids are not restricted to conditions of perfect periodicity. For non-periodic structures, eqs. (2^{I}), (3^{I}) and (4^{I}) can be assumed to represent original definitions of the quantities m^*, $\frac{1}{M}$ and $m_{d.s.}$ whereas the state of the electron can be described by an adequate set of quantum numbers in place the wave vector $\vec{k}$ characteristic of the state of the electron in periodic structures. We shall now proceed to compute the values of the differential effective masses for electrons in InSb. Here, a number of experimental results point to spherical structure of the conductivity band, (thus, e. g. experiments on variations in the electric conductivity in a longitu-

dinally aplied magnetic field) Hence, the dispersion formula for InSb will be of the form

$$\varepsilon(\vec{k}) = \varepsilon(k) \tag{7}$$

With respect to the non-quadratic form of $\varepsilon(k)$, it would be possible to take into account the next, higher term in the Taylor expansion, thus assuming

$$\varepsilon(k) = ak^2 + bk^3 \tag{8}$$

In the next step, with this expression, it would be possible to determine various effective mass quantities and to find the values of a and b from comparison with experimental data. If necessary, powers higher than k^3 in the expansion of $\varepsilon(k)$ should be taken into account.

Here, however, a different procedure will be adopted. Indeed our starting point will be given by Kane's formula (9), (1957), recently derived along theoretical lines, which explicitly gives $\varepsilon(k)$ in InSb.

Hence, the exprimental confirmation of the results of the present computations can be considered to provide the justfication of our general procedure and, at the same time that of Kane's formula.

Kane proposes the following expression for the energy of an electron in the conductivity band:

$$\varepsilon(k) = \frac{\hbar^2 k^2}{2m_0} + \frac{1}{2}\left[\left(\Delta\varepsilon_G^2 + \frac{8}{3}\hbar^2 k^2 P^2\right)^{1/2} - \Delta\varepsilon_G\right] \tag{9}$$

The formula contains, in addition to universal constants, only two structural parameters which should be determined experimentally, namely:

$\Delta\varepsilon_G$ the width of the energy gap, and the quantity P, which can be related to the cyclotron effect and determined from formula (10):
with m_c denoting the cyclotron mass (see Appendix).

$$\frac{4}{3}p^2 = \Delta\varepsilon_G \frac{m_0 - m_c}{m_0 \cdot m_c} \tag{10}$$

Eq. (9) was derived by highly interesting consideration of a general nature not involving knowledge of the form of the InSb lattice potential, but basing on its symmetry properties and characteristics as resulting from well-known and rather simple experimental facts (a single resonance maximum in the cyclotron effect, behauiour of the electric resistivity in a magnetic field, an extremely narrow forbidden band). Thus, Kane could adopt the most appropriate perturbation method and restrict the problem to $\vec{k}\vec{p}$ and spin-orbital interactions indepedently of k. Kane's formula may indeed be considered to account adequately for the structure of the conductivity band, at least for electrons of up to 0.3 ev, since, as that author proved, neglected interactions of various other kinds begin to play a part for electrons whose energies exceed this value.

The energy mass, m^*, as determined from Kane's formula, is conveniently represented in the form of an expansion. It is readily proved, from eq. (9), that

$$m^* = m_c \left[1 + \sum (-1) \frac{n \ldots (2n-3)}{n!} 2^{n-1} \left(\frac{m_c}{m_0} \right)^{n-2} \left(\frac{m_0 - m_c}{m_0} \right)^n \left(\frac{\varepsilon}{\Delta \varepsilon_G} \right)^{n-1} \right] \tag{11}$$

The differential state density effective mass $m_{d.s.}$ is expressed in m^* according to

$$m_{d.s.} = m^{*1/2} \left(m^* + \frac{\partial m^*}{\partial \varepsilon} \varepsilon \right)^{3/2} \tag{12}$$

The tensor $\frac{1}{M}$ is given by the following expression:

$$\frac{1}{M} = \begin{vmatrix} \frac{1}{m_1} \cos^2 \alpha_1 + \frac{1}{m_2} \sin^2 \alpha_1, & \left(\frac{1}{m_1} - \frac{1}{m_2} \right) \cos \alpha_1 \cos \alpha_2, & \left(\frac{1}{m_1} - \frac{1}{m_2} \right) \cos \alpha_2 \cos \alpha_3 \\ \left(\frac{1}{m_1} - \frac{1}{m_2} \right) \cos \alpha_2 \cos \alpha_1, & \frac{1}{m_1} \cos^2 \alpha_2 + \frac{1}{m_2} \sin^2 \alpha_2, & \left(\frac{1}{m_1} - \frac{1}{m_2} \right) \cos \alpha_2 \cos \alpha_3 \\ \left(\frac{1}{m_1} - \frac{1}{m_2} \right) \cos \alpha_3 \cos \alpha_1, & \left(\frac{1}{m_1} - \frac{1}{m_2} \right) \cos \alpha_3 \cos \alpha_2, & \frac{1}{m_1} \cos^2 \alpha_3 + \frac{1}{m_2} \sin^2 \alpha_3 \end{vmatrix} \tag{13}$$

wherein

$$\frac{1}{m_1} = \frac{1}{\hbar^2} \frac{\partial^2 \varepsilon}{\partial k^2} = \frac{1 + (a-2)\, a + b}{m^* (1+a)^3}$$

$$\frac{1}{m_2} = \frac{1}{\hbar^2} \frac{1}{k} \frac{\partial \varepsilon}{\partial k} = \frac{m^{*1/2}}{m_{d.s.}^{3/2}}$$

and

$$a = \frac{1}{m^*} \frac{\partial m^*}{\partial \varepsilon} \varepsilon$$

$$b = -\frac{2}{m^*} \frac{\partial^2 m^*}{\partial \varepsilon^2} \varepsilon^2$$

$$\frac{k^i}{k} = \cos \alpha_i$$

Thus, the quantities m^*, $m_{d.s.}$ and $\frac{1}{M}$ are seen to be increasing functions of the energy. Fig. 1 shows a graph of the four differential mass coefficients as previously defined.

It is noteworthy that, notwithstanding the fact that the band structure is spherical, the effective mass tensor $\frac{1}{M}$ by no means reduces to a scalar. Hence, the change in velocity of the electron in the field of force does not, in general, oecur

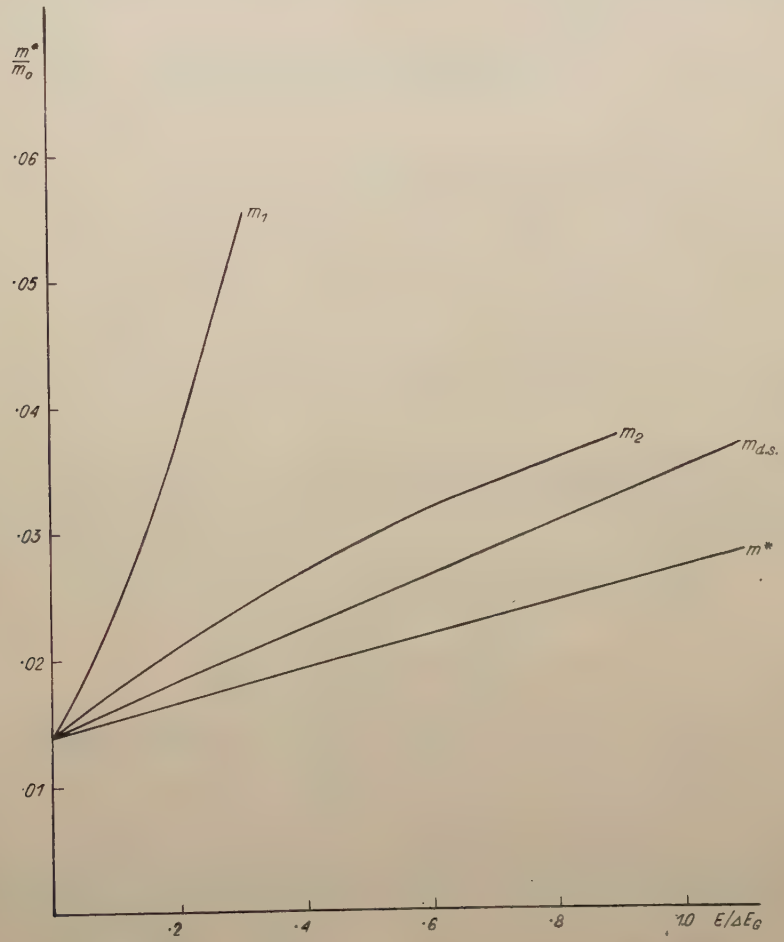

Some differential effective masses for InSb. Effective energy mass — m^*; state-densities — $m_{d,s}$; dynamical masses as functions of electron anergy (calculated with $m_c = 0.014$) — m_1, m_2.

in the direction of the force, but depends also on the direction of cristal-momentum of the electron.

Scalarity of the effective dynamic mass is exclusively a property of a structure that is at the same time parabolic and spherical (see Appendix):, it thus represents a case that does not occur in normal conditions among the semi-conductors known at present.

Some Integral Effective Mass Quantities in InSb—n

State density mass $M_{d.s.}$.

The quantity is defined by the well-known formula accounting for the electron concentration in the band:

$$n = \frac{2(2\pi kT)^{3/2} M_{d.s.}^{3/2}}{h^3} \frac{2}{\sqrt{\pi}} F_{1/2}(\eta) \tag{14}$$

wherein

k — Boltzmanns constant

h — Plancks constant

$\eta = \frac{\varphi}{kT}$ and φ — energy of Fermi level

$$F_i(\eta) = \int_0^{\tilde{}} \frac{x^i dx}{1 + e^{x-\eta}} \quad \text{(Fermi's integral)}$$

The expression can also be derived in the Kane's type band. The quantity $M_{d.s.}$ is obtained from the differential coefficient $m_{d.s.}$ by integration according to eq. (15) (see Appendix):

$$M_{d.sq} = \left[\frac{\int_0^{\tilde{}} \frac{m_{d.s.}^{3/2} \cdot x^{1/2}}{1 + \exp(x - \eta)} dx}{F_{1/2}(\eta)} \right]^{2/3} \tag{15}$$

Exact calculation of $M_{d.s.}$ from eq. (15) reduced to the numerical computation of a sequence of Fermi type integrals and is a highly toilsome affair. Since, however, the $\varepsilon(k)$ dependence in not expressed quite exactly by Kane's formula (especially at energies $\varepsilon > 0.3$ eV), it seems justified to introduce an approximation that greatly simplified the computations, albeit at the cost of some small increase in error.

It is readily proved (see Appendix) that, assuming the linear approximation

$$m_{d.s.}^{3/2} = s + t \frac{\varepsilon}{\Delta\varepsilon_G} \tag{16}$$

instead of the exact expression for $m_{d.s.}^{3/2}$ in eq. (15), a relatively simple, approximate form of $M_{d.s.}$ is obtained:

$$M_{d.s.}^{3/2} = s + t \frac{kT}{\Delta\varepsilon_G} \frac{F_{3/2}(\eta)}{F_{1/2}(\eta)} \tag{17}$$

The following values have been assumed: $s = 0.00165$, $t = 0.0055$. The error of this computation does not exced 10 %. Here, the values of m_c and $\Delta\varepsilon_G$ had to be

taken from other sources. For m_c, a value of 0.014 (in m_0) was assumed, representing the average of m_c[1]) as measured in the cyclotron effect at 4.2^0 K: $m_c = 0.013$, and at 300^0 K: $m_c = 0.015$.

The value of $\Delta\varepsilon_G$ $\left(\text{at } 0^0 \text{ K } \Delta\varepsilon_G = 0.24 \text{ ev } \frac{d\Delta\varepsilon_G}{dt} = 2.17 \cdot 10^{-4}\text{ev}\right)$ was assumed in accordance with the optical data found in the literature.

Some results of the computations are given in Table 1, wherein the coordinates $T(^0\text{K})$ and n (concentration of free electrons) are employed, as is usually the case in describing the state of the electrons in a sample.

Table 1 $M_{d.s.}(T, n)$

T \ n	10^{15}	10^{16}	10^{17}	10^{18}	10^{19}
50°K	.0148	.0151	.0172	.0239	.0394
100°K	.0155	.0159	.0176	.0242	.0410
300°K	.0194	.0198	.0206	.0266	.0451

From Table 1, the effective state density mass in InSb increases with the temperature and the electron concentration. The author feels he should stress that, at 300^0 K. the transition from electron concentration 10^{16} cm^{-3} to 10^{19} cm^{-3} involves an increase in $M_{d.s.}$ to more than double. It is this integral effective state density mass that is obtained in measurements of the thermoelectromotive force α (see Appendix).

Dispersion Coefficients A and r

In the expression of the thermoelectromotive force

$$\alpha = \frac{k}{e}(A - \eta) \tag{18}$$

where e denotes the elementary charge, the well-known dispersion coefficient A representing the mean kinetic energy of the carriers in kT units appears. The coefficient itself has been the object of many an investigation, whence it is known to possess a number of interesting properties.

In the first place, for applicability of Boltzmann statistics and of the parabolic band approximation the values of A for most dispersion mechanisms range from 2

[1]) If the result of measurements of m_c in the cyclotron effect at room temperature is analyzed more closely the conclusion is reached that the true value of the effective mass at the bottom of the band at the temperature considered is somewhat smaller than the value of 0.013 characteristic of low temperatures. Since the computations were approximate, the present author refrained from introducing the temperature variations in m_c. Besides, to obtain the latter variations, some kind of extrapolation would have to be adopted.

to 4. A value of 2 corresponds to dispersion on acoustical phonons, whilst that of 4 to dispersion on ions. If both mechanisms exist simultaneously, intermediate values appear; the dependence of the latter on the rate of participation of either mechanism is discussed e. g. in the paper by A. I. Anselm and V. I. Klatchkin (1952). Degeneracy has been investigated by a rigorous treatment only for pure dispersion mechanisms (J. Tauc 1953, O. Madelung and H. Weiss 1954). In cases when dispersion can be accounted for by introducing the notion of relaxation time, the formula for A assumes the form

$$A = kT \frac{L_1}{L_0} \tag{19}$$

with

$$L_i = -\frac{2}{3} e \int v \cdot l \cdot \varepsilon^i D(\varepsilon) \frac{\partial f_0}{\partial \varepsilon} d\varepsilon \tag{20}$$

The following relation can be proved to hold for dispersion on acoustical phonons and Kane's structure (see Appendix):

$$l = \frac{\pi \hbar^4 c_{ll}}{\varepsilon_1^2 kT} \frac{m^*}{m_{d.s.}^{3/2}} \tag{21}$$

being a modification of the respective formula of deformation potential theory (J. Bardeen, W. Schockley 1950), where as $D(\varepsilon)$ is determined from eqs. (4[1]) and 12); finally, A is obtained in the form

$$A = \frac{\int \frac{m^{*2}}{m_{d.s.}^3} x^2 \frac{\partial f_0}{\partial x} dx}{\int \frac{m^{*2}}{m_{d.s.}^3} x \frac{\partial f_0}{\partial x} dx} = \frac{\pi_2}{\pi_1} \tag{22}$$

wherein

$$x = \varepsilon / kT \quad \text{and} \quad \pi_i = \int \frac{m^{*2}}{m_{d.s.}^3} x^i \frac{\partial f_0}{\partial x} dx$$

For strong degeneracy, with respect to the deltoidal form of $\frac{\partial f_0}{\partial x}$ $A \to \eta$. The difference $(A - \eta)$, being a second order quantity, requires a separate calculation. In the present case, the result will differ but negligibly from the one obtained for the parabolic band.

The situation is entirely different in the absence of strong degeneracy. For Boltzmann statistics, we have

$$A = \frac{\int \frac{m^{*2}}{m_{d.s.}^3} x^2 e^{-x} dx}{\int \frac{m^{*2}}{m_{d.s.}^3} x e^{-x} dx} \tag{22[1]}$$

at energy values of $\varepsilon < 0.3$ ev, the quantity $\frac{m^{*2}}{M_{d.s}^{3}}$ can be approximated as follows (at higher energies, the contribution to the integral in negligible):

$$\frac{m^{*2}}{m_{d.s.}^{3}} = a_0 + a_1 x + a_2 x^2 \tag{23}$$

the quotient of integrals (22^{I}) reduces to the approximate expression

$$A = \frac{2!\, a_0 + 3!\, a_1 + 4!\, a_2}{a_0 + 2!\, a_1 + 3!\, a_2} \tag{22^{II}}$$

assuming $m_c = 0.014$ and $\Delta\varepsilon_G = 0.175$ ev; $A = 1.66$ ($T = 300^0$ K).

If dispersion is not phonon acoustical but phonon-optical, the quantity A can no longer be expressed by eq. (22) (as it is not possible to define the quantity l, and the problem becomes highly involved nathematically; Boltzmann's equation then becomes Voterra's integral equation, which must be solved by variational methods). A case of this kind was discussed by E. H. Sondheimer and O. I. Hogath (1953) and applied to Kane's structure by H. Ehrenreich (1957). According to the latter author, $A = 2.5$ at 300^0 K.

As to the coefficient r in the formula

$$R = \frac{r}{n \cdot e \cdot c} \tag{24}$$

with

R denoting Hall's constant
n — the carrier concentration,
c — the velocity of light, and
e — the elementary charge,

it is independent of the dispersion mechanism at high field intensities, and assumes the value $r = 1$. On the other hand, however, non-parabolicity of the structure, by a computation analogous to the one yielding A, leads to an increase in r: $r = 1.26$:, For strong degeneracy r again tends to 1.

Phonon -Acoustical Mobility Mass

We shall also deal with the mass coefficient in Shockley's well-known mobility formula:

$$\mu_{ph} = \frac{(8\pi)^{1/2}\, e \hbar^4 c_{ll}}{3 m_\mu^{5/2} (kT)^{3/2} \varepsilon_1^{\,2}} \tag{25}$$

It is the general opinion that, in pure germanium and in pure silicium, the carriers at room temperature are dispersed on the acoustical phonons exclusively.

Consideration of the steps leading to $m_\mu^{5/2}$ in eq. (29) yields a relation between m_μ and the integral state density mass $M_{d.s.}$ already derived (in the case of Kane's band structure — see Appendix):

$$m_\mu = M_{d.s.}^{3/5}\, m_\pi^{2/5} \tag{26}$$

The quantity m_π in the foregoing formula is given by eq. (27):

$$m_\pi = \frac{\frac{2}{\sqrt{\pi}} F_{1/2}(\eta)}{\int \frac{m^{*2}}{m_{d.s.}^3} \frac{\exp(x-\eta)}{\{1+\exp(x-\eta)\}^2}\, x \cdot dx} = \frac{\frac{2}{\sqrt{\pi}} \cdot F_{1/2}(\eta)}{\pi_1} \tag{27}$$

It is seen that m_π is closely related to the coefficient π_1 in eq. (22) for A. From eq. (27), m_π was computed by expanding in a series of Fermi functions and taking several terms, with an accuracy of 15 — 20 %. Substituting the respective values of m_π together with those of $M_{d.s.}$ from Table 1 in eq. (26), the dependence of m_μ on the concentration n and temperature T was obtained. The results are shown in Table 2.

Table 2 m_μ

T \ n	10^{15}	10^{16}	10^{17}	10^{18}	10^{19}
50°K	.0156	.018	.025	.048	.13
100°K	.0165	.018	.023	.047	.11
300°K	.0193	.025	.029	.042	.09

The value of m_μ is seen to exceed considerably both the effective cyclotron mass and the effective state density mass. The concentrational variability of the quantity considered is a much more pronounced one. It is highly characteristic that, contrary to $M_{d.s.}$, the quantity m_μ can be a decreasing function of the temperature (at constant concentration). Namely, in sufficiently impure samples, m_μ decreases with higher temperatures.

The foregoing results of the computation of mass coefficients in InSb, and, more especially, the Table of integral effective state density mass values (Table 1) and mobility mass values, point not only to far reaching divergences in the numerical values of these coefficients, but also to a different form of their temperature and concentration dependence.

These are the forms — certainly "anomalous" ones from the classical point of view — that have been observed in investigations on the thermoelectromotive force and carier mobility in InSb. An account of these experiments will be given elsewhere.

The author wishes to express his very great indebtedness to Proffessor A. F. Joffe for his valuable discussions. It was Professor Joffe's initiative that the author took up the problem of effective mass in InSb.

Appendix

State Density

In the "classical" theory of effective mass, the density of states (i. e. the number of states per unit energy ε and unit body angle Ω) is given by the relation

$$d(\varepsilon) = \frac{(2m_{ef})^{3/2}\sqrt{2}}{h^3} \tag{4a}$$

which is independent of the angle (isotropy); hence, it is always possible to employ state density per unit energy:

$$D(\varepsilon) = 4\pi d(\varepsilon) = \frac{4\pi}{h^3}(2m_{ef})^{3/2}\sqrt{\varepsilon} \tag{4}$$

Quite generally, in the description of the state of an electron by a set of numbers x_0, x_1, x_2 in x-space, a function $d_0(x, \ldots)$ will also exist, which we shall term the state density per x-space element:

$$d_0(x_1, x_2, x_3)\, d\tau_x = dN$$

with $d\tau_x = dx_0\, dx_1\, dx_2$, and $dN =$ the number of states per element $d\tau_x$.

In considering an isotropic problem (the only case reasonably possible in generalizing over homogeneous and amorphic structures), $d_0(x)$ will be a function of the energy only:

$$d_0(x) = d_0(\varepsilon) \tag{4b}$$

We shall now write an expression, analogous to (4a), for the density of states in the general case:

$$d_0 = \frac{(2m_{d.s.})^{3/2}\sqrt{\varepsilon}}{h^3} \tag{4a'}$$

which we shall consider a definition of the generalized differential effective state density mass $m_{d.s.}$.

In concrete cases of computation, we are interested in periodic structures only. Isotropic periodic structures (InSb) are also entirely within the scope of the foregoing general notation (4). Anisotropic structures, however, require that we start from the more fudamental equation (4a). Clearly, the differential state density mass, as defined by eq. (4a) can now be a function not only of the energy, but also of the angle:

$$d(\varepsilon, \vartheta, \varphi) = \frac{(2m_{d.s.})^{3/2}\sqrt{\varepsilon}}{h^3} \tag{4a}$$

The form of $m_{d.s.}$ as defined by (4a) is obtained through finding the Jacobian of the transition from the coordinates k_1, k_2, k_3 to ε, ϑ, φ. In the former system, the

state density in an element $d\tau_k = dk_1\, dk_2\, dk_3$ is constant and amounts to $\frac{2}{(2\pi)^3}$:

$$\frac{2}{(2\pi)^3}\, d\tau_k = dN \tag{4c}$$

We have

$$dk_1\, dk_2\, dk_3 = \frac{D(k_1\, k_2\, k_3)}{D(\varepsilon, \vartheta, \varphi)}\, d\varepsilon\, d\vartheta\, d\varphi = \frac{1}{\sin\vartheta}\, \frac{D(k_1\, k_2\, k_3)}{D(\varepsilon, \vartheta, \varphi)}\, d\varepsilon \cdot d\Omega \tag{4d}$$

Substituting (4d) in (4c) we have

$$\frac{2}{(2\pi)^3}\, \frac{1}{\sin\vartheta}\, \frac{D(k_1\, k_2\, k_3)}{D(\varepsilon, \vartheta, \varphi)}\, d\varepsilon\, d\Omega = d(\varepsilon, \vartheta, \varphi)\, d\varepsilon \cdot d\Omega \tag{4e}$$

i. e.

$$d = \frac{2}{(2\pi)^3} \cdot \frac{1}{\sin\vartheta}\, \frac{D(k_1\, k_2\, k_3)}{D(\varepsilon, \vartheta, \varphi)}$$

or

$$D = \frac{2}{(2\pi)^3} \cdot \iint \frac{D(k_1\, k_2\, k_3)}{D(\varepsilon, \vartheta, \varphi)}\, d\vartheta\, d\varphi$$

and, by the difinition of eq. (4^{I})

$$m_{d.s.} = \frac{1}{2}\left[\frac{h^3}{4\pi\sqrt{\varepsilon}} \iint \frac{D(k_1\, k_2\, k_3)}{D(\varepsilon, \vartheta, \varphi)}\, d\vartheta\, d\varphi\right]^{2/3} \tag{4^{II}}$$

Kane's Formula

In numerical computations, we employed the following form of Kane's formula:

$$\varepsilon = \frac{\hbar^2 k^2}{2m_c} + \frac{1}{2}\left[\Delta\varepsilon_G^2 + 2\hbar^2 k^2\, \Delta\varepsilon_G\, \frac{m_0 - m_c}{m_0 \cdot m_c}\right)^{1/2} - \Delta\varepsilon_G\Bigg] \tag{9^{I}}$$

Eq. (9^{I}) is derived from (9) by substituting eq. (10) therein. The quantity m_c defined in (10) is the cyclotron mass, which can be obtained from measurements at low temperatures with samples of very high purity.

In these conditions, it is the electrons at the very bottom of the band that come to be investigated, for which $\vec{k} \to 0$. By transition to the limit in eq. (9) for $\vec{k} \to 0$ it is readily found that

$$\varepsilon_{\vec{k}\to 0} = \frac{\hbar^2 k^2}{2m_c} \tag{9a}$$

Thus, for such electrons, we have once more derived the quadratic approximation Hence, in their case, the "classical" concept of effective mass holds and in cyclotron measurements $m_{ef} = m_c$.

Effective Mass Quantities in InSb

From the definition (2^{II}) and eq. (9^{I}), the energy effective mass m^* can be determined in accordance with eq. (11).

The form of eq. (11) which is that of a simple power series in powers of $\frac{\varepsilon}{\Delta\varepsilon_G}$, is well adapted to the problem of determining all the remaining effective mass quantitiens in InSb as the latter will be given by the expansion (11) together with its first and second derivatives:

$$\frac{\partial m^*}{\partial\varepsilon/\Delta\varepsilon_G} = m_c \sum_{n=2}^{\infty} (-1)^n \frac{1\ldots(2n-3)}{n!}\, 2^{n-1}(n-1)\left(\frac{m_c}{m_0}\right)^{n-2}\left(\frac{m_0-m_c}{m_0\cdot m_c}\right)^n\left(\frac{\varepsilon}{\Delta\varepsilon_G}\right)^{n-2} \tag{11a}$$

$$\frac{\partial^2 m^*}{\partial(\varepsilon/\Delta\varepsilon)^2} =$$

$$= m_c \sum_{n=1}^{\infty} (-1)^n \frac{1\ldots(2n-3)}{n!}\, 2^{n-1}(n-1)(n-2)\left(\frac{m_c}{m_0}\right)^{n-2}\left(\frac{m_0-m_c}{m_0\cdot m_c}\right)^n\left(\frac{\varepsilon}{\Delta\varepsilon_G}\right)^{n-3} \tag{11b}$$

By simple computations, in accordance with eq. (4^{II}) and with respect to

$$\frac{D(k_1\, k_2\, k_3)}{D(\varepsilon, \vartheta, \varphi)} = \frac{2m^*\varepsilon}{\hbar^2}\frac{\partial k}{\partial\varepsilon}$$

wherein

$$\frac{\partial k}{\partial\varepsilon} = \frac{1+\frac{1}{m^*}\frac{\varepsilon}{\Delta\varepsilon_G}\frac{\partial m^*}{\partial\varepsilon/\Delta\varepsilon_G}}{\hbar\Delta\varepsilon_G^{1/2}\left(\frac{2}{m^*}\frac{\varepsilon}{\Delta\varepsilon_G}\right)^{1/2}}$$

the differential state density mass reduces to

$$m_{d.s.} = \left[m^{*1/2}\left(m^* + \frac{\partial m^*}{\partial\varepsilon/\Delta\varepsilon_G}\cdot\frac{\varepsilon}{\Delta\varepsilon_G}\right)\right]^{2/3} \tag{12}$$

Eq. (13) results immediately from Bloch's theorem on the motion of a wave packet, as applied to a band described by a formula of the form $\varepsilon(\vec{k}) = \varepsilon(k)$. It is seen that the reciprocal mass tensor can also be computed from eqs. (11), (11a) and (11b).

By the form of eq. (13), the dynamic mass is seen not to be a scalar, to the sole exception of the case

$$\frac{\partial^2\varepsilon}{\partial k^2} = \frac{1}{k}\frac{\partial\varepsilon}{\partial k}, \qquad \text{i. e. } \varepsilon = \text{const. } k^2$$

Hence, the parabolical and spherical energy structure, i. e. the case of the "classical" concept of effective mass, is the only one to admit of the scalar form to the effective dynamic mass.

Integral Mass Quantities

State Density Mass $M_{d.s.}$

On integrating the product of the state density $D(\varepsilon)$, as given by eq. (4) and of the electron distribution function (Fermi) $f(\varepsilon) = \dfrac{1}{1 + \exp\left(\dfrac{\varepsilon}{kT} - \eta\right)}$ over the energy, we obtain the number of electrons in the band, $n = \int D(\varepsilon)\, f(\varepsilon)\, d\varepsilon$.

On expressing $D(\varepsilon)$ by $m_{d.s.}$ according to eq. (4), we have

$$n = \frac{2\,(2\pi\, kT)^{3/2}}{h^3}\,\frac{2}{\sqrt{\pi}}\,F_{1/2}(\eta)\left[\frac{\int \dfrac{m_{d.s.}^{3/2}\, x^{1/2}}{1 + \exp\,(x - \eta)}\, dx}{F_{1/2}(\eta)}\right] \tag{14}$$

Thus, it has been possible to express the concentration by an equation that is formally identical with the "classical" expression (the "classical" concept of effective mass) with the only difference that the respective power of the effective mass is now replaced by the expression in square brackets. Denoting the latter, in accordance with the general procedure adopted in the present paper, by $[\,] = M_{d.s.}^{3/2}$ the definition of the integral state density mass is obtained:

$$M_{d.s.} = \left[\frac{\int m_{d.s.}\; x^{1/2}\, f dx}{F_{1/2}(\eta)}\right]^{2}, \tag{15}$$

Dispersion Coefficients

Here, the non-quadratic form of $\varepsilon(k)$ should be acounted for in the expression for the mean free path l or the relaxation time τ. According to W. Shockley ("Electrons and Holes in Semi-Conductors", 1950),

$$\frac{1}{\tau} = \int W_{0j}\, d\Omega_j \tag{I}$$

wherein

$$W_{0j} = \frac{|U_{j0}|^2}{\hbar^2}\, 2\pi\varrho_i \tag{II}$$

the probability for transition of an electron of energy ε_0 from state 0 to state j, $|U_{j0}|^2$ denoting the square of the transition matrix element $|U_{j0}|^2 = \dfrac{AT}{V}$ ϱ_j is given by the relation:

$$\frac{V}{h^3}\, dp_1\, dp_2\, dp_3 = \varrho_j\, d\Omega_j\, d\varepsilon \quad (\vec{p} = \hbar\vec{k}) \tag{III}$$

in the case under consideration

$$dp_1\, dp_2\, dp_3 = \frac{1}{\sqrt{2\varepsilon}}\, \frac{m_{d.s.}^{3/2}}{m^*}\, d\Omega_j d\varepsilon \qquad \text{IV}$$

as

$$|\Delta_p \varepsilon| = V_j = \frac{\sqrt{2\varepsilon}\, m^*}{m_{d.s.}^{3/2}} \qquad \text{(V)}$$

thus

$$dp_1\, dp_2\, dp_3 = \frac{1}{V_j}\, d\Omega_j\, d\varepsilon \qquad \text{(VI)}$$

$$\varrho_j = \frac{V}{\hbar^3 v_j} = \frac{V}{\hbar^3}\, \frac{m_{d.s.}^{3/2}}{m^*}\, \frac{1}{\sqrt{\varepsilon}} \qquad \text{(VII)}$$

$$\frac{1}{\tau} = \frac{\sqrt{2}}{\pi}\, \frac{1}{\hbar^4}\, V |U_{j0}|^2\, m_{d.s.}^{3/2}\, \varepsilon^{1/2} \qquad \text{(VIII)}$$

however, with respect to

$$A = \frac{\varepsilon_1^2\, k}{V \cdot c_{ll}} \qquad \text{(IX)}$$

$$\frac{1}{\tau} = \frac{\sqrt{2}}{\pi}\, \frac{1}{\hbar^4}\, \frac{\varepsilon_1^2\, kT}{c_{ll}}\, m_{d.s.}^{3/2}\, \varepsilon^{1/2} \qquad \text{(X)}$$

or

$$l = \tau v_j = \frac{\pi\, \hbar^4\, c_{ll}\, m^*}{\varepsilon_1^2\, kT\, m_{d.s.}^3} \qquad (21)$$

On the Quantity r

A outline will now be given of the computation leading to r for Boltzmann statistics and dispersion on acoustical phonous only.

According to A. I. Anselm and I. V. Klatchkin (1953), accounting for the modified state density mass in Hall's constant, we may write

$$R = \frac{3\sqrt{2}}{32\pi}\, \frac{\hbar^3}{M_{d.s.}^{3/2}\, e}\, \frac{\int l^2\, \frac{\partial f}{\partial \varepsilon}\, \varepsilon^{1/2}\, d\varepsilon}{\int l\, \frac{\partial f}{\partial \varepsilon}\, \varepsilon d\varepsilon} \qquad \text{(XI)}$$

hence, by eq. (24) and substituting (21),

$$R = \frac{\frac{\sqrt{2}}{\sqrt{\pi}} \int \frac{m^{*2}}{m_{d.s.}^3}\, e^{-x}\, x^{1/2}\, dx}{\left[\int \frac{m^*}{m_{d.s.}^{3/2}}\, e^{-x}\, x d\, x^2\right]^2} \qquad \text{(XII)}$$

Approximating $\frac{m^{*2}}{m_{d.s.}^{3}}$ and $\frac{m^{*2}}{m_{d.s.}^{3/2}}$ by several terms of the expansion in povers of $x(x = \varepsilon/kT)$, the numerator reduced to a sum of simple Gauss integrals $\int x^{n+\frac{1}{2}} e^{-x}\,dx$, whereas the denominator, or, preferably, the expresion in square brackets reduces to well- known integrals of the type $\int x^n e^{-x}\,dx$.

On the Mobility μ_{ph}

$$\mu = \frac{j}{n \cdot e \cdot c} \tag{XIII}$$

From Boltzmann's equation

$$j = \frac{16}{3}\frac{\sqrt{2}}{\pi}\frac{e^2}{\hbar^3\,kT}\,E\int \tau(\varepsilon)\,\frac{m^*}{m_{d.s.}^{3/2}}\,\frac{\exp\left(\frac{\varepsilon}{kT}-\eta\right)}{\left[1+\exp\left(\frac{\varepsilon}{kT}-\eta\right)\right]^2}\,\varepsilon^{1/2}\,d\varepsilon \tag{XIV}$$

by eq. (19)

$$n = \frac{2}{\hbar^3}\,2^{1/2}\,4\pi\int \frac{m_{d.s.}^{3/2}\,\varepsilon^{1/2}}{1+\exp\left(\frac{\varepsilon}{kT}-\eta\right)}\,d\varepsilon \tag{XV}$$

substituting in (XV) the quantities (XIII) and (XIV) together with τ from eq. (X) and on appropriate transformations, we have

$$\mu_{ph} = \frac{2}{3}\sqrt{2\pi}\,\frac{\hbar^4\,e\,C_{ll}}{\varepsilon_1^3\,(kT)^{3/2}}\,\frac{\sqrt{\pi}}{2}\,\frac{\int \frac{m^*}{m_{d.s.}^{3}}\,\frac{\exp(x-\eta)}{[1+\exp(x-\eta)]^2}\,x\,dx}{\int \frac{m_{d.s.}^{3/2}\,x^{1/2}\,dx}{1+\exp(x-\eta)}} \tag{25}$$

or

$$\mu_{ph} = \frac{2}{3}\sqrt{2\pi}\,\frac{\hbar^4\,e\,C_{ll}}{\varepsilon_1^2\,(kT)^{3/2}}\,\frac{1}{m_{\mu}^{5/2}} \tag{26}$$

wherein

$$m_{\mu}^{5/2} = \frac{2}{\sqrt{\pi}}\,\frac{\int \frac{m_{d.s.}^{3/2}\,x^{1/2}\,dx}{1+\exp(x-\eta)}}{\int \frac{m^*}{m_{d.s.}^{3}}\,\frac{\exp(x-\eta)}{[1+\exp(x-\eta)]^2}\,x\,dx} \tag{27}$$

REFERENCES

Anselm, A. I., Klatchkin, V. I., *Zh. eksper. teor. Fiz.*, **92**, 297 (1952).
Bardeen, J., Shockley, W., *Phys. Rev.*, **80**, 72 (1950).
Bloch, F., *Z. Phys.*, **52**, 718, 555 (1929).
Ehrenreich, H., *J. Phys. Chem. Solids* **1**, 131 (1957).

Fan, H. Y., Spitzer, W. G., *Phys. Rev.*, **99**, 1893 (1955).
Hogarth, D. J., Sandheimer, E. H., *Proc. Roy. Soc.*, A **53**, 219 (1953).
Kane, E. O., *J. Phys. Chem. Solids* **1**, 244 (1957).
Kipp, A. F., Kittel, C., *Phys. Rev.*, **98**, 2, 368 (1955).
Kopeć, Z., *Zh. tekh. Fiz.*, **26**, 2451 (1956).
Madelung, O., Weiss, H., *Z. Naturforsch.*, **9a**, 527 (1954).
Tauc, J., *Czech. J. Phys.*, **3**, 120 (1953).

RECTIFICATION OF PHOTOELECTRIC SPECTROMETER

By Kazimierz W. Ostrowski

II. Chair of Physics, Mining and Foundry Academy, Cracow

(Received September 4, 1959)

In the present paper formulas are derived for the tolerance of the disposition of the spectrometer camera exit-slit. Other formulas accounting for the curvature of the spectral line set a limit to the admissible height of the exit-slit. A practical rule for the rectification of the spectrometer is also given, the principal feature of which consists in the use of the Hartmann diaphragm. From higher order diffraction, the effect of neighbouring lines on the data recorded is assessed. Computation is adapted to the ИСП 22 spectrograph.

1. *Introduction*

In direct spectrometry, instead of the photographical plate a photoelectric detector (photomultiplier, photosensitive G.—M. counter) is introduced; the latter is displaced parallel to the focussing plane, within which displacement of the exit-slit occurs. During the measurement, the width of the slit is fixed so as to entirely comprise the spectral line. It is but rarely that a slit of lesser width than the line is used. In this case continuous recording is obtained with an instrument provided with an automatically recording milliampermeter wherein motion of the paper tape is coupled to that of the exit-slit with selsyns.

Although direct spectrometry has now been in industrial use for about 15 years, there exists as yet no systematic treatment of the problem of rectifying the camera with the photoelectric detector accounting for such factors as the power of separation, curvature of line, ambient temperature, pressure and atmospheric moisture content.

Some papers (Hanau and Wolfe 1948, Bryon and Nahstoll 1948, Naish 1951, 1952, Mostyn 1952, Soda 1953, Hagenmah 1954, and Carlsson 1954) give these problems passing consideration, and this but from an experimental standpoint. The present author intends to complete the foregoing papers by giving computations of the admissible tolerance in disposing the camera with the photoelectric detector. Such computations may be of interest, as similar problems have been dealt with in the case of grating spectrometers (Minkowski 1942, Rupert 1952, Fastie 1952 a, b.)

These authors considered i. a. the problem of chosing the curvatature radii of the entrance and exit-slits so as to eliminate aberration and astigmatism at all wavelengths when using a long slit.

2. Assessement of tolerance in disposing exit-slit

Assume a prismatic spectrometer to have been adjusted as spectrograph. By displacing a very narrow exit- slit parallel to the focussing plane, the profile of the line can be determined. The latter will be wider then natural for three reasons:

1. the plane of motion of the slit is at a distance g from the focussing plane, which moreover can differ for the various spectral regions,
2. the exit-slit generally subtends a non- zero angle, γ with the spectral line,
3. the spectral line possesses curvature of radius ϱ,

a. Assessment of admissible distance g between focussing plane and plane of motion of slit

Fig.1 shows the situation dealt with. R denotes the line-width measured at $g \neq 0$ assuming the width of the exit-slit, the intrinsic width of the line, and the width

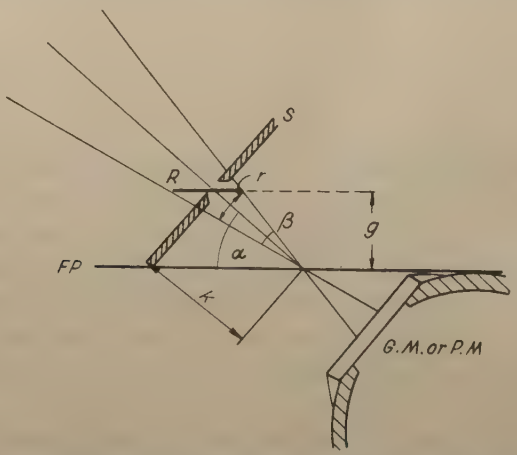

Fig. 1 Position of exit-slit S with respect to focussing plane FP

resulting from diffraction on the prims to be infinitesimally small. Introducing the notation g, α, β, R, r, k as in Fig. 1, we have, by elementary considerations:

$$R = \frac{r}{\sin\alpha} = \frac{k \sin\beta}{\sin\alpha} = \frac{g \sin\beta}{\sin^2\alpha}, \tag{1}$$

or

$$g = \frac{R \sin^2\alpha}{\sin\beta},$$

wherein sin β is a quantity identical with the relative aperture of the camora i. e. the ratio of the radius of the objective lense and its focal length. In the present considerations, values of g will be admitted for which $R = d$, with d denoting the width

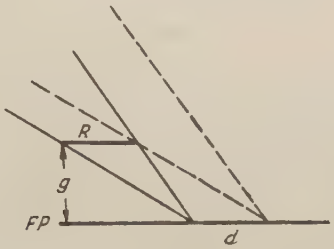

Fig. 2. Intrinsic width of line, d, and admissible width R as resulting from distance g of slit from focussing plane

of the spectral line (Fig. 2). If this width be assumed as the "instrument" line-width i. e. a half-width of the zero order diffraction maximum, then d is given by the well-known formula of the theory of optical instruments:

$$d = \frac{\lambda \sin \alpha}{\sin \beta}. \tag{2}$$

For the ИСП 22 spectrograph used by the present author in investigating photosensitive G.—M. counters (Ostrowski 1959), the following values of d and α hold (Prokofiev 1951):

Table 1

2000 Å	$d =$ 5.6 microns	$\alpha = 47°$
2570 Å	9.0 "	41°
5600 Å	23.0 "	37°

According to catalogue, the relative aperature of the objective lense in the ИСП 22 spectrograph is 0.05 for the spectral region of about 2570 Å. If these values are substituted in eq. (1), an admissible distance of about 0.1 mm is obtained. Let us compare this value and that assumed by Prokofiev for the same spectrograph when using photographic plates. In this case d is limited by the grain-size (ca. 20 microns). Prokofiev assumens the admissible distance of the plate and focussing plane to be 0.5 mm. It should be stressed that additional widening arises in the plane from dispersion of radiation in the emulsion, especially at greater wavelengths, for which gelatine exhibits lesser absorption. Resulting from non-perpendicular incidence, the long-wave side of the line will show greater diffluence, Hence adjustment of the photoelectric spectrometer requires a greater degree of accuracy; however, its separating power is higher, too. Similarly, temperature will affect the precision of adjustment to a greater degree (resulting in variations of the position of the line and in variations of g). On the other hand, such variations can be set right within

a very short time by investigating the profile of the appriopriate line, whereas the photographic method makes it necessary to make test photographs. The value of g can be modified by introducing appropriataly cut props between the spectrometert and the camera; of a set of these are to hand, the camera can be set to the degree of accuracy required.

b. Assessment of maximum admissible angle between slit and line

Hitherto it has been assumed here that the height of the entrance-slit is so small that inclination in the exit-slit has no widening effect upon the of profile the line. Fig. 3 shows a spectral line L and profiling slit S. As admissible angle γ, the one will be here assumed at which the of edge of the slit is the diagonal of the spectral line. Then

$$\operatorname{tg} \gamma = \frac{d}{l}. \tag{3}$$

For $d = 10$ microns and $l = 10$ mm, the admissible angle is 0.05^0. Simultaneous setting of the slit to this degree of accuracy and continual control of the spectral line profile is a very tedious affair. The present author proposes to make this task easier as follows: an appropriate (narrow) line is subjected to separation with a Hartmann diaphragm placed just before the entrance-slit (Fig. 4). When profiling the

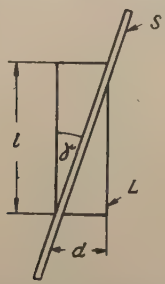

Fig. 3. Relative position of line and narrow exit-slit

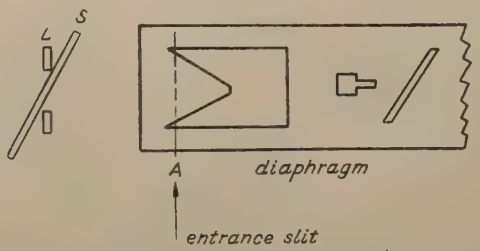

Fig. 4. Division of line for obtaining sufficiently small angle γ (method of blending of two maxima)

line two maxima are obtained; these can be made to coincide into one, presenting double intensity, if the camera is constructed so as to admit of rotating the slit through several degrees of the arc. The method proposed makes observation independent of the widening of the line profile arising from curvature. The higher the entrance--slit, the easier it becomes to attain parallel setting of the line and the exit-slit with an increasing degree of accuracy.

3. Limitation in height of entrance-slit relating to line curvature

The spectral line presents the shape of a parabola whose convexity is directed towards the short-wave end of the spectrum. This results form accounting for refrac-

tion outside the principal section of the prism. The radius of curvature of the line is given by the well- known Kaiser (1900) formula:

$$\varrho = \frac{n^2 f}{2(n^2-1)} \operatorname{ctg} i, \tag{4}$$

with f denoting the focal lenght of the collimator,

n — the refractive index for the line considered, and

i the angle of incidence, at minimum deviation (in the principal plane).

Fig. 5 shows the spectral line L, account being taken of the curvature. It will be here assumed that the admissible effective height l of the exit-slit is the one at

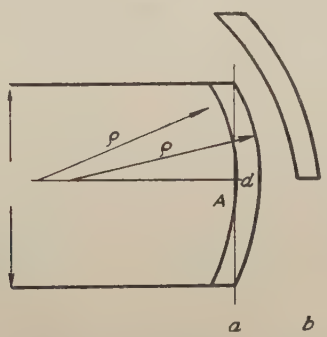

Fig. 5. Relating to definition of admissible effective height of exist-slit (admissible height of spectral line)

which the tangent A to the first edge of the line becomes the chord of the second one. Using a slit whose breadth is double that of the line, it is possible the comprise the latter entirely. By the theorem of Pitagoras,

$$l = 4\sqrt{\varrho^2-(\varrho-d)^2} \tag{5}$$

Neglecting d^2 with respect to $2\varrho d$, we have

$$l = 4\sqrt{2}\cdot\sqrt{\varrho d}. \tag{6}$$

The admissible *entrance-slit* height will be smaller in proportion to the magnifying factor of the spectrograph (for ИСП, this amount to about 1.5). If the exit-slit is several times wider than the line, then the admissible effective height is obtained by substituting the former's width for d in eq. (6). The paper by Gates (1952) brings a detailed computation of ϱ as function of the refractive index, for different angles of the prism. The following table has been prepared from Gates' graphs.

Table 2

	60° prism			45° prism
	n(quartz)	ϱ/f	for $f = 60$ cm	ϱ/f
1900 Å	1.65	0.5	$\varrho = 30$	1.00
2500 Å	1.6	0.6	36	1.05
4000 Å	1.55	0.7	42	1.15

It is seen that in direct spectrometry the prisms of smaller angle are of greater advantage. Computation yields the following results for the height of the exit-slit in the case of the ИСП 22 spectrograph:

Table 3

$\varrho = 35$ cm	d (microns)	l (mm)
	5	7.4
	10	10.4
	20	14.8
	40	20.8
	80	29.5
	100	33.0

The present author has carried out the computations for coincidence of the optical axis of the spectrometer and the centre of the entrance-slit. Were the axis to coincide with the edge of the slit, the admissible height would amount to one half of that computed (Fig. 5b). The correction γ as proposed by the author automatically for the inclination of the exit-slit accounts for deviation of the centre of the slit from coincidence with the optical axis of the spectrometer. Eq. (6) serves to determine experimentally the radius of curvature. For this, we proceed to find the difference in height between two positions of the camera that yields a difference in position of the centres of the profiles equal to the width of profile of the spectral line. That difference in height, when read on the scale of the arrangement for vertical displacement of the plates, will equal $l/2$. Then eq. (6) will yield the radius of curvature. From the theoretical point of view the line-width adopted and the way the width has beenn defined are not essential. Practically this will affect nothing but the degree of accuracy in measuring the radius of curvature.

Since in direct -reading spectrometry it is of importance that the recorded frequency of counting be maximum, and since this is in proportion with the area of the entranceslit, it seems of interest to consider *the problem of an exit-slit with curvature.* Let ϱ_1 and ϱ_2 denote the radii of curvature of the slit and the line, respectively. The height of the slit as in the situation of Fig. 6 will be assumed to be still admissible, if the slit and the line have the same width. From eq. (6), with the notation x instead of d (the latter is to denote the line-width ontly), we have:

$$l = 4\sqrt{2\varrho_1 x} \tag{7}$$

and

$$l = 4\sqrt{2\varrho_2 (x + d)}. \tag{8}$$

On eliminating x between both equations, we have

$$l = 4\sqrt{\frac{2\varrho_1 \varrho_2 d}{\varrho_1 - \varrho_2}}. \tag{9}$$

The latter is a generalisation of eq. (6), to which it reduces by substitution of $\varrho_1 = \infty$. If $\varrho_1 \approx \varrho_2$, and denoting the mean value of the radius by ϱ and the difference $|\varrho_1 - \varrho_2|$ by $\Delta\varrho$, we have finally:

$$l = 4\varrho\sqrt{\frac{2d}{\Delta\varrho}}. \tag{10}$$

With $d = 10$ microns, $\varrho = 35$ cm and $\Delta\varrho = 2.5$ cm (corresponding to the range of 2000—2500 Å), we obtain $l = 3.8$ cm. What has been said above concerning eq. (6) still holds for eq. (10).

Finally, let us consider the divergence between a circle and a parabola of the same curvature. A spectral line is stricly, a section of a parabole .Tha equations of

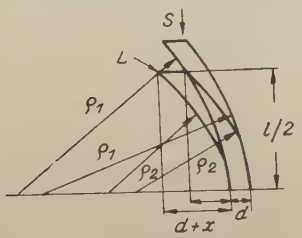

Fig. 6. Relating to definition of admissible effective height of exit-slit (with curved slit)

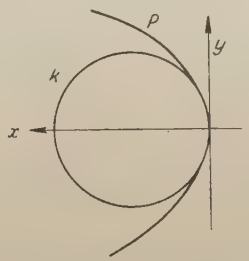

Fig. 7. Relating to computation of divergence between abscissae of circle and parabola

the circle and parabola are of the following form, respectively (cf. Fig. 7):

$$y_k^2 + (x_k - \varrho)^2 = \varrho^2;$$

$$y_p^2 = 2\varrho x_p.$$

The condition $y_k = y_p$ yields $x_k^2 + 2\varrho(x_p - x_k) = 0$. x_k is approximated from eq. (6). Finally, the following approximate formula is obtained:

$$x_k, - x_p = \frac{l^4}{8192 \cdot \varrho^3}. \tag{11}$$

With $\varrho = 35$ cm, the value of the difference begins to be of significance at $l = 25$ cm. It is seen cleary that the significance of substituting the parabola by a circle of the same radium of curvature is negligible.

The construction of curved slits is easily carried out by evaporation onto a quartz plate and subsequent incision (Polster 1951). The paper by Firestone and Randall (1938) deals with the construction of a curved slit of adjustable curvature. Fastie (1953) and Crosswile and Fastie (1954 and 1956) used 10 cm slits of 20 cm radius of curvature for grating spectrometers.

4. Diffractional effect of neighbouring lines on recorded intensity

It is a well-known fact that a spectral line results from a pattern of diffraction on the prism. Diffractions on the slit does not affect the resulting picture of the line in a way essential to our present considerations. The half-width of the zero order maximum is termed the "instrument line-width" and is given by the formula cited previously:

$$d = \frac{\lambda \sin \alpha}{\sin \beta} \tag{2}$$

wherein α is the angle of inclination of the beam with respect to the focal plane, and $\sin \beta$ — the relative aperture of the camera. The diffractional minima occur at a distance of the instrument width. From the Fresnel-Huygens principle, the consecutive approximate values of the diffractional maxima can be computed using the formula

$$A = \left(\frac{\sin \varphi/2}{\varphi/2}\right)^2, \tag{12}$$

wherein $\varphi = 2\pi n$. The following table contains the results up to order 500.

Table 4

n	A	n	A
0	1	9.5	1.1×10^{-3}
1.5	4.6×10^{-2}	10.5	9.0×10^{-4}
2.5	1.6×10^{-2}	15.5	4.3×10^{-4}
3.5	8.3×10^{-3}	20.5	2.4×10^{-4}
4.5	5.2×10^{-3}	30.5	1.0×10^{-4}
5.5	3.4×10^{-3}	50.5	4.0×10^{-5}
6.5	2.4×10^{-3}	100.5	1.0×10^{-5}
7.5	1.8×10^{-3}	200.5	2.5×10^{-6}
8.5	1.4×10^{-3}	500.5	4.0×10^{-7}

Consider the following example: let the recorded line be P 2136.199 Å and the perturbing one — the intense Cu 2135.976 Å line. These are wavelengths for which the dispersion of the ИСП 22 spectrograph amounts to 3.5 Å/mm, yielding a separation of 60 microns for the two lines. The instrument width of 6 microns enters 60 microns ten times. If the width of the exit-slit is 20 microns, then the slit stretches over orders from 7 to 12 of Cu 2135.976 Å. To compute the number of orders comprised, the slit should be projected upon the focussing plane along the beams perpendicular to the slit. Hence in the example under consideration not 3 but 5 orders are comprised. Thus, the effect of the Cu line will amount to something like an additional $5^0/_{00}$ of the Cu line intensity. If the last line is of an intensity of e. g. 100 times that of the P line, then one half of of the effect recorded is due to diffractiona

perturbation. The problem arises of how to account for the effect under consideration. It would seem right to introduce appropriate corrections for the perturbating line, accounting for its distance from the line measured, as well as for other factors. However, it would seem more correct to proceed along the following lines; Table 4 shows the effect of diffraction to be solely a quadratic diminishing function of the order of the spectrum. This effect is, thus, a far-reaching one. A number of neighbouring lines affect the line recorded, yielding a certain background. Hence the most correct approach consists in giving the effect of diffraction the treatment of a background. The background may be considered to be due largely to diffraction.

5. *Conclusions*

The foregoing cosiderations lead to the conclusions that, although the demand for high luminosity in photoelectric spectrometers is consistent, their construction should fulfill somewhat different conditions than those observed in the construction of spectrographs. Since the slit is to comprise the line with excess, it is possible partly to renounce conformily in favour of high liminosity. It may be of advantage to use high slits, high 45° prisms (instead of the 60° prisms commonly in use) having great focal lengths, and cylindrical lenses. With these conditions, higher luminosity and a greater radius of curvature will be obtained.

The author wishes to thank Professor Dr L. Jurkiewicz for his critical remarks and his valuable discussions.

REFERENCES

Bryon, F. R., Nahstoll, G. A., *JOSA*, **38**, 510 (1948).
Carlsson, C., *Spectrochem. Acta*, **6**, 211 (1954).
Crosswhile, H. M., Fastie, W. S., *JOSA*, **44**, 349 (1954).
Crosswhile, H. M., Fastie, W. S., *JOSA*, **46**, 110 (1956).
Fastie, W. S., *JOSA*, **42**, 641 (1952), **42**, 647 (1952); **43**, 1174 (1953).
Firestone, F. A., Randall, H. M., *Rev. sci. Instrum.*, **9**, 404 (1938).
Gates, A., *Jour. Phys.*, *20*, 275 (1952).
Rupert, C. S., *JOSA*, **42**, 779 (1952).
Hagenmah, N. D. *Z. angew. Phys.*, **6** 318 (1954).
Hanau, H., Wolfe, R. A., *JOSA*, **38**, 377 (1948).
Hulton, Müller, *Ark. Fys.*, **3**, 393 (1952).
Kayser, *Handbuch der Spektroskopie*, Leipzig (1900).
Minkowski, R., *Astrophys. J.*, **96**, 306 (1942).
Naish, J. M., *J. sci. Instrum.*, **28**, 138 (1951).
Naish, B., Ramsden, W., *Spectrochem., Acta*, **5**, 295 (1953).
Mostyn, R., Jury, R. V., *Spectrochem., Acta*, **5**, 257 (1953).
Ostrowski, K. W., *Acta phys. Polon.*, **18**, 231 (1959).
Polster, A., *JOSA 41*, 290 (1951).
Prokofiev, W. K., *Fotograficheskie metody kolichestviennovo spektralnovo analiza metallov i splavov*, Vols. I, II, (Moskva 1951).
Sawyer, R. L., *Experimental Spectroscopy*, N. Y. 1951 II. Ed.
Soda, M. S., *J. sci. industr. Res.*, **12 B**, 563 (1953).

MEASUREMENT OF THE SLOW NEUTRON SPECTRUM OF A NEUTRON BEAM FROM THE WWRS REACTOR BY MEANS OF A CRYSTAL NEUTRON SPECTROMETER

By D. A. O'Connor J. Sosnowski

Institute of Nuclear Research, Polish Academy of Sciences, Warsaw

(Received September 19, 1959)

The efficiency of a crystal neutron spectrometer was determined experimentally using a double crystal arrangement. On the basis of these results the slow neutron spectrum of a neutron beam was determined in the range of neutron wavelength 0.5 — 2.5 Å. The variation of crystal reflectivity with wavelength was compared with a theoretical expression for this dependence.

The inherently high energy resolution for thermal neutrons of the crystal spectrometer makes it a very convenient instrument for many types of neutron measurements, such as cross section measurements etc. Difficulties in determining the energy dependence of the efficiency of the crystal spectrometer hinder its application in precise neutron spectrum measurements and in this respect it is much less convenient than the mechanical chopper devices. Sturm [1] has used theoretically derived expressions for the efficiency in a study of a reactor spectrum. In the present work an attempt was made to measure the efficiency experimentally.

Theory

We consider first a single crystal spectrometer consisting of entrance collimator, monochromating crystal, exit collimator and neutron counter. If with the exit collimator and counter set at an the angle Θ with respect to primary beam, the crystal is rotated to give the maximum intensity of Bragg reflected neutrons, then the counting rate of the counter is given by (1):

$$P(\Theta) = An(\lambda)\ \varepsilon_\lambda \cos\Theta \int\int I_1(\lambda, \alpha).\ R(\lambda, \beta)\ I_2(\lambda, \alpha - 2\beta)\, d\alpha\, d\beta \qquad (1)$$

where $n(\lambda)d\lambda$ is the flux of neutrons entering the first collimator of wavelength $\lambda - -\lambda + d\lambda$; $I_1(\lambda, \alpha)$ is the efficiency of the first collimator i. e. the probability that a neutron of wavelength λ entering the collimator at an angle α in the plane of diffrac-

tion with respect to the collimator axis, will pass through the collimator; $I_2(\lambda, \alpha)$ is an analogous quantity for the second collimator; $R(\lambda, \beta)$ is the reflection coefficient of the crystal i. e. the probability that a neutron of wavelength λ will be Bragg reflected by a crystal mosaic blok lying at an angle β with respect to the effective centre of the mosaic block angular distribution; ε_λ is the efficiency of the neutron counter and A is a constant depending on the constant geometrical factors of the system. The limits of integration in equation (1) are determined by the geometry of the system.

In equation (1) only the first order of reflection is included, in general one should include higher orders and $P(\Theta)$ will be the sum of a number of similar expressions for λ, $\lambda/2$, $\lambda/3$ etc.

In the present case it was demonstrated experimentally (see later section on results) that $I_1(\lambda, \alpha)$ and $I_2(\lambda, \alpha)$ could be regarded as independent of λ and both could be represented by the same expression:

$$I(\alpha) = e^{-\frac{\alpha^2}{2\Phi^2}}$$

Substituting in equation (1) for $I_1(\alpha)$ and $I_2(2\beta-\alpha)$ and integrating with respect to α in the limits $-\infty$ to ∞ we obtain:

$$P(\Theta) = B.n(\lambda)\, \varepsilon_\lambda \cos\Theta \int R(\lambda, \beta)\, e^{-\frac{\beta^2}{\Phi^2}}\, d\beta \tag{2}$$

where B is new constant which includes a function of Φ. To determine $n(\lambda)$ it is now necessary to determine ε_λ and $R(\lambda, \beta)$ and to eliminate terms due higher order reflections. ε_λ can be calculated from the known contants of the counter.

If the form of the dependence of $R(\lambda, \beta)$ on β is known, or is known to be independent of λ, then the dependence of $R(\lambda, \beta)$ on λ can be determined experimentally using a double crystal spectrometer in the (1, −1) setting. Consider an arrangement consisting of entrance collimator, first crystal, second crystal, exit collimator and counter. Neglecting for the moment higher order reflections we can write for the counting rate in the (1, −1) position:

$$\begin{aligned} P_{\lambda\lambda}(\Theta) &= C.\, n(\lambda)\, \varepsilon_\lambda \cos\Theta \int I_1(\alpha)\, I_2(\alpha)\, d\alpha \int R^2(\lambda, \beta)\, d\beta \\ &= D.\, n(\lambda)\, \varepsilon_\lambda \cos\Theta \int R^2(\lambda, \beta)\, d\beta \end{aligned} \tag{3}$$

where it is assumed that the two crystals are identical. From equations (2) and (3) it is seen that if the form of the dependence of $R(\lambda, \beta)$ on β is known then the variation of $R(\lambda, \beta)$ with λ can be found from measurements of the ratio $P_{\lambda\lambda}(\Theta)/P(\Theta)$ as a function of λ. In particular if $R(\lambda, \beta)$ is given by

$$R(\lambda, \beta) = R'(\lambda)\, e^{-\frac{\beta^2}{2\eta^2}} \tag{4}$$

i. e. the reflection curve has a Gaussian shape, then:

$$\frac{P_{\lambda\lambda}(\Theta)}{P(\Theta)} = \text{constant} \cdot R'(\lambda) \tag{5}$$

In fact for an ideal mosaic crystal $R(\lambda, \beta)$ is given by [2]:

$$R(\lambda, \beta) = \frac{We^{-\frac{\beta^2}{2\eta^2}}}{1 + We^{-\frac{\beta^2}{2\eta^2}}} \tag{6}$$

where η is a measure of the mosaic spread of the crystal and W is a known function of λ. Using this expression for $R(\lambda, \beta)$ it is clear that the ratio $P_{\lambda\lambda}(\Theta)/P(\Theta)$ will not be a simple function of $R(\lambda, \beta)$. However the form of equations (2), (3) and (6) suggests that if for $R(\lambda, \beta)$ we substitute a simple Gaussian expression of the form given by equation (4), the resultant error should be relatively small. It should be noted that in equation (2) $R(\lambda, \beta)$ is multiplied by the Gaussian expression $\exp -\frac{\beta^2}{\Phi^2}$ and in equation (3) $R(\lambda, \beta)$ is raised to the second power which again should give a closer approximation to a Gaussian expression. The accuracy of this approximation will obviously depend on the parameters of the collimators and crystals used, but for the moment we shall continue to use expressions (4) and (5) and return to an estimation of the errors involved on the basis of the experimental results in a later section.

When higher orders of reflection are not negligible then the method outlined above must be modified. In practice over a considerable range of values of λ, from 0.2 Å to 1.5 Å, the second order reflection may be neglected. Between 1.5 Å and 2.5 Å the second order component considerably increases but the third and higher orders are negligible. Including the second order, equation (2) becomes

$$P(\Theta) = Bn(\lambda)\,\varepsilon_\lambda \cos\Theta \int R_1(\lambda, \beta)\, e^{-\frac{\beta^2}{\Phi^2}}\, d\beta + B.n\left(\frac{\lambda}{2}\right) \varepsilon_{\frac{\lambda}{2}} \cos\Theta \int R_2(\lambda, \beta)\, e^{-\frac{\beta^2}{\Phi^2}}\, d\beta$$
$$= P_1(\Theta) + P_2(\Theta) \tag{7}$$

where $R_1(\lambda, \beta)$ and $R_2(\lambda, \beta)$ are the reflecting powers for first and second order reflections for a first order wavelength setting of λ. The ratios $P_1(\Theta)/P(\Theta)$ and $P_2(\Theta)/P(\Theta)$ can be determined by measuring the transmission of calibrated $1/v$ filters (see reference 1) for the reflected beam.

Including the effect of second order contamination, the double crystal measurement gives:

$$P_{\lambda\lambda}(\Theta) = C \cdot n(\lambda)\,\varepsilon_\lambda \cos\Theta \int R_1^2(\lambda, \beta)\, d\beta + Cn\left(\frac{\lambda}{2}\right) \varepsilon_{\lambda/2} \cos\Theta \int R_2^2(\lambda, \beta)\, d\beta \tag{8}$$

In fact it was found that the term in $R_2^2(\lambda, \beta)$ was negligible compared with that in $R_1^2(\lambda, \beta)$. Using the value of $P_1(\Theta)$ obtained by the filter measurements we obtain from (7) and (8):

$$\frac{P_{\lambda\lambda}(\Theta)}{P_1(\Theta)} = \text{constant} \cdot R_1'(\lambda) \tag{9}$$

Apparatus and methods

Measurements were made on a double crystal neutron spectrometer which has already been described [3]. The collimators used were steell Soller slit type of nominal half — angle 10 min. Two copper single crystals were used, both having a polished surface cut parallel to the (111) plane according to methods which have been described [4]. The cut surfaces were of dimensions approximately 100 × 40 mm. Two neutron counters were used of identical construction, one filled with boron trifluoride of natural boron isotopic composition and the other filled with B^{10} — enriched boron trifluoride, the latter counter being used for measurements at $\lambda < 0.5$ Å. The calculated efficiency of these counters is given by

$$\varepsilon_\lambda = e^{-3.53\times10^{-1}\lambda}(1 - e^{-6.35\times10^{-1}\lambda}) \text{ natural boron}$$

$$\varepsilon_\lambda = e^{-1.88\times10^{-1}\lambda}(1 - e^{-3.38\lambda}) \text{ enriched boron.}$$

The source of neutrons was the No 4 horizontal hole of the WWRS reactor. The situation of the end of the hole with respect to the core is shown in Figure 1. Between the end of the hole and the nearest fuel elements an air — filled aluminium

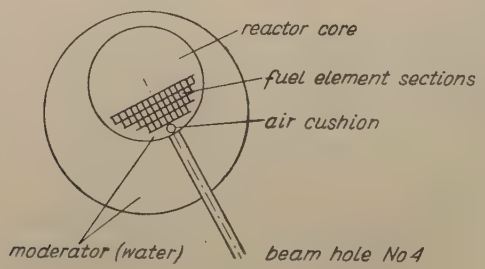

Fig. 1

can be inserted into the light water moderator, thus increasing the fast neutron flux available from the hole. This air cushion is of effective thickness about 75 mm, and when in position leaves a water layer of about 30 mm between the hole and the nearest fuel elements. Measurements were made with and without this air cushion, at a reactor power of 2 MW and with a moderator water temperature of 25 to 30°C. The stability of the reactor power was such that a monitor counter proved unnecessary, in fact the day to day reproducibility of results was better than 0.5 %.

The $1/v$ filters used were plates of a glass containing 11 % by weight of B_2O_3. Plates of four different thicknesses were available and they were calibrated using a singly reflected beam of 1 Å neutrons. The dependence of absorption cross section was not tested but assumed, which is justfied for $\lambda > 1$ Å and for the boron content used.

Results

In figure 2 there are given curves of $P(\Theta)$ as a function of wavelength for the range 0.1 to 2.5 Å for the two cases (a) with air cushion and (*b*) without air cushion. These curves have been corrected for a background counting rate which was taken to be that given when the crystal was rotated through 30 min from the Bragg position. The background was relatively constant except for very small Bragg angles and

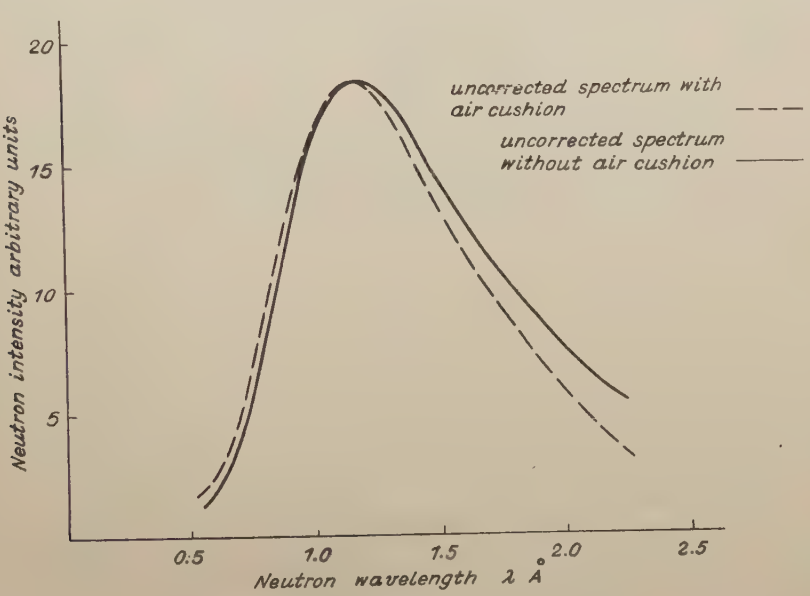

Fig. 2

amounted to about 1 % of the peak intensity at the maximum of the curve. The small narrow (about 10 min wide) valleys in the curves, produced by parasitic reflections in the crystal have been smoothed out. The statistical errors are everywhere very small but the reproducibility of the intensities is of the order of 0.5 %.

Single crystal rocking curves were taken for both crystals at wavelengths of 0.5, 1.0, 1.5, 2.0 and 2.5 Å. The curves obtained are all practically identical as will be seen from Figure 3 where points obtained at various wavelengths have been collected together on one curve by normalising at the maximum. The half — width of this curve is 10.8 ± 0.5 min. This was compared with the curve obteined by rotating the second collimator in the primary beam at very low reactor power, which gave a half-width of 18.0 ± 0.5 min.

Both these curves are well approximated by Gaussian functions and using the notation introduced earlier we obtain $\Phi = 5.6 \pm 0.15$ min and $\eta = 2.3 \pm 0.5$ min.

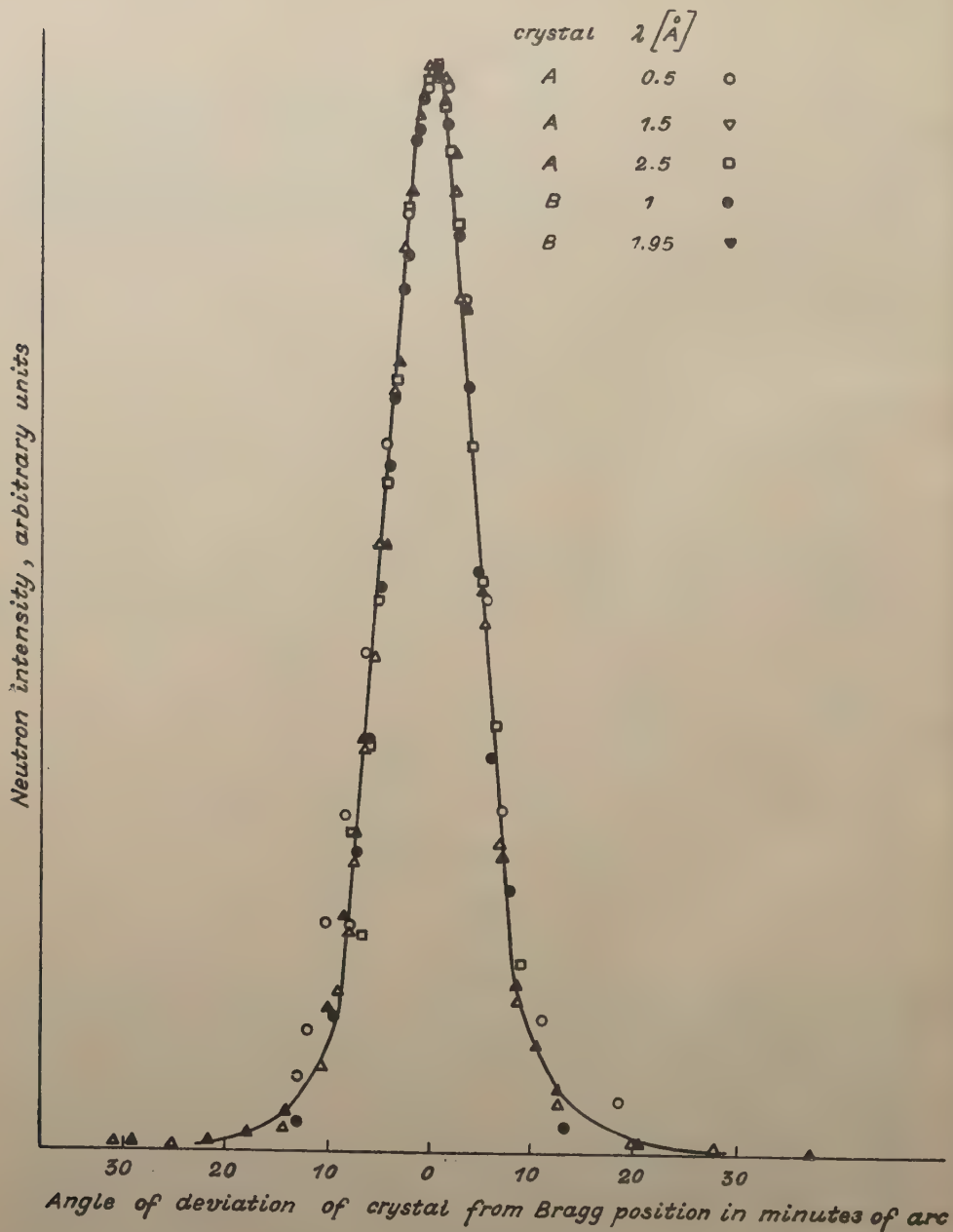

Fig. 3

The fact that the rocking curves are practically identical for all values of λ justifies our assumption that $I_1(\alpha)$ and $I_2(\alpha)$ are independent of λ. It would further appear that the shape of the $R(\lambda, \beta)$ function is also independent of λ, since there is no possibility

that changes in the width of the $R(\lambda, \beta)$ distribution with change in λ could be compensated by opposite changes in the width of the $I(\alpha)$ function, both in fact might be expected to increase with λ.

Measurements of the content of higher order reflections in the singly reflected beam were made with the boron filters mentioned above in the range 1.0 to 2.3 Å. Two filter thicknesses were used so that theoretically the percentange of first second and third order neutrons could be determined. In fact below 2.0 Å the third order was negligible. Above 2.0 Å the measurements were not accurate enough to give the third order with any certainty but the calculated first order intensity was the same within ± 2 % when the third order was assumed to be negligible and when it was included. The composition of the beam (with air cushion) as a function of λ is shown in Figure 4.

The reflectivity of the crystals as a function of λ was measured for several values of λ in the range 0.25 to 2.5 Å. For $\lambda < 1.0$ Å $R_1'(\lambda)$ equation (5) was used as a basis of calculation. Above 1 Å the results obtained from the filter measurements were combined with those from the double crystal measurements using equation (9).

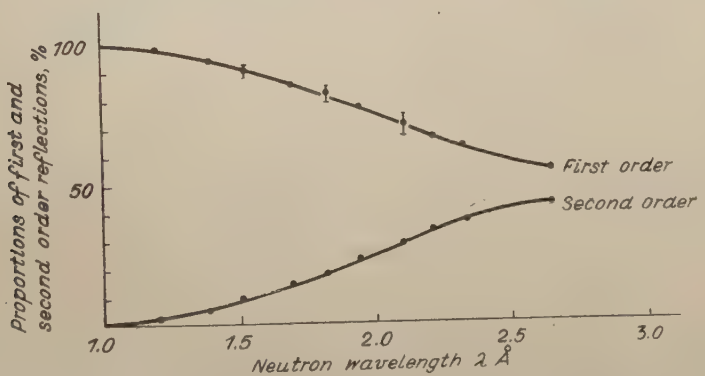

Fig. 4

After correcting for higher order reflections, and for the total spectrometer efficiency we obtain curves for $n(\lambda)$. These are shown in Figure 5 for the two cases with and without air cushion together with a Maxwell distribution for an equilibrium temperature of 350°K. The portion of the curve below 0.5 Å is omitted since for shorter wavelengths the accuracy of determination of the efficiency is progressively poorer. Both curves show a maximum at 1.04 ± 0.01 Å, which corresponds to a Maxwell spectrum of temperature 350 ± 7°K. This is about 50°K above the temperature of the moderator which is normally in the range 25 — 30°C. Introduction of the air cushion results in an increase in the intensity of faster neutrons and a decrease in intensity of the "colder" neutrons. Above 2.5 Å both curves fall below the Maxwell spectrum.

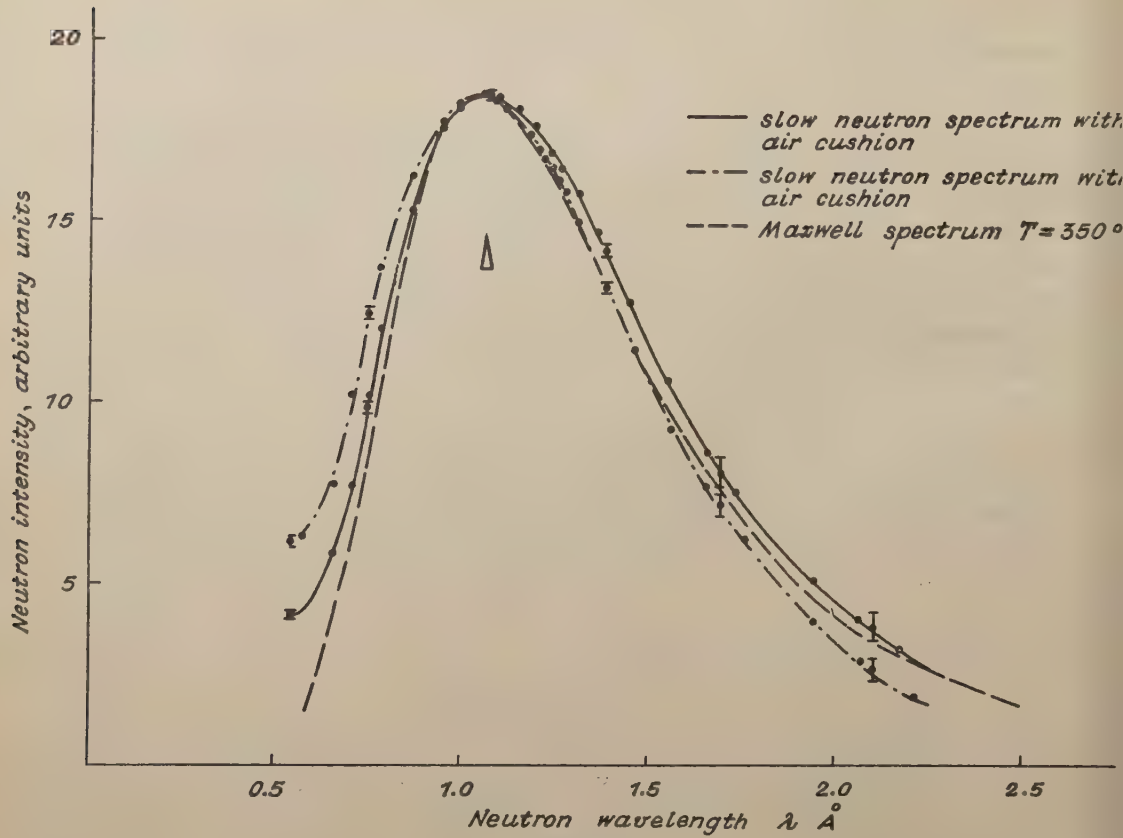

Fig. 5

Discussion of results

On the basis of the results it is now possible to make some estimate of the probable errors inherent in the method of measurement of the crystal reflectivity.

The fact that the shape of the rocking curve does not change with wavelength suggests that the widths of the collimator function and the crystal reflectivity curve are constant.

The absence of the increase with wavelength in collimator function width which should result from total reflection of neutrons by the collimator material, is probably due to the presence of a thin film of oil on the steel shims of the collimator.

The curve obtained for the crystal reflectivity (figure 6) shows that above about 0.5 Å secondary extinction in the crystal increases rapidly with increase in wavelength and the crystal reflectivity reaches a "saturation" level above I.0 Å wykreślić. This means that the shape of the $R(\lambda, \beta)$ curve must change significantly between 0.5 and 1.0 Å.

However calculations of the $R(\lambda, \beta)$ curve according to equation (6) and using the value $\eta = 2.3$ minutes, gave curves which, while departing from Gaussian shape

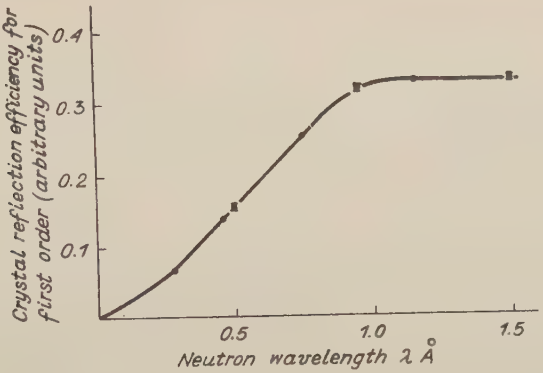

Fig. 6

considerably for $\lambda > 0.5$ Å had effective widths which corresponded to the experimental value within the limits of the rather lange, ± 0.5 minute, experimental error.

The most important possible source of error in estimating the crystal reflectivity is the assumption that $P_{\lambda\lambda}(\Theta)/P_1(\Theta)$ can be taken as a measure of the integrated reflectitivity of the crystal. The quantity actually measured is given by:

$$\frac{P_{\lambda\lambda}(\Theta)}{P(\Theta)} = \text{constant} \frac{\int R^2(\lambda, \beta)\, d\beta}{\int R(\lambda, \beta)\, e^{-\frac{\beta^2}{\Phi^2}}\, d\beta} \tag{10}$$

The quantity to be used as the effective crystal efficiency is from equation (2):

$$\int R(\lambda, \beta)\, e^{-\frac{\beta^2}{\Phi^2}}\, d\beta. \tag{11}$$

Using the theoretical expression for $R_1(\lambda, \beta)$ (6) with $\eta = 2.3$ minutes, the values of expression (10) and (11) were calculated by numerical integration and compared. The dependence of the integrated efficiency (11) on λ is given in figure 7. It was found that for this particular case the ratio of expressions (10) and (11) was constant to within 4 % in the range $0.5 < \lambda < 2.0$ Å. The simplifications inherent in the method would therefore appear to be justified. Comparison of the theoretical curve, figure 7, with that actually obtained, figure 6, shows that in fact the secondary extinction was considerably stronger than that to be expected theoretically.

It is possible that the value of η used in the calculations is higher than the true value. A relatively small decrease in η will considerably flatten the theoretical curve. The flatter the curve the smaller will be the error resulting from the approximations in the method of measurement of the crystal reflectivity, since for large secondary extinction the detail of the shape of the $R(\lambda, \beta)$ curve has a relatively small influence on the integrals involved. Other factors which may possibly explain the marked flattening observed are the primary extinction which may not be negligible in a crystal

of very small mosaic spread (the mosaic blocks might be expected to be of larger dimensions than in crystals of greater mosaic spread) and nuclear absorption, which increases with wavelength.

On the basis of this discussion it is possible to estimate the overall accuracy in the measurements of $n(\lambda)$. The possible systematic error due to the method will

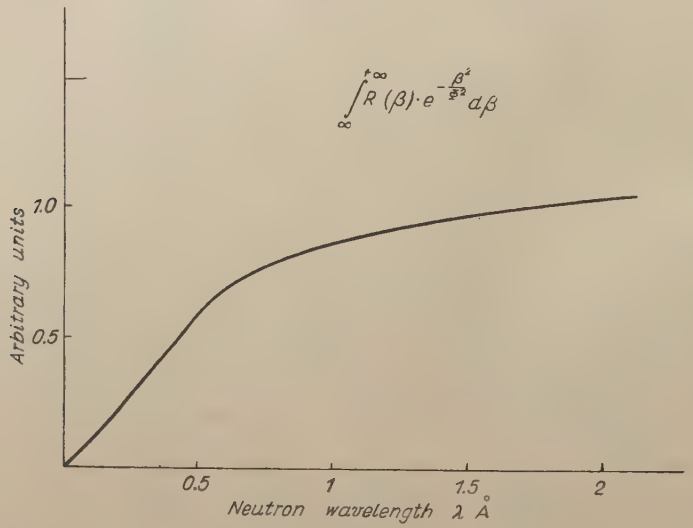

Fig. 7

be a maximum of ± 2 %. The overall error is calculated to be about ± 3 % between 0.5 Å and 1.0 Å and above 1.0 Å increases to about ± 9 % at 2.0 Å the increase being due to the possible errors in the estimation of the percentage of higher order reflections at the longer wavelengths.

Acknowledgements

The authors wish to thank Prof. Bronisław Buras for his encouragement and interest in this work, and Ryszard Kula and Stefan Szafran for their technical assistance in the measurements.

LITERATURE

[1] Sturm, W. G., *Phys. Rev.*, **71**, 757, (1947).
[2] Bacon, G. E., Lowde, R. D., *Acta cryst.*, **1**, 303 (1948).
[3] O'Connor, D. A., Bońkowski, L., *Report No 46, Institute of Nuclear Research*, Warsaw (1958).
[4] Modrzejewski, A., Buras, B., Czarnecki, R., *Archiwum Hutnictwa* IV, 81 (1959).

COLLISION RECOMBINATION IN Tl_2S

By J. W. Ostrowski

Institute of Physics, Polish Academy of Sciences, Warsaw

(Received November 17, 1959)

The relaxation of photoconductivity in semiconductor microcrystalline Tl_2S layers was investigated. The hypothesis of collision recombination of the free current carriers in the process of decay of the photoconductivity was put forward and verified. The phenomenological model of recombination: $r = \alpha np^2$ was proposed (r — number of acts of recombination per cm^3 and sec, α — coefficient of recombination, n, p — concentration of free electrons and holes, respectively). A recombination coefficient $\alpha = 10^{-30}$—10^{-31} cm^6 sec^{-1} and a relaxation time of $\tau = 0.5$—5 msec were measured. The equation of the recombination curve was derived. The temperature dependence of the relaxation time and electric conductivity was investigated. The parameters determining the conditions of recombination, namely: the concentration of the free current carriers, their mobility, the conductivity, the position of the Fermi level and that of the acceptor level, were evaluated.

1. *Introduction*

The hypothesis of collision recombination of the free current carriers in the process of decay of the photoconductivity in semiconductor microcrystalline Tl_2S layers was proposed and experimentally verified.

The collision recombination appears when any free current carrier in a single act process passes its entire recombination energy to another free carrier and recombines either with an opposite free carrier or with the center in the forbidden gap.

Considering the most simple case of an intrinsic semiconductor wherein the concentration of carriers able to recombine is n, the probability for recombination W, as for radiative and phonon recombination, is proportional to n, whereas in the collision mechanism, which is one involving three carriers, we have

$$W \sim n^2,$$

whence

$$\tau \sim n^{-2}.$$

As yet, papers on the mechanism of collision recombination are few in number. No theory of the mechanism is available, and experimental data are scarce. T. S.

Moss (1953) was the first to recognize the collision model of recombination in order to provide a partial interpretation of his results.

J. A. Hornbeck and J. R. Haynes (1954) in their paper on the recombination of minority carriers with capture centres in p-type silicon, mention i. a. having noticed inverse proportionality of the relaxation time and the square of the concentration of the majority carriers.

The first to deal exclusively with collision recombination were J. W. Ostrowski and L. Sosnowski (1954); the respective measurements were carried out on thallium sulphide microcrystalline layers.

L. Pincherle (1955) mentions a nonpublished notice of 1950 by Fan and Pincherle where the authors express the opinion that the life-time of the minority carriers may be inversely proportional to the square of the concentration of the majority carriers. Pincherle, basing on the Auger effect theory, evaluates the coefficient of recombination α at $10^{-29} > \alpha > 10^{-33}$ cm^6 sec^{-1}.

At the beginning of 1955 appeared a paper (N. Sclar, E. Burstein), dealing with collision recombination and the remaining two, possibilities, i. e. radiative and phonon mechanisms. The authors carried out their measurements at the temperature of liquid helium, at a low concentration of the carriers in the range 10^9—1.6×10^{11} cm^{-3}.

L. Bess (1957) computed the cross section for collision recombination and life-time of the carriers assuming participation of intermediate states situated in the energy gap.

The Proceedings of the Conference on Semiconductors held at Rochester in 1958 bring the summary by P. T. Landsberg and A. R. Beattie (1958) of an attempt at computing theoretically the relaxation time for collision recombination.

The foregoing review of the literature shows, firstly, that papers, both theoretical and experimental, dealing with collision recombination, are as yet few in number, and, secondly, that whatever data are available come from widely different semiconducting materials such as PbS, Si, Ge, and Tl_2S single crystals and polycrystalline layers at various temperatures.

2. Material Investigated

The material investigated consisted of microcrystalline, polycrystalline p-type Tl_2S layers of thickness ranging from 0.3—1.5 μ, evaporated in vacuum at about 450°C on to the cooled wall of the glass cell in which the sample was subsequently enclosed (A. Wolska 1953).

The Tl_2S layers were investigated with the electron microscope and electron diffraction method by Kur and Toruń. The microscope image revealed the existence of two crystalline phases. This was confirmed by the diffraction patterns. Moreover, the layers were found to be highly inhomogeneous as to crystal structure. Hence it was not possible to give an exact interpretation of the layer structure. The linear dimensions of the crystals ranged from 0.06 to 1 μ.

Thus, in the case under consideration, the symbol Tl_2S is more a technical abbreviation than that of a chemical compound.

The layers exhibit photosensitivity within 0.4—1.2 μ, maximum sensitivity occurring at 0.83 μ. The forbidden gap computed from the long-wave boundary of absorption, amounted to 1.1 eV.

In addition, the layers exhibit a photovoltaic effect of a sensitivity distribution resembling that of the photoconductivity.

The resultant dark resistivity, for various samples, amounted to 0.2—10 MΩ.

3. Phenomenological Considerations

3.0. Introduction

Table of Symbols

n_0, p_0 — concentration of free electrons and holes, respectively, in darkness (at thermodynamic equilibrium);

n, p — momentary concentration of free electrons and holes, respectively;

n_m, p_m — steady state concentration of free electrons and holes, respectively, in conditions of illumination;

n_i — free electrons concentrations in the presence of background illumination;

Δn — variation in free electron concentration resulting from superposition of a light impulse on the background illumination;

N_a — concentration of acceptors;

n_a — concentration of electron-invested acceptors;

N_d — concentration of donors;

N_p — density of states in valence band;

E_a — energy of acceptor level as referred to the top of valence band;

F — Fermi level as referred to the top of valence band;

r_0 — number of acts of recombination in the dark per cm^3 and sec;

r_i — number of acts of recombination due to illumination, per cm^3 and sec;

r — total number of acts direct collision recombination, per cm^3 and sec;

W — probability for collision recombination;

α — coefficient of the collision recombination;

g_0, g_i — number of free current carriers generated in dark and by light, respectively, per cm^3 and sec;

τ — relaxation time;

$\tau_{1/2}$ — time during which the photoconductivity decays to one half of its maximum value (half-relaxation time);

$\tau_{1/2\Delta}$ — time during which the additional photoconductivity resulting from superposition of a light impulse on the constant illumination decays to one half of its initial value;

σ_0, σ — dark and total conductivity, respectively;

σ_i — conductivity for background illumination;

$X = \frac{\sigma}{\sigma_0}$

$X_i = \frac{\sigma_i}{\sigma_0}$

d — thickness of layer;

μ — "effective" mobility of free current carriers;

J — intensity of light incident on 1 cm^2 of layer;

S — photosensitivity, defined as $S = d\sigma/\sigma dI$;

γ — number of photons absorbed within range of photosensitivity of layer, per energy unit of light;

M — light source intensity;

l — distance from light source to semiconductor layer;

Z — the part of radiative energy of the black-body (of temperature 2200°C) that is absorbed by the layer wirthin the range of photosensitivity;

Q — number of photons emitted per 1 sec by 1 cm^2 of the surface of the black-body at 2200°C;

H — energy radiated per 1 sec from 1 cm^2 of surface of the black-body at 2200°C;

T_w — temperature of light source;

η — coefficient accounting for light absorption and scattering along the path to the layer;

ϑ — time during which the photoconductivity decayed in the measurement of the maximum amplitude of photoeffect.

Let us now approach the mechanism of collision recombination, confining the problem to phenomenological considerations.

From the facts that: 1)dark conductivity was of the p-type, 2) absorption of 10^{18} photons per cm^3 and sec, the life-time of the carriers being about 10^{-3}sec, raised the conductivity to no more than the double of its value in darkness (every photon absorbed is assumed to give rise to an electron-hole pair), and 3) the intrinsic carrier concentration can amount to about 10^{10} cm^{-3}, the following model may be derived: In the dark, the concentration n_0 of free electrons is very low, whereas that of the holes, p_0, is comparatively high, thus:

$$n_0 \ll p_0 \tag{2}$$

Due to illumination, the concentration of the electrons and that of the holes increase by an equal amount, which considerably exceeds the value of the electron concentration in darkness:

$$p - p_0 = n - n_0 \cong n;$$

hence it may be assumed that, in the presence of illumination in the steady state,

$$p = n + p_0 \tag{3}$$

Various specialized models for collision recombination that seemed plausible with respect to the semiconductor investigated were discussed and tested by the experimental data available. Here, account was taken of the possibility of a process involving intermediate recombination centres in the forbidden gap. The ensuing considerations refer to the model which was found to yield the best agreement with the experimental results.

The case will be considered where the dominant process is one of the recombination of a free hole with a free electron, the recombination energy being transferred to another free hole in the neighbourhood. The probability for such a collision, per unit time and per electron, is proportional to the square of the hole concentration:

$$W = \alpha p^2 \tag{4}$$

The number of acts of recombination per unit time is thus

$$r = \alpha n p^2 \tag{5}$$

Assume that, in one act of recombination and one act of optical generation, one electron-hole pair vanishes and arises, respectively, with every photon absorbed generating one pair.

The equation of the kinetics of the process under consideration is

$$\frac{d(n+p)}{dt} = g_0 + g_i - r_0 - 2r_i \tag{6}$$

Here, the notion of "effective" mobility has been introduced on purely practical grounds; the meaning thereof will be discussed in detail in Section 3.5; here, let it suffice that the relation

$$\sigma = \mu \cdot e\,(n + p),$$

is assumed, justifying the presence of the sum $n + p$ in the derivative of eq. (6).

The number of photons absorbed per sec by 1 cm^3 of the layer is equal to that of the acts of generation; thus,

$$g_i = 2\gamma \frac{1}{d} J \tag{7}$$

in the dark, at thermodynamic equilibrium, we have

$$g_0 = r_0 \tag{8}$$

equilibrium of the process is assumed to be preserved in conditions of illuminations.

By eqs. (3), (5), (7) and (8), eq. (6) of the kinetics assumes the form

$$\frac{dn}{dt} = \frac{1}{d} \gamma J - \alpha n (n + p_0)^2 \tag{9}$$

The actual concentration of the electrons is equal to the product of the number of those arising per sec per cm^3 and of their life-time:

$$n = \frac{1}{2} g_i \tau; \tag{10}$$

by eq. (7), this yields

$$n = \gamma \frac{1}{d} J \cdot \tau \tag{11}$$

Assuming the "effective" mobility of the carriers μ not to depend on the illumination, the following relations are obtained for conductivity in the dark and in the presence of illumination, respectively:

$$\sigma_0 = e\mu p_0 \tag{12}$$

$$\sigma = e\mu (n + p) \tag{13}$$

The relaxation time τ, defined as the reciprocal of the probability for the collision recombination considered,

$$W = \frac{1}{\tau},$$

is given by

$$\frac{1}{\tau} = \alpha p^2 \tag{14}$$

The parameter

$$X = \frac{\sigma}{\sigma_0} \tag{15}$$

which is directly given by experiment, is a measure of how the semiconductor reacts to illumination; assuming constant (at a fixed temperature) mobility of the carriers and accounting for eqs. (11), (12) and (13), this may be rewritten as follows:

$$X = \frac{n_m + p_m}{p_0} = \frac{2n_m}{p_0} + 1 \tag{16}$$

The following quantities are directly or almost directly given by experiment, and hence are independent of the model adopted: σ_0, σ, d, X, γ, J, $\tau_{1/2}$, and S.

With the foregoing quantities, and assuming the model already proposed, the quantities p_0, n, μ, α, τ will be computed, as well as the following relations which can be verified experimentally:

$$\begin{aligned} \tau_{1/2} &= f_1 (p_0, X) \\ \sigma &= f_2 (J) \\ S &= f_3 (J, X) \end{aligned} \tag{17}$$

We now proceed to carry out the programme outlined above.

3.1. Relaxation Time

As we require an expression for the time of decay of the photoconductivity, eq. (9) should be integrated at $J = 0$. On separation of the variables, the latter is rewritten as follows:

$$\frac{dn}{n(n+p_0)^2} = \alpha\, dt$$

Integration, with the initial condition $n(0) = n_m$, yields

$$t = \frac{1}{\alpha p_0^2}\left[\ln\frac{(n+p_0)\,n_m}{n\,(n_m+p_0)} + p_0\left(\frac{1}{n_m+p_0} - \frac{1}{n+p_0}\right)\right] \tag{18}$$

From eq. (18), an expression for the half-time of decay of the photoconductivity $\tau_{1/2}$ is readily derived; substituting $n(\tau_{1/2}) = \frac{1}{2}\, n_m$, and accounting for eq. (16), we have

$$\tau_{1/2} = \frac{1}{\alpha p_0^2}\left[\ln\frac{X+3}{X+1} - 2\,\frac{X-1}{(X+1)\,(X+3)}\right] \tag{19}$$

Eq. (19) admits of experimental verification within proportionality.

It is noteworthy that, as the light intensity increases, i. e. for greater values of X, the time $\tau_{1/2}$ decreases.

From eq. (14), by eq. (16), the relaxation time τ is obtained as follows:

$$\tau = \frac{4}{\alpha p_0^2\,(X+1)^2} \tag{20}$$

Eqs. (19) and (20) yield a relation between the relaxation time τ and the half-time of decay of the photoconductivity $\tau_{1/2}$ measured experimentally:

$$\tau = \tau_{1/2}\,\frac{4}{(X-1)^2 \ln\dfrac{X+3}{X+1} - 2\,\dfrac{X^2-1}{X+3}} \tag{21}$$

In experimental conditions, the ratio $\tau : \tau_{1/2}$ differs but insignificantly from unity.

From eqs. (20) and (21), both the relaxation time τ and the half-time $\tau_{1/2}$ are seen to be inversely proportional to the square of the carrier concentration in the dark, in accordance with the theoretical considerations due to Landsberg and Beattie (1959)

When the semiconductor is subjected to constant, intense illumination — back ground illumination — and light impulses are superposed on this background, the relaxation time for reverting from the state arising from the additional light impulse to the steady state for background illumination will be a function of the intensity of the constant background illumination. By analogy to the derivation of eq. (19), the relaxation time $\tau_{1/2\Delta}$ is now readily obtained. With

$$n(\tau_{1/2}) = n_i + \tfrac{1}{2}\,\Delta n \tag{22}$$

and

$$n_m = n + \Delta n$$

and assuming intense background illumination and a weak light impulse:

$$n_i \gg p_0; \quad p_0 \gg \Delta n,$$

we have

$$\tau_{1/2\Delta} = \frac{1}{\alpha p_0^2}\left[\ln\left(1+\frac{X-X_i}{X_i^2-1}\right) - \frac{X-X_i}{(X_i+1)^2}\right] \tag{23}$$

The half time of decay of the excess conductivity decreases as the background illumination increases, in analogy to the time $\tau_{1/2}$.

In the presence of very intense background illumination and weak light impulses i. e. in conditions when the conductivity in the dark is much smaller than that in the presence of illumination (a situation that can be obtained in very sensitive layers only) and when the relaxation time τ is proportional to the half-time of decay $\tau_{1/2\Delta}$ (the decay of the conductivity due to the light impulse is here considered to be exponential), a simple, approximate relation $\tau(\sigma_i)$ can be derived. Namely, by eq. (14), with eqs. (3), (12) and (13) (with σ_i instead of σ in the latter one), we have

$$\tau \sim (\sigma_i + \sigma_0)^{-2},$$

whence, with respect to $\sigma_0 \ll \sigma_i$,

$$\tau \sim \sigma_i^{-2} \tag{24}$$

In the paper by Sosnowski and Ostrowski (5), eq. (24) was derived on the ground of simplified assumptions; it has been also obtained experimentally (Fig. 7).

3.2. Conductivity

An expression for the second relation of eq. (17) will now be derived.

We now consider the steady state case, i. e. $dn/dt = 0$.

Eq. (9) yields $J = \alpha(d/\gamma)\, n(n+p_0)^2$, whence, by eqs. (11), (12) and (16), we have

$$J = \frac{\alpha d\, p_0^3}{8\gamma\, \sigma_0^3}\left(\sigma^3 + \sigma^2\,\sigma_0 - \sigma\sigma_0^2 - \sigma_0^3\right) \tag{25}$$

Similarly to the expressions for $\tau_{1/2}$ and $\tau_{1/2\Delta}$, the function $\sigma = f_2(J)$ can be verified to proportionality.

For very great light intensities, when it may be assumed that $\sigma_0 \ll \sigma$, eq (25) reduces to the simple relation

$$J \sim \sigma^3 \tag{26}$$

which is correct for other models of collicion recombination, too.

This constitutes an easy, experimental criterium for collision recombination. There are no grounds for considering this criterium to be reciprocally univocal: the present considerations are phonomenological and do not account for all the possi-

ble mechanisms of collision recombination. However, the fulfillment of the condition of eq. (26) points to the possibility of collision recombination, and, inversely, if collision recombination occurs, eq. (26) should be fulfilled.

3.3. Sensitivity

In the present Section, an expression for the sensitivity

$$S = \frac{1}{\sigma}\frac{d\sigma}{dJ}$$

will be derived.

Differentiation of eq. (25), on simple transformations and substitution of $X = \sigma/\sigma_0$, yields

$$S = \frac{8\gamma}{\alpha d\, p_0^3} \cdot \frac{1}{X(X+1)(3X-1)}, \tag{27}$$

which contains measurable quantities nad a constant factor, and, thus, can serve as a criterium of the model adopted.

The sensitivity will now be expressed as a function of the light intensity. Eqs. (27) and (25) yield

$$S = \frac{X^2-1}{X(3X-1)} \cdot \frac{1}{J} \tag{28}$$

For $1 < X < 2$, the first factor in eq. (28) (which depends on X solely) increases rather rapidly, whereas for $X \geqslant 2$ it varies very slowly, the more so as X increases; hence, for high values of X (in the presence of intense illumination), we have

$$S \sim \frac{1}{J}, \tag{29}$$

and, by eq. (26),

$$S \sim \sigma^{-3} \tag{30}$$

Eqs. (19), (23), (25) and (30) provide the answer, on an experimental basis, as to whether the model adopted accounts adequately for the prosesses occurring in the Tl_2S layers

3.4. Relations between the Principal Quantities

It is now possible to give some relations between the measurable quantities and the quantities p_0, α and μ. The formulas of Sections 3.0 — 3.3 yield, on elementary transformations:

$$p_0 = \frac{2\gamma \frac{1}{d} J\tau}{X-1} \tag{31}$$

and

$$\alpha = \frac{d^2(X-1)^2}{(\gamma J)^2(X+1)^2} \cdot \frac{1}{\tau^3} \tag{32}$$

$$\mu = \frac{\sigma_0 d(X-1)}{2e\gamma J\tau} \tag{33}$$

3.5. *Mobility*

It has been hitherto assumed that the mobility of the free carriers does not depend on the light intensity, and that it fulfills eq. (13). In polycrystalline layers exhibiting also photovoltaic properties, the "effective" mobility of current carriers can be considered in a double sense: on the one hand, this is the resultant of the volume and surface mobilities for intercrystalline transitions, and — on the other — the average mobility of the holes and electrons. If volume mobility prevails, we have

$$\mu \sim T^{-\varkappa}, \qquad \text{where } \tfrac{1}{2} \leqslant \varkappa \leqslant 3,$$

i. e. a decrease of the mobility as the temperature rises, whereas if barrier mobility predominates, the latter increases exponentially with the temperature. It should be mentioned here that measurements point to the latter case.

The problem of how the mobility behaves as illumination varies, remains open; on the one hand, the mobility should be expected to vary with the illumination, since the intercrystalline barries generally decrease in the presence of illumination; on the other hand, the fact that it is the concentrational and not the barrier mechanism of photoconductivity that predominates in Tl_2S is an indication that the barriers play but a secondary role and, hence, that the mobility is independent of the illumination. Eqs. (19) and (23) — (30) were derived on the assumption of constant "effective" mobility; hence, if the shapes of the functions $\tau_{1/2}(X)$, $\sigma(X)$, $S(X)$ and $\tau_{1/2}(X_i)$ are found to be in agreement with the experimental results, the assumption that the mobility does not vary perceptibly in the presence of illumination should also be considered to be correct.

3.6. *Temperature Dependence*

It is interesting to know the temperature dependence of the time τ and the coefficient α. From the present phenomenological considerations, no conclusions can be derived as to the temperature dependence appearing explicitely. The only conclusion from eq. (20) is that the temperature dependence of $\tau_{1/2}$ is of an implicite nature, involving the dependence of the carrier concentration in the dark, p_0, and the parameter X.

Eqs. (19) and (23) can be rewritten as follows:

$$\tau_{1/2} = \frac{1}{\alpha p_0^2} f_1(X), \qquad \tau_{1/2d} = \frac{1}{\alpha p_0^2} f_2(X_i)$$

If the temperature varies, the remaining experimental parameters being kept constant, a decrease in the temperature will lead to a rise in X (or X_i, too) and, hence, to a decrease in the values of the functions $f_1(X)$ and $f_2(X_i)$; on the other hand, the hole concentration p_0 will decrease, leading to a rise in the factor $1/p_0^2$ (the variation in α is negligible). Experimental results point to the same order of magnitude for the relative variations of the increasing and decreasing factors. Hence it is possible to obtain experimental conditions such that if the temperatures are varied within a finite, though may be not very wide range, constant values of the time $\tau_{1/2}$ and $\tau_{1/2\,d}$ are measured. Before a discussion of the results is presented it should be noted that such conditions have been obtained in practice.

4. *Measurements*

4.1. *Feeding System*

The light source consisted of a 100 W bulb. The light intensity was controlled by varying the distance of the source from the semiconducting layer.

As far as possible, the pulse method was adopted, so that full use could be made of electronic devices.

Rectangular light pulses were obtained by screening off the light with an appropriate mechanical modulator.

The layer was fed from a DC voltage source consisting of an anode battery; the fall in voltage across the layer range from 1 V to 200 V.

The variable fall in voltage across the oscilloscope input load due to the variation in conductivity of the layer illuminated by the flashes from the modulator was, on amplification, applied to vertically deflecting oscilloscope plates and brought to observation on the screen. In order to preserve the form of the conductivity variation, DC current amplifiers were used. The constant component of the fall in voltage due to conductivity in the dark was eliminated by appropriate compensation.

4.2. *The Parameter X*

The parameter $X = \sigma/\sigma_0$ or $X_i = \sigma_i/\sigma_0$ was measured either with a galvanometer connected in series with the layer, by measuring the current through the latter, or with an oscilloscope, by measuring the layer resistivity at which compensation occured, as observable on the oscilloscope screen by the "zero" position of the image.

With respect to the necessity of eliminating long-lifetime processes of the order of seconds, the oscilloscope provided the advantage over the galvanometer of reducing the time of measurement to tenths of a second.

4.3. Half-Times of Decay

The time τ was measured as follows: first, the maximum amplitude of the signal on the oscilloscope was measured, the modulator being rotated sufficiently slowly for the duration of flasch and darkness to provide for the full development and decay of the conductivity variation. Then the duration of darkness was shortened so that the conductivity should have time to fall to one half its full amplitude, which could be checked by the decrease in amplitude of the image on the screen; the duration of the flash, however, had to be kept at a sufficiently high value for the conductivity to have time to develop fully, which was obtained by an appropriate shape of the modulator.

The rotation frequency of the modulator was measured by appropriate synchronisation with the frequency of a pulse generator. Synchronisation was controled on the screen of an auxiliary oscilloscope.

Observation of the decay of photoconductivity with the galvanometer already reveals a process consisting in a rather slow decrease of the conductivity lasting up to a minute and sometimes amounting to about 10 % of the total photoconductivity. This effect was considered to be one of a nature different from that of the recombination investigated. The long-lifetime process is eliminated by applying periods of darkness of sufficiently short duration ϑ at the moment of measuring the maximum amplitude of the photoeffect. The values of ϑ ranged from 20 to 90 msec. At longer times ϑ, the result obtained ceased to be reproducible; probably perturbation by slow processes intervened.

4.4. Conductivity

The conductivity in light and darkness was measured by measuring either the current through the layer, or its resistivity. The current was measured with a galvanometer connected in series with the layer. The latter's resistivity was measured either by the bridge method, or by finding the appropriate resistivity in a compensating circuit at "zero" position of the image on the oscilloscope screen.

4.5. Sensitivity

The sensitivity was determined either by graphical differentiation of the conductivity curve

$$\sigma = f(J),$$

or by measuring the rise in current resulting from superposition of a constant, additional light pulse on the illumination of intensity J, to which purpose a galvanometer connected in series with the layer was used, or else by measuring the height of the image on the oscilloscope screen in its dependence on the light intensity.

4.6. The Number of Light Generated Carriers

Computation of the concentration of the carriers of one sign set free by light per sec, i. e. of the right hand side of the expression

$$\frac{1}{2} g_i = \frac{\gamma}{d} J, \tag{34}$$

amounted to finding all three quantities one by one, with the rather evident assumption that one photon absorbed generates a single free electron (and a single hole).

The intensity (in W) of the white light incident on 1 cm^2 of the layer, accounting for absorption and scattering, is computed from the expression

$$J = \frac{M}{4\pi l^2} \cdot \eta \tag{35}$$

($\eta = 0.8$).

The number of photons absorbed is computed from the expression

$$\gamma = \frac{ZQ}{H} \tag{36}$$

for $T_w = 2200°C$ and the photosensitivity range of 0.4—1.1 μ.

The values of Z, Q and H are to be found in the appropriate Tables.

The mean thickness d of the layer could be determined to a gross approximation only. All direct measurements (as e. g. by optical methods) pointed to considerable inhomogenity of the thicknes; this resulted also from pictures obtained with the electron microscope. Evaluation of the thickness from measurements of the area and mass of the layer yielded results that agreed within about 50 %. The thickness of the layers ranged from 0.3 to 1 μ.

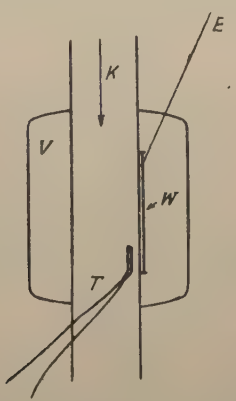

Fig. 1. Schematic arrangement showing a glass cell for temperature dependence measurements. K — tube for flow of liquid (alcohol), V — vacuum chamber for deposition of layer w by evaporation, T — thermocouple suspended in tube near layer, E — electrodes.

4.7. Obtainment and Measurement of Temperature of the Layer

In order to obtain various temperatures within the layer and to measure them, glass cells of a special shape for enclosing the layer were constructed (Fig. 1). The temperature of the layer varied as that of the alcohol circulating in continuous flow along the glass wall (support). The thermocouple measured the temperature of the alcohol flowing through the tube.

The temperature of the layer ranged from $+40°$ to $-60°$C.

4.8. Discussion of Experimental Error

The highest amount of error was inherent in the measurement of the layer thickness. However, because of the inhomogeneous composition of the layer and, especially, its polycrystalline structure, no degree of accuracy in determining the thickness could essentially reduce the intrinsic impossibility of strictly determining the "geometry" for physical processes.

If the layer thickness is not known with accuracy, none of the quantities referred to unit volume are known exactly. However, their exact knowledge is not of foremost importance for the present investigation; what is really important is that their dependence on the light intensity and the temperature be known as exactly as possible, and this, in fact, was measured with a much higher degree of accuracy.

The principal source of error in all the measurements resided in certain slow processes, of which little is known as yet, consisting in a slow rise in the conductivity in the presence of illumination and a decrease thereof when the layer is placed in the dark.

The general character of the fundamental relationships remained the same, notwithstanding the presence of individual quantitative differences which, as we have seen, was not of essential significance.

5. Results and Discussion

5.1. Conductivity as a Function of the Illumination

The measurements of the conductivity in its dependence on the intensity of illumination were carried out at various temperatures. These measurements, which presented no complications, yielded the first experimental corroboration of the mechanism of collision recombination

Since it was the variation of the expression

$$f(\sigma) = \sigma^3 + \sigma^2\sigma_0 - \sigma\sigma_0^2 - \sigma_0^3$$

that was essential [cf. eq. (25)], this was plotted in arbitrary units on the axis of ordinates in Fig. 2, whereas the light intensity was plotted on that of the abscissae, also in arbitrary units. If the recombination model adopted is correct, straight lines through

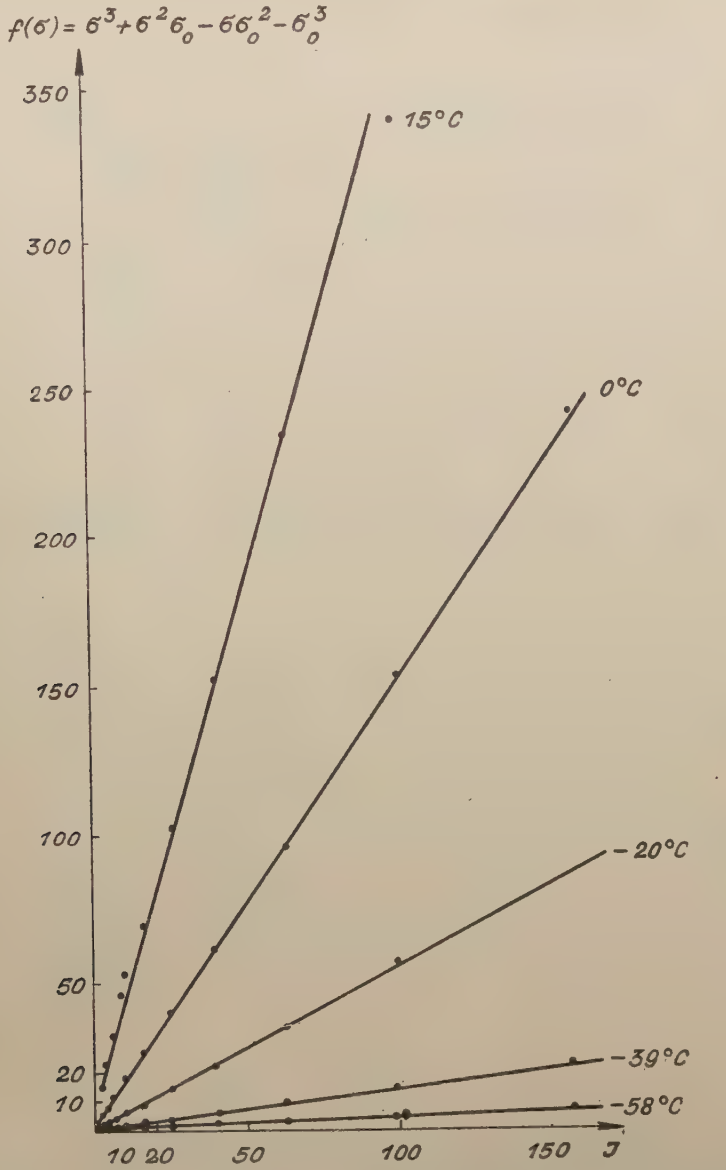

Fig. 2. Comparison of $f(\sigma) \sim I$ calculated from eq. 25 (solid lines) with the experimental data (dots). Arbitrary units.

the origin of the coordinates should result. It is seen from Fig. 2 that the experimental dots coincide satisfactorily with straight lines.

In the presence of very intense illumination $i_0 \ll i$, thus yielding conditions for which eq. (26) is correct. The results of the respective measurements are shown

in Fig. 3. The curve is clearly seen to tend towards a straight line of slope 1/3, in agreement with eq. (26).

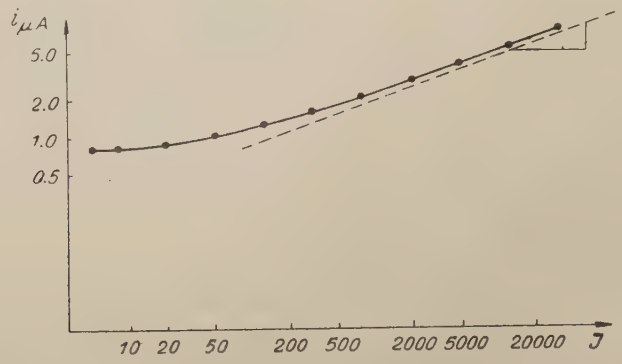

Fig. 3. Comparison of $\sigma \sim I^3$ at strong illumination, assuming $i \sim \sigma_1$ (dashed line) with the experimental data (solid line). Electrical current i in μA, I light intensity in arbitrary units.

5.2. The Half-Time of Decay as a Function of the Illumination

Figs. 4 and 5 bring the measurements of the half-time of decay of the photoconductivity as a function of the parameter X. The continuous line therein represents the $\tau_{1/2}(X)$ dependence in agreement with eq. (19), representing a factor depending explicitely on X; the dots represent direct measurements of $\tau_{1/2}$. The theoretical curve is determined as to its form only; its position was adjusted to suit that of the experimental dots. The agreement is seen to be satisfactory.

The dependence of the time $\tau_{1/2\Delta}$ on the parameter X_i was also confirmed by experimental results. The continuous line in Fig. 6 represents the results obtained in measuring $\tau_{1/2\Delta}$ as a function of X_i (the experimental dots are not shown; X_i and $\tau_{1/2\Delta}$ were measured to a rather high degree of accuracy), whereas the dots represents the values of the function

$$\ln\left[1+\frac{X-X_i}{X_i^2-1}\right]-\frac{X-X_i}{(X_i+1)^2}$$

[cf. eq. (23)]; the difference $X-X_i$ was determined to a lesser degree of exactitude, the respective values being small as compared to those of X and X_i. In this case, too, agreement may be said to be rather satisfactory, within the limits of experimental error.

Measurements of $\tau_{1/2\Delta}$ as a function of the conductivity σ_i in the presence of very intense, variable background illumination are found to be in rather good agreement with eq. (24). The experimental results are shown in Fig. 7; the experimental dots lie satisfactorily on a straight line of slope -2. It should be noted that eq. (24) is an approximation.

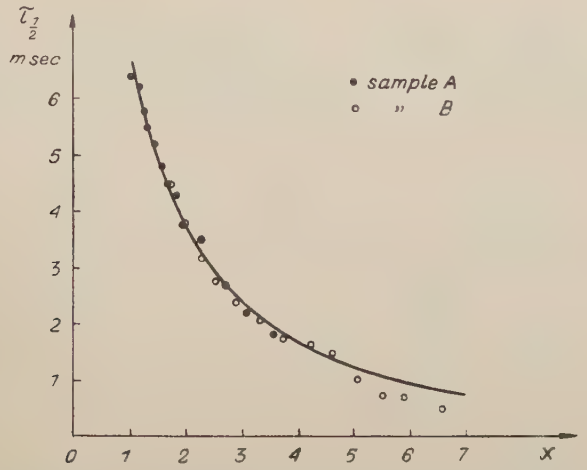

Figs. 4 and 5. Comparison of $\tau_{1/2}$ (X) from eq. 19 (solid line) with the experimental data (dots), the calculated curve being placed on the experimental dots to show the agreement of shape.

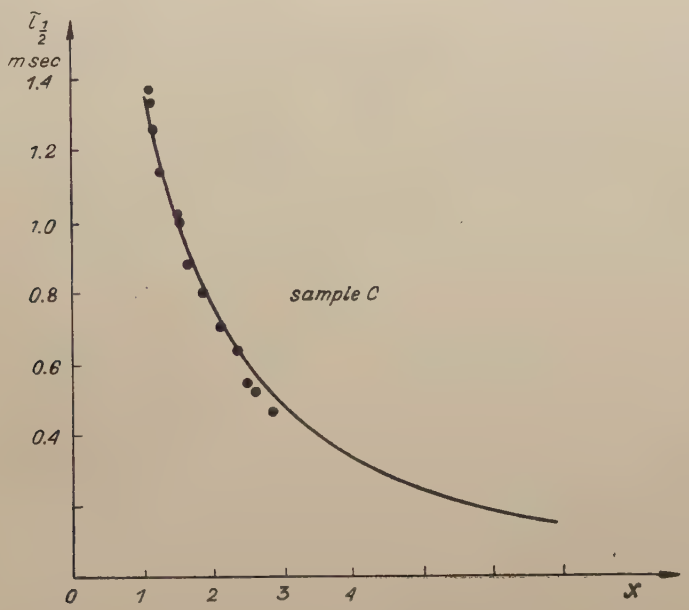

Fig. 5

5.3. *Sensitivity*

The sensitivity as a function of the illumination is represented in Fig. 8, the ordinates representing the experimental values of S, whereas the function

$$\frac{1}{X(X+1)(3X-1)},$$

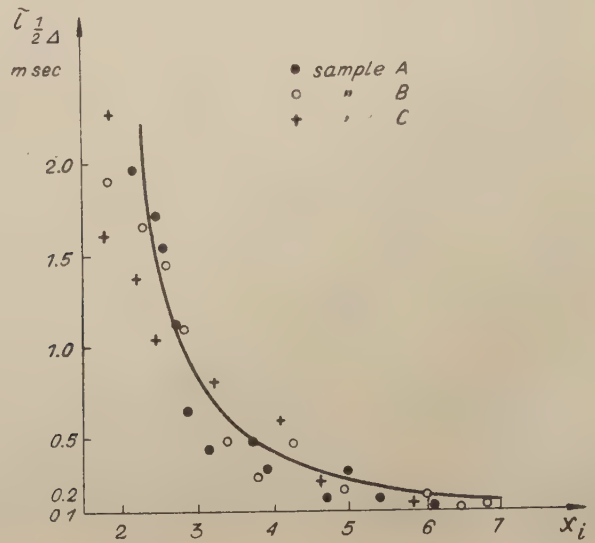

Fig. 6. Comparison of $\tau_{\frac{1}{2}\Delta}(X)$ from eq. 23 with the experimental data (solid line). The dots and crosses represent the values of the function in eq. 23, the difference $X-X_i$ being determined with a great error.

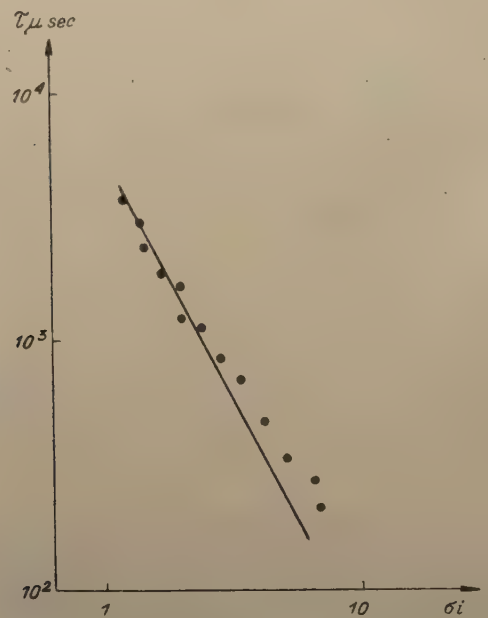

Fig. 7. Comparison of τ (in μ sec) dependence on σ_i (in arbitrary units) at strong illumination (solid line) calculated from eq. 24 with the experimental data (dots) in log-log scale.

in agreement with eq. (27), has been plotted on the axis of abscissae. If the model adopted is correct, straight lines through the origin should result. Here, too, the experimental dots are seen to coincide satisfactorily with the respective straight lines. Line 1 in Fig. 8 was obtained at a lower temperature than line 2 and, hence,

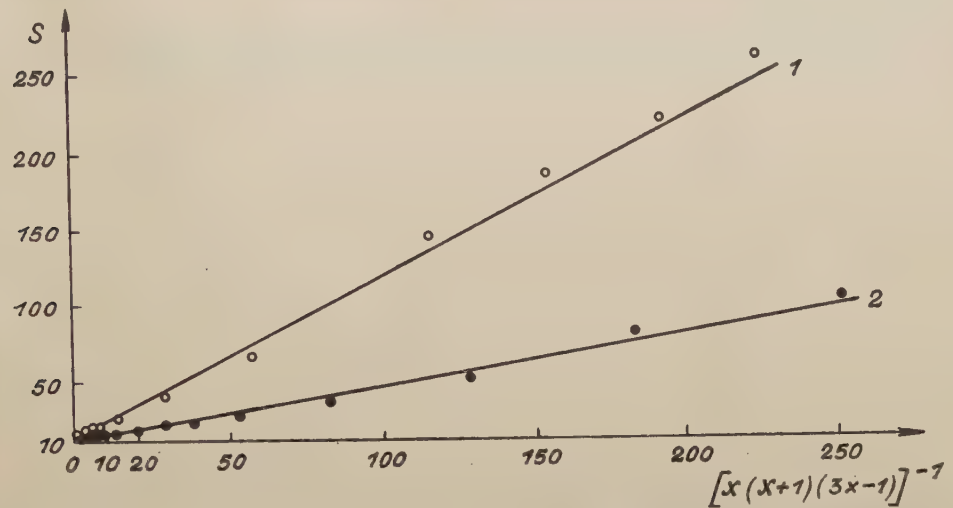

Fig. 8. Comparison of S sensitivity (in arbitrary units) *vs.* $[X(X+1)(3X-1)]^{-1}$ calculated from eq. 27 (solid lines) with the experimental values for two temperatures (dots).

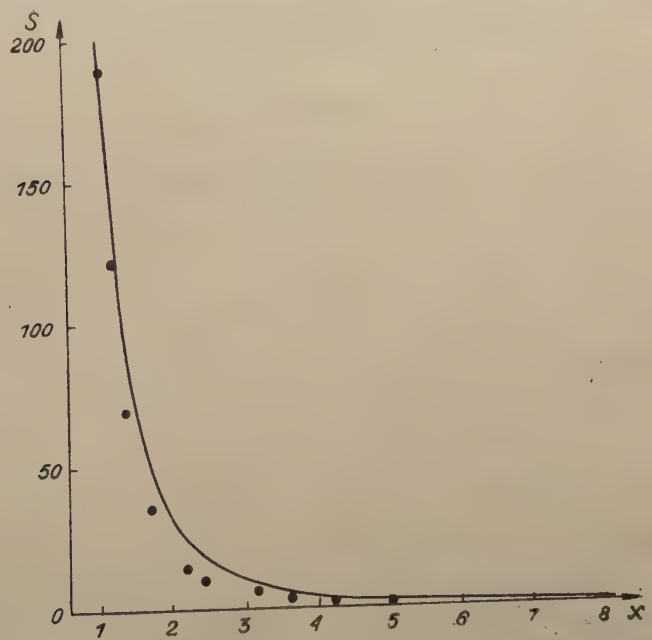

Fig. 9. Comparison of S sensitivity (in arbitrary units) *vs.* X parameter calculated from eq.27 (solid line) with the experimental data (dots).

its inclination with respect to the axis of abscissae is greater, in agreement with eq (27), as the factor $1/p^2$ now assumes a larger value. Fig. 9 represents the variation of the sensitivity as a function of the parameter X; the continuous line corresponds to eq. (27) with the assumption that the factor $8\gamma/\alpha p^2 d$ is constant; the dots represent experimental results.

For very intense illumination, eq. (28) assumes the form of eq. (29). Fig. 10 shows the dependence of the sensitivity on the intensity of illumination.

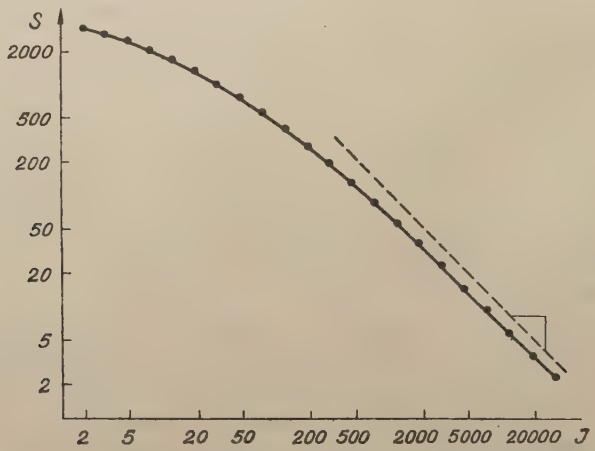

Fig. 10. Comparison of $S \sim I^{-1}$ at strong illumination from eq.29 (dashed line) with the experimental data (solid line) in log-log scale.

5.4. *Shape of the Relaxation Curve*

The foregoing experimental results yield the shape of the relaxation curve for photoconductivity:

$$\sigma = \sigma_0 f(t).$$

From eq. (19), on substituting $X = \frac{\sigma_{max}}{\sigma_0} = \frac{n_m + p_0}{p_0}$ and $y = \frac{2n + p_0}{p_0}$ and assuming e. g. $X = 4$, we have

$$t = \ln 0.6 \frac{y+1}{y-1} - 2\left[\frac{1}{y+1} - \frac{1}{5}\right]. \tag{37}$$

In order to compare the relaxation curve of eq. (37) with the one for exponential decay, an exponential was normalized so as to have two points, namely, the origin and the half-time of decay, in common with the curve of eq. (37). The curve is traced in Fig. 11. Decay of the photoconductivity is seen to set in at a somewhat higher rate than would correspond to the exponential,whereas subsequently it is a much slower process.

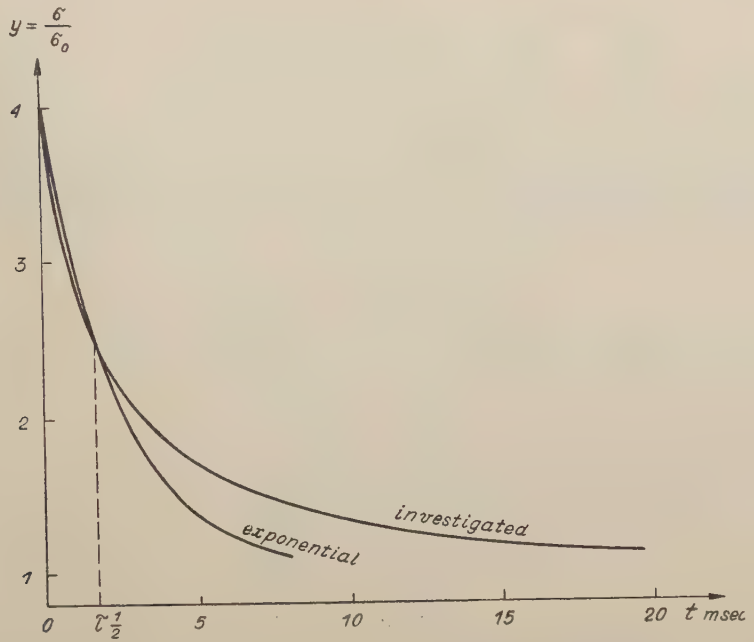

Fig. 11. Comparison of the investigated relaxation curve with the exponential curve. The former first falls quicker and then slower than the latter one.

5.5. *Numerical Values of Principal Quantities*

$$T_w = 2200°\text{C}$$
$$J = 6.4\times10^{-4}\ \text{cm}^{-2}\ \text{W}$$
$$Z = 1.4\times10^{-2}$$
$$Q = 2.26\times10^{21}\ \text{cm}^{-2}\ \text{sec}^{-1}$$
$$H = 2.12\times10^{2}\ \text{cm}^{-2}\ \text{W}$$
$$\gamma = 1.5\times10^{17}\ \text{joule}^{-1}$$
$$d = 0.5\times10^{-4}\ \text{cm}.$$

With the foregoing numerical values and by eqs. (36), (37) and (38), the number of carriers generated by light per sec and cm^3 of the layer can now be computed at

$$\tfrac{1}{2}\, g_i \cong 2\times10^{18}.$$

The fundamental eq. (10) yields an electron concentration of

$$n_m = 4\times10^{15}\ \text{cm}^{-3}$$

for a relaxation time of 2 msec.

Eq. (31) now yields the darkness concentration p_0 by substitution of the appropriate value of X, at

$$p_0 = 1.6\times10^{16}\ \text{cm}^{-3}.$$

Eq. (32), by substitution of the values obtained, yields numerically the coefficient α at room temperature,

$$\alpha = 1.4 \times 10^{-30} \text{ cm}^6 \text{ sec}^{-1}.$$

By direct measurement of the current flowing through the layer and the latter's dimensions, the value of the conductivity in the dark at room temperature is obtained:

$$\sigma_0 = 5 \times 10^{-5} \text{ Amp Volt}^{-1} \text{ cm}^{-1}.$$

Eq. (33) yields the value of the current carriers mobility, i. e. the mean "effective" mobility of holes and electrons:

$$\mu = 2 \times 10^{-2} \text{ cm}^2 \text{ Volt}^{-1} \text{ sec}^{-1}.$$

The sensitivity varied widely according to the illumination and temperature. At room temperature, in the dark, with light impulse from a 100 W bulb placed at a distance of 100 cm, the sensitivity amounted to

$$S = 600 \text{ cm}^2 \text{ W}^{-1},$$

the active surface being 1.2 cm^2.

The results obtained with various samples of different photosensitivity, thickness and resistivity in the dark exhibited some amount of dispersion; however, considering the diversity of the material used, the latter was, in fact, surprisingly small.

In Table 1, the approximate values of the various quantities at room temperature are assembled.

Table 1

n_m	$10^{15}-10^{16}$	cm^{-3}
p_0	$10^{16}-10^{17}$	cm^{-3}
α	$10^{-30}-10^{-32}$	$\text{cm}^6 \text{ sec}^{-1}$
μ	$5 \times 10^{-2}-5 \times 10^{-3}$	$\text{cm}^2 \text{ Volt}^{-1} \text{ sec}^{-1}$
σ_0	$10^{-4}-10^{-5}$	$\text{Amp Volt}^{-1} \text{ cm}^{-1}$

The value obtained for the coefficient of recombination α lies within the theoretical limits predicted by Pincherle (cf. p. — 346), who evaluated it at

$$10^{-29} > \alpha > 10^{-33}.$$

Hitherto the literature brings no instance of the coefficient of recombination having been determined experimentally.

The small value of the "effective" mobility of the carriers is in accordance with the hypothesis that the principle obstacle in the path of the carriers moving in the electric field resides in the surface effects predominating in polycrystalline material.

5.6. *Temperature Dependences*

Fig. 12 brings graphs of the temperature dependence of the conductivity, for various sample. The latter exhibit but small differences in the inclination of the curves representing the variation of the conductivity in darkness, whereas the curves representing the conductivity dependence in the presence of light of various intensities, and resembling straight lines, exhibit almost constant inclination. The relations

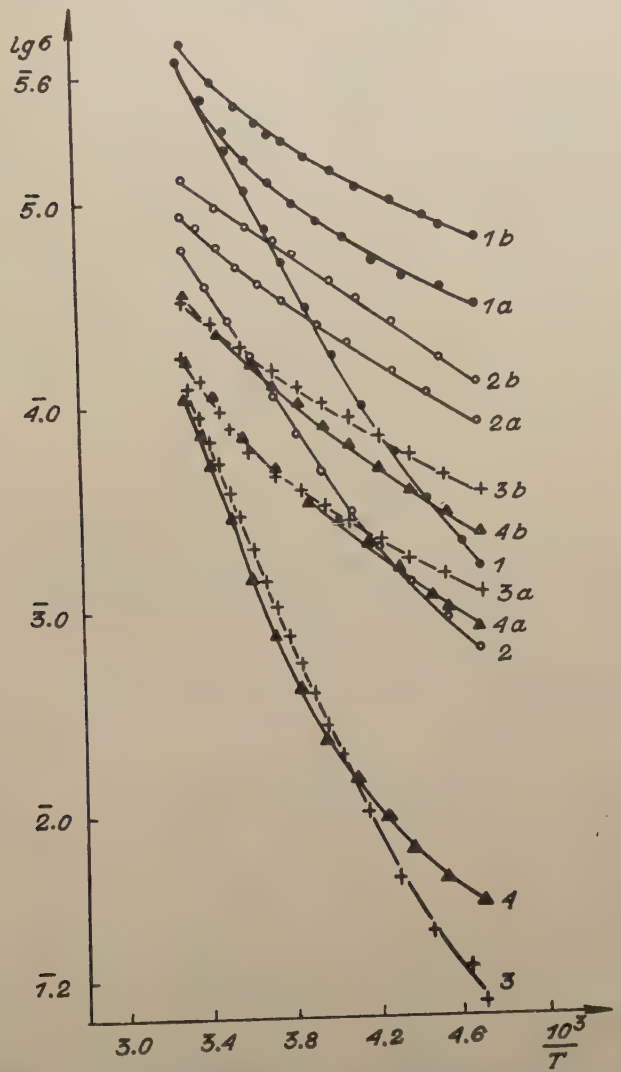

Fig. 12. Conductivity σ *vs.* reciprocal temperature. The curve 1—4 correspond to the dark conductivity of the various samples, the curves 1a — 4a and 1b — 4b to the weaker and stronger background illumination respectively.

in Fig. 13 are analogous to those of Fig. 12. The linear sections of the σ $(10^3/T)$ dependences as obtained with four values of the light intensity differing by almost one order of magnitude are seen to retain an almost constant steepness.

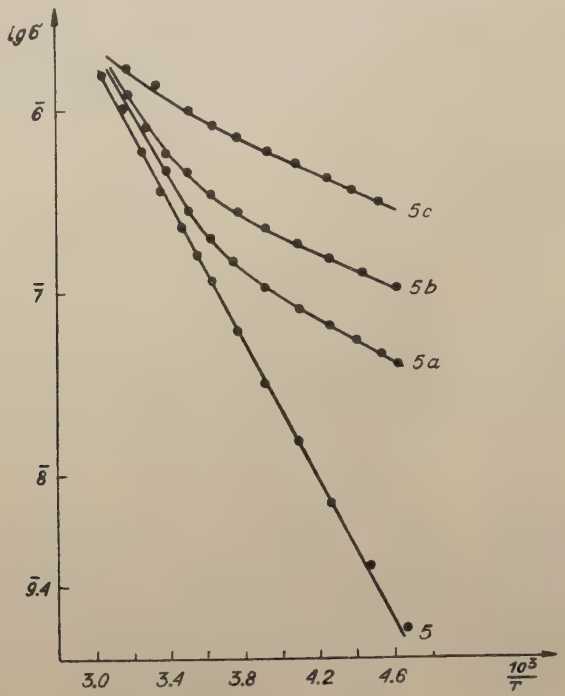

Fig. 13. Conductivity *vs.* reciprocal temperature. The curve 5 was taken in darkness and the curves 5*a* — 5*c* at different increasing background illumination intensities

The tangents of the angles (β) of inclination for the various curves are assembled in Table 2. The initial section of the σ $(10^3/T)$ have been considered.

Table 2

Current number of curve	tg β
1	2.1
2	1.7
3	2.6
4	2.6
5	1.9
1 *a*, *b*	0.5
2 *a*, *b*	0.53
3 *a*, *b*	0.6
4 *a*, *b*	0.6
5 *a* — 5 *c*	0.51

In accordance with the relation $\sigma_0 \sim \mu p_0$, curves 1—5 (Figs. 12 and 13) illustrate the temperature dependence of the product

$$\mu\left(\frac{1}{T}\right) \cdot p_0\left(\frac{1}{T}\right) \tag{38}$$

whereas curves 1 *a*, *b* — 5 *a*, *b*, *c* in their final, linear part illustrate that of the product

$$\mu\left(\frac{1}{T}\right) \cdot \tau\left(\frac{1}{T}\right), \tag{39}$$

since now we have

$$n \gg p_0,$$

which leads to $\sigma \sim \mu n$, and with respect to $n \sim \tau$ ((10), (11)) we have finally eq. (39), which holds for a given sample and a given intensity of illumination.

From eqs. (38) and (39) it is seen that the functions $p_0(T)$ and $\mu(T)$ are obtained if the function $\tau(T)$ is known experimentally.

Fig. 14 illustrates the temperature dependence of the relaxation time τ. The upper curve resulted at a slightly larger value of X i. e. a somewhat more intense light impulse, than the lower one, a circumstance of no great importance. The relaxation time is seen to descrease linearly as the temperature rises.

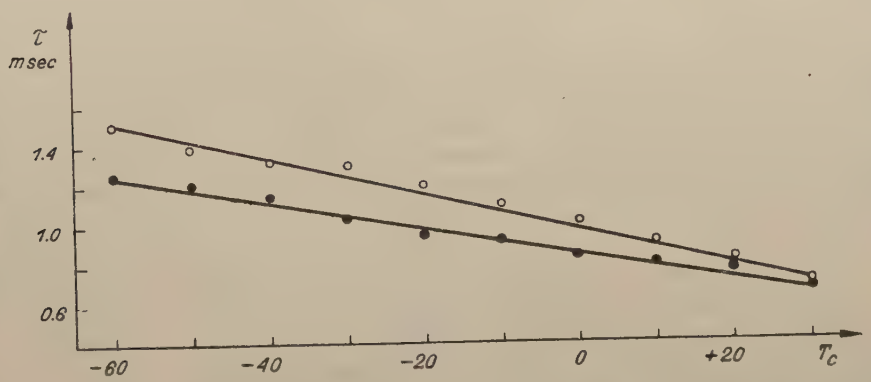

Fig. 14. Relaxation time τ *vs.* temperature. The upper curve corresponds to the stronger pulse illumination.

Since the variation of $\tau(T)$ with the temperature is linear and rather slow, the character of the temperature dependence $\mu\ (1/T)$ of the mobility ensures the exponential shape of the product in eq. (39). Fig. 15 illustrates the experimental temperature dependence of the mobility on the basis of the results yielding eq. (39) and the dependence of the time τ on the reciprocal value of the temperature. The mobility is seen to fall exponentially with the reciprocal temperature, a fact that — together with the low numerical value — may be considered to confirm the hypo-

thesis of the predominant effect of the surface barriers at the microcrystalline boundaries.

The form of eq. (38), together with the exponential decrease of the mobility with $1/T$ (Fig. 15), yields the temperature dependence of the concentration in darkness p_0. Restricting to the sample of Fig. 13, the $p_0(1/T)$ function is found as follows:

$$p_0 \sim 10^{-\frac{(1.91-0.56)\times 10^3}{T}} = e^{-\frac{3.1\times 10^3}{T}} \tag{40}$$

wherein 1.91 is the angular coefficient of the strainght line in 5 Fig. 13, and 0.56 — that of μ $(10^3/T)$ in Fig. 15. From the shape of p_0 $(10^3/T)$, the position of the acceptor states accounting for the conductivity in the dark can be evaluated.

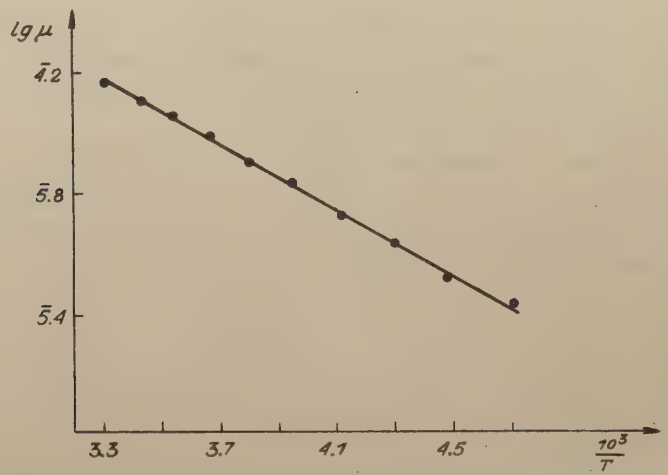

Fig. 15. Mobility μ *vs.* reciprocal temperature calculated from eq. 39 and from τ (T) measurements shown in fig. 14.

Let us now consider the problem from a more general point of view. The holes in the valence band are assumed to arise from electron capture by the acceptors; the latter, moreover, undergo investing by electrons from donors, although these are present in a number far inferior to that of the acceptors.

The corresponding formulas are:

$$n_a = N_a \exp\left(-\frac{E_a - F}{kT}\right) \tag{41}$$

$$p_0 = N_p \exp\left(-\frac{F}{kT}\right) \tag{42}$$

Let us consider two cases: First assume all acceptors to be invested by electrons from the valence band, $n_a = p_0$; thus, there are very few donors, so that

$$p_0 \gg N_d. \tag{43}$$

With $n_a = p_0$ and by eqs. (41) and (42), we have

$$2N_a \exp\left(-\frac{E_a}{kT}\right) \cdot \exp\left(\frac{F}{kT}\right) = N_p \exp\left(-\frac{F}{kT}\right)$$

whence
thus, eq. (42) yields

$$p_0 = \sqrt{2N_p N_a} \exp\left(-\frac{E_a}{2kT}\right) \tag{44}$$

Now assume the other case, namely

$$p_0 \ll N_d; \tag{45}$$

here,

$$n_a = p_0 + N_d \cong N_d,$$

whence, by eq. (41),

$$2N_a \exp\left(-\frac{E_a}{kT}\right) \cdot \exp\left(\frac{F}{kT}\right) = N_d,$$

and eq. (42) yields

$$p_0 = 2N_p \frac{N_a}{N_d} \exp\left(-\frac{E_a}{kT}\right) \tag{46}$$

From eqs. (44) and (46), the acceptor activation energy for the first case is seen to amount to the double of that for the second. There is no possibility of deciding between the assumptions of eqs. (43) and (45) by direct experiment since neither the concentration N_d of the donors nor that of the acceptors N_a could be made accessible to measurement.

We shall now attempt to prove that case I does not occure. For this, the right hand side of eq. (44) will be computed:

$$N_p = \frac{2(2\pi m \cdot kT)^{3/2}}{h^3} = 2.38 \times 10^{19};$$

in the foregoing, the effective mass of a hole is assumed to be equal to the mass of a free electron, and $T = 290°\text{K}$.

$$\exp\left(-\frac{E_a}{2kT}\right) = \exp\left(-\frac{0.54}{\text{k} \cdot 290}\right) = 2 \times 10^{-5},$$

whence, with $p_0 \cong 5 \times 10^{16}$, we have

$$N_a \cong 10^{22}\ \text{cm}^{-3},$$

a result that cannot be retained in view of the fact that the number of atoms per cm^3 of Tl_2S is evaluated at the order of 10^{22}.

Let us now consider case II. Eq. (46) yields

$$\frac{N_a}{N_d} = 35,$$

a number of acceptors 35 times greater than that of the donors, which is quite reasonable. With respect to the condition of eq. (45), it seems permissible to put e. g. $N_d = 3 \times 10^{17}$ and $N_a = 10^{19}$, these being figures that are within reasonable limits.

Thus, eq. (46) is the one to be retained; it yields the following evaluation for the position of the acceptors:

$$E_a \cong 0.27 \text{ eV};$$

this is an approximation, as resulting from earlier evaluations (as, e. g. of p_0), and additionally because of the lack of information as to the value of the effective mass of the holes in the valence band.

By eq. (42), assuming the resultant, effective mass of the holes and electrons to be equal to the mass of a free electron, the position of the Fermi level F et room temperature can be assessed as follows:

$$F \cong 0.15 \text{ eV}.$$

If a hydrogen type model of the acceptors is assumed, the dielectric constant of the material investigated can be evaluated; this leads to

$$\varepsilon \cong \sqrt{\frac{13.5}{0.27}} \cong 7,$$

which is a reasonable value.

Thus, the following approximate model results for darkness and room temperature:

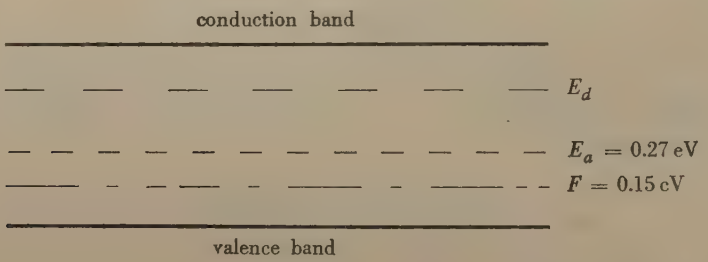

To conclude, it may be mentioned that, in accordance with the considerations of Section 3.6, the time $\tau_{1/2\Delta}$ was found to be temperature independent throughout the range of $+20°$ to $-40°$C. This latter fact corroborates the general trend of the present considerations.

5.7. *Conclusion*

In Table 3, numerical data obtained with the layer with which the greatest amount of measurements had been carried out, and which could be considered to present average properties are assembled. The concentration n_m and the relaxation time τ are given for illumination with a 100 W bulb from a distance of 100 cm.

Table 3

approximate values	n_m	cm^{-3}	4×10^{15}
	p_0	cm^{-3}	1.6×10^{16}
	α	$cm^6\ sec^{-1}$	1.4×10^{-30}
	μ	$cm^2\ Volt^{-1}\ sec^{-1}$	2×10^{-2}
	σ_0	$Amp.\ Volt^{-1}\ cm^{-1}$	5×10^{-5}
	τ	m sec	2
	E_a	eV	0.27
Values assessed on the assumption of $m^* = m_e$	F	eV	0.15
	$\frac{N_a}{N_d}$		35
Reasonable values	N_a	cm^{-3}	10^{19}
	N_d	cm^{-3}	3×10^{17}

The model of collision recombination as adopted is, in general, confirmed by experiment. Nevertheless, it is certainly no more than an approximate one. It seems that material of the kind used is hardly adapted to the verification of the finer, quantitative consequences resulting from more detailed assumptions in the model.

In semiconductor material of this type of structure, having a vast surface and an inhomogeneous composition with many impurities, a number of local energy levels situated at various depths of the energy gap should be expected to exist. It is thus hardly feasible to eliminate entirely the possibility of recombination of the carriers through the centres. However, the experimental results seem to indicate that recombination through intermediate states is not predominant here. May be the time of intermediate recombination is longer than that for the direct process. The long-

-lifetime processes observed may well consist in the investing of traps of some kind or other.

Further research work on the mechanism of collision recombination should be conducted with material of a type free from the disadvantages of the polycrystalline one investigated. In the first place, monocrystals of high photosensitivity, a high concentration of free carriers and a well-determined distribution of impurity levels should be recommended.

Acknowledgments

The author wishes to express his thanks to Professor dr L. Sosnowski for suggesting this problem and for helpful discussions, He is also grateful to Dr. J. Mycielski for discussions concerning some problems in the present paper. The author would like to acknowledge the assistance of Miss I. Turska in performing the experiments. The material investigated was made available to the author by Dr. T. Piwkowski.

REFERENCES

Bess, L., *Phys. Rev.*, **105**, 1468 (1957).
Hornbeck, J. A. and Haynes, J. R., *Phys. Rev.*, **97**, 311 (1955)
Kur, J. and Toruń, A. (not published).
Landsberg, P. T. and Beattie, A. R., *J. Phys. Chem. Solids.*, **8**, 73 (1959).
Moss, T. S., *Proc. Phys. Soc.* LXVIB, 993 (1953).
Ostrowski, J. W. and Sosnowski, L., *Bull. Acad. Polon. Sci.* Cl. III, II, 385 (1954).
Pincherle, L., *Proc. Phys. Soc.* LXVII B, 319 (1955).
Sclar, N. and Burstein, E., *Phys. Rev.*, **98**, 1757 (1955).
Wolska, A., *Bull. Acad. Polon. Sci.* Cl. III, **1**, 179 (1953).

DIELECTRIC PERMITTIVITY VARIATIONS IN $BaTiO_3$ SINGLE CRYSTALS AND CERAMICS RESULTING FROM HYDROSTATIC PRESSURE[1]

By J. Klimowski and J. Pietrzak

Institute of Experimental Physics, A. Mickiewicz University, Poznań

(Received December 7, 1959)

The effect of hydrostatic pressure on the dielectric properties of $BaTiO_3$ monocrystals and ceramic below and above the Curie point was investigated. Curves of the permittivity *versus* the temperature, for various voules of the pressure, were obtained. The maximum hydrostatic pressure was 2.000 kG/cm². The reciprocal value of the dielectric permittivity, $1/\varepsilon$, was found to decrease linearly below the Curie point and to rise linearly above the Curie point, as the pressure increased, both in monocrystals and in ceramic. The Curie point and Curie-Weiss temperature (i. e. the temperarute of the catastrophe for the cubic phase) decrease linearly as the pressure rises, at a rate of -4.1×10^{-3} °C/at and -3.6×10^{-3} °C/at for the crystal and -4.5×10^{-3} °C/at for ceramic. The Curie-Weiss constant is not modified by pressure. The maximum value of the permittivity of a monocrystal rises with the pressure and the $\varepsilon(T)$ curve becomes steeper; in ceramic, ε decreases and the curve flattens down. The results obtained within the region above the Curie point were compared with Devonshire's theory. Using the authors' experimental results, the coefficient of voluem electrostriction η was computed. Moreover, dalayed effects resulting from hydrostatic pressure pulses were investigated.

Introduction

A number of papers dealing with the effect of hydrostatic pressure on ferroelectric properties have been published. Vul and Vereshtchagin (1945) found that the capacity of a polycrystalline $BaTiO_3$ plate increased as a result of hydrostatic pressure and the relative variation of the capacity per unit pressure amounted to 1.2×10^{-5} cm²/kG. Koch (1958) investigated time variations of the dielectric permittivity in a $BaTiO_3$ single multi-domain crystal and ceramics by pulse-wise applying and removing of hydrostatic pressure. Merz (1950) found that the Curie point decreased linearly by -5.8×10^{-3} °C/at in a monocrystal subjected to hydrostatic pressure.

The present investigation deals with the effect of hydrostatic pressure on the

[1]) The present investigation was subventioned in part by the Institute of Physics of the Polish Academy of Sciences.

dielectric permittivity of $BaTiO_3$ monocrystals and ceramics both below and above the Curie point. The results obtained above the Curie point are compared with Devonshire's theory.

1. Experimental Method

a) Preparation of Samples

$BaTiO_3$ monocrystals and ceramic were used for investigation. The crystals were grown by Remeika's method, and had the shape of plates 0.2 — 0.3 mm thick of an area of 4 — 10 mm^2. Silver electrodes were formed on the surfaces by evaporation *in vacuo*. Only monocrystals presenting a rectangular hysteresis loop and a dielectric permittivity of about 300 at room temperature were used in the investigation.

Ceramic samples were prepared from polycrystalline barium titanate by well-known methods (Trzebiatowski and co-workers, 1952). Podwered $BaTiO_3$ was compressed at 4 tons/cm^2 to form discs 6 mm in diameter. The latter were sintered for 3 hours at 1380°C, yielding material of low porosity. On polishing the discs down to a thickness of 0.6 — 2 mm, silver electrodes were chemically formed on the surfaces.

b) High Pressure Apparatus

The apparatus for producing high pressures is shown in Fig. 1. Hydrostatic pressures of up to 2.000 at were produced within a piezostat by a screw compressor and 1 : 20 pressure multiplicator filled with paraffine oil.

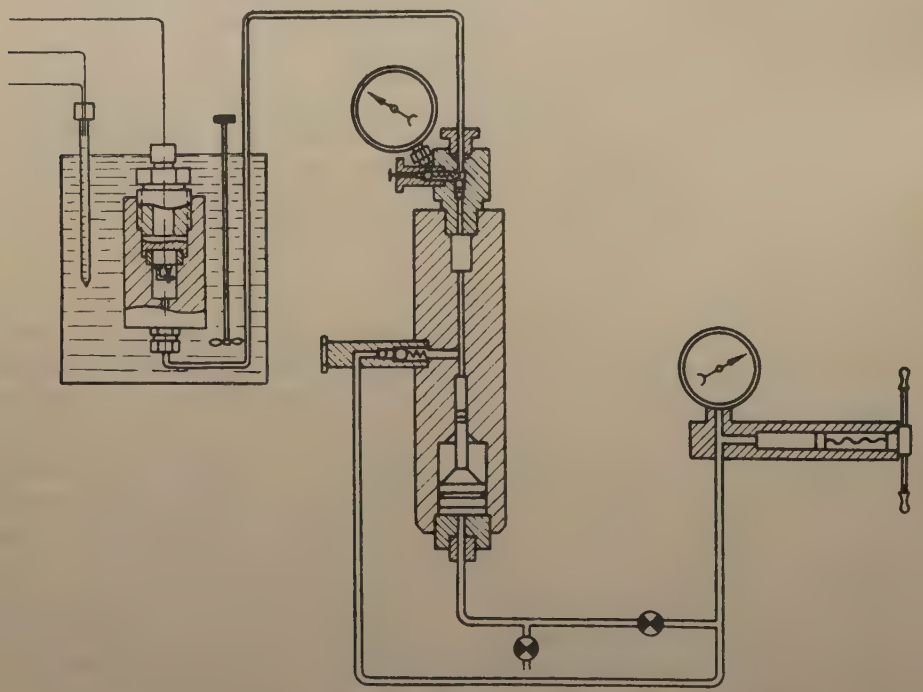

Fig. 1. Apparatus for producing hydrostatic pressure, with piezostat

The pressure within the piezostat was measured with a tube manometer, the accuracy amounting to ± 10 kG/cm^2. The electric leads connecting the crystal or ceramic sample with the measuring device passed through the plug in the piezostat (Fig. 2) giving rise to a capacity of about 7 pF. The temperature was measured with a thermo-

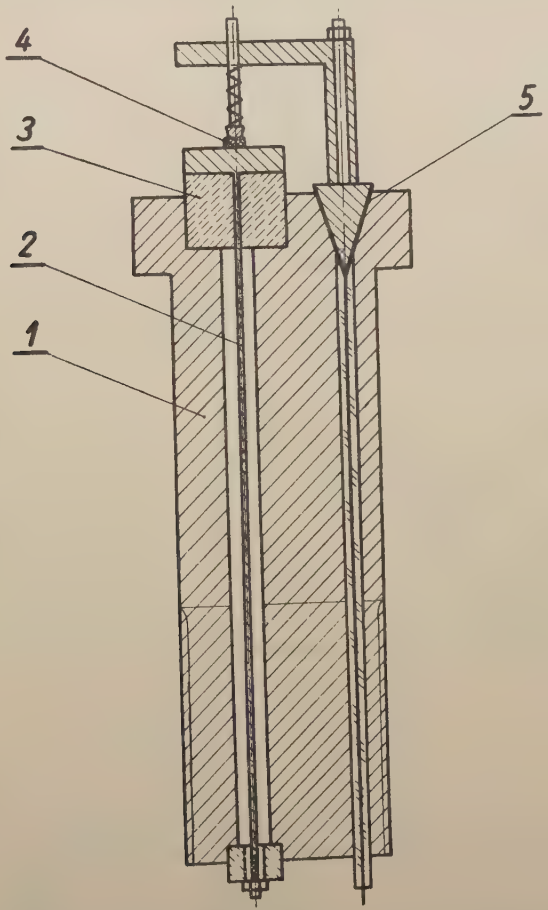

Fig. 2. Plug with electric leads: 1. plug, 2. leads, 3. insulation, 4. sample, 5. insulation (mica)

couple situated at a distance of about 1 mm from the sample on the side of the grounded electrode. The thermo- electric force was measured with a Diesselhorst compensator.

c) *Electric Measurements*

The dielectric permittivity of $BaTiO_3$ monocrystals and ceramic was measured on a Schering type bridge. The device is shown schematically in Fig. 3. The accuracy in measuring the capacity amounted to ± 0.2 pF. The measuring field did not exceed

10 V/cm, and the measuring signal had a frequency of 2 kc/sec. Each measurement of the capacity *versus* the temperature at constant pressure was carried out by cooling the sample from 180°C. The rate of cooling amounted to 30°C per hour and was constant throughout each measurement. The variations of the stray capacity resulting from changes in temperature and pressure did not exceed ± 0.1 % and were practically negligible.

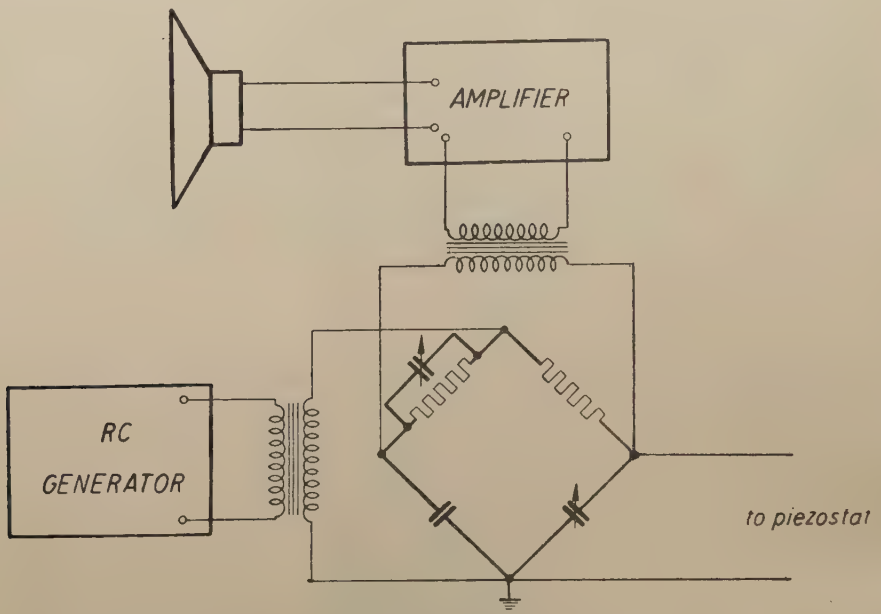

Fig. 3 Scheme for measuring capacity

2. Results

A. Fig. 4 shows the dielectric permittivity of a monocrystal as plotted *versus* the temperature, at various fixed values of the hydrostatic pressure. As the pressure rises, the Curie point (the temperature corresponding to maximum ε) shifts linearly towards lower temperatures by -4.1×10^{-3}° C. cm²/kG, and the maximum value of the permittivity rises monotonically. The Curie-Weiss temperature Θ at pressure σ (the extrapolated temperature at which $\varepsilon^{-1}$is 0) decreases as the pressure rises; however, the decrease is smaller than that of the Curie point, and amounts to $-3.6\times$ $\times10^{-3}$ °C · cm²/kG (Fig. 5). The Curie-Weiss constant, which amoumts 1.1×10^{4} °C, undergoes no modification. Hence, as the hydrostatic pressure rises, the interval between the Curie point T_C and the Curie-Weiss temperature Θ diminishes.

Measurements of the dielectric permittivity as a function of the temperature and hydrostatic pressure carried out on $BaTiO_3$ ceramics (Fig. 6) proved a rise in the pressure to produce a linear decrease in the Curie point and Curie-Weiss tem-

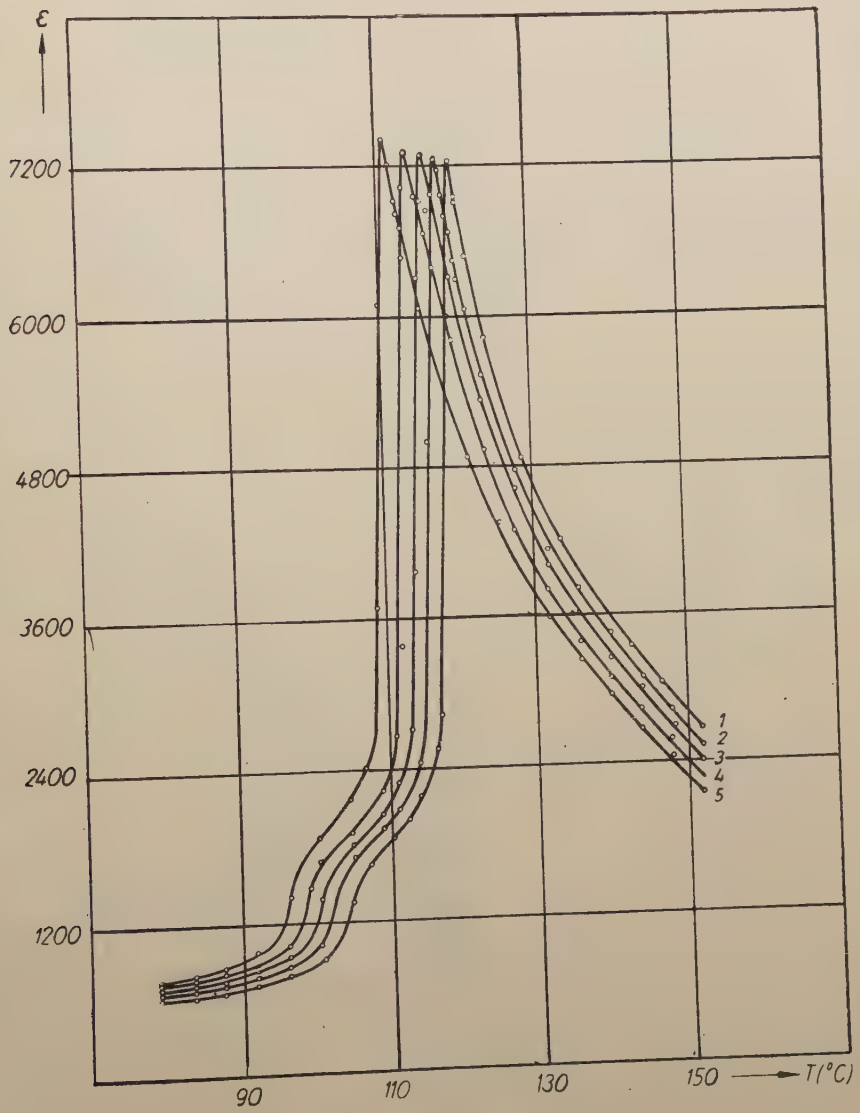

Fig. 4. Permittivity of $BaTiO_3$ crystal *versus* the temperature, at various values of the hydrostatic pressure:

1 — 0 kG/cm²,
2 — 500 kG/cm²,
3 — 1.000 kG/cm²,
4 — 1.500 kG/cm²,
5 — 2.000 kG/cm²,

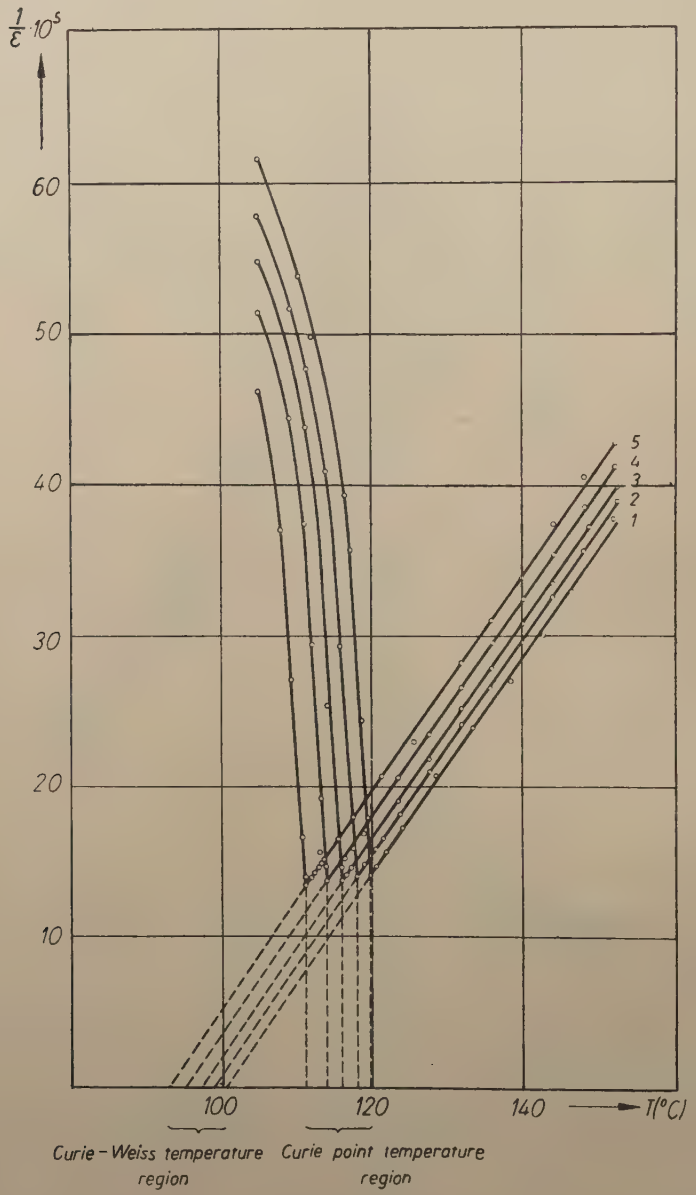

Fig. 5. Temperature dependance of $1/\varepsilon$ for crystal, at the hydrostatic pressure values of Fig. 4.

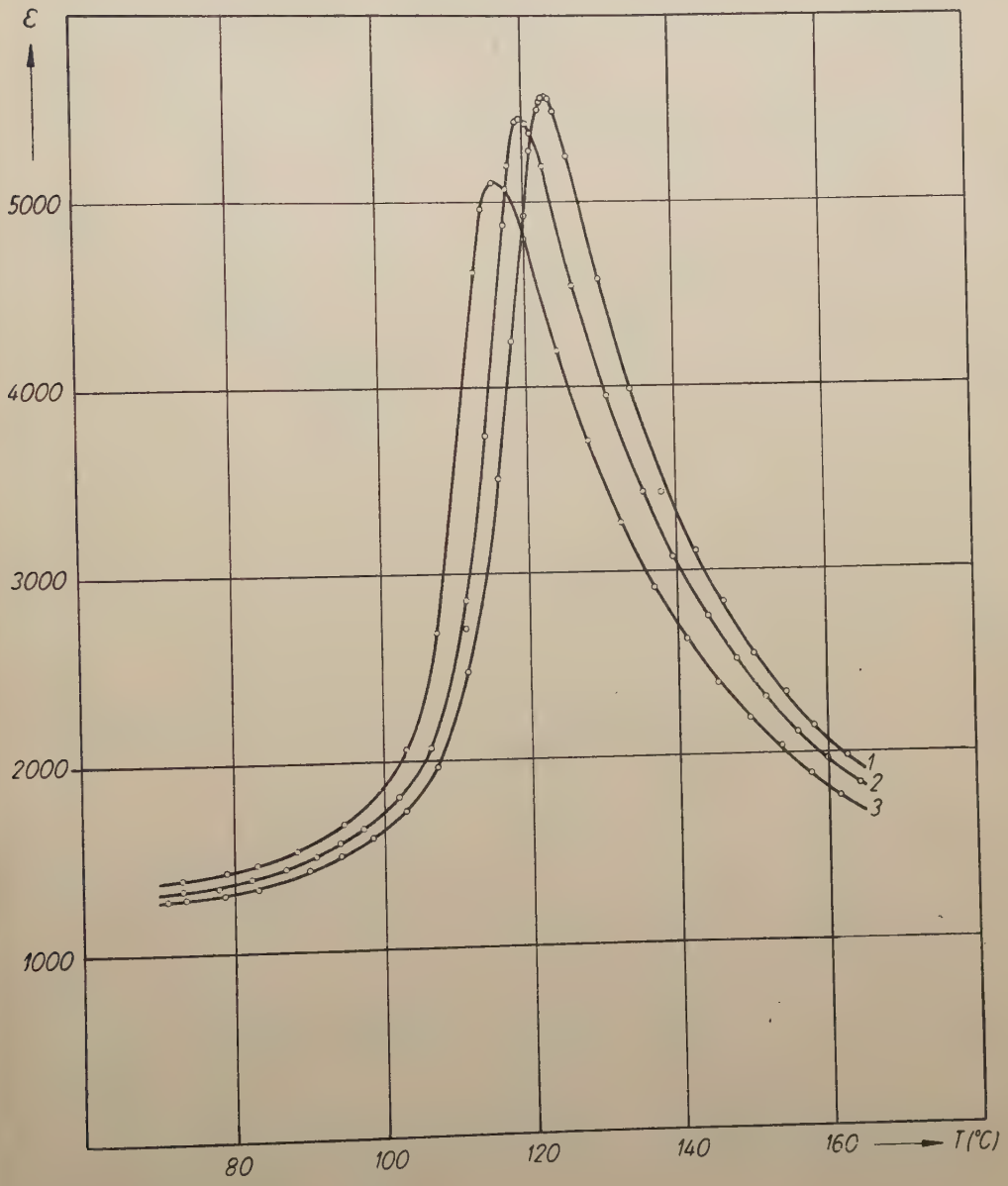

Fig. 6. Permittivity of ceramic *versus* the temperature, at various values of the hydrostatic pressure:
1 — 0 kG/cm²,
2 — 740 kG/cm²,
3 — 1.600 kG/cm²,

perature amounting to -4.5×10^{-3} °C · cm²/kG (Fig. 7). This value exceeds the one for a crystal and is in agreement with results obtained by Jaffe and co-workers (1957). The Curie-Weiss constant is pressure-independent and equals 0.9×10^{4} °C. The essential difference between the results obtained with $BaTiO_3$ monocrystals and

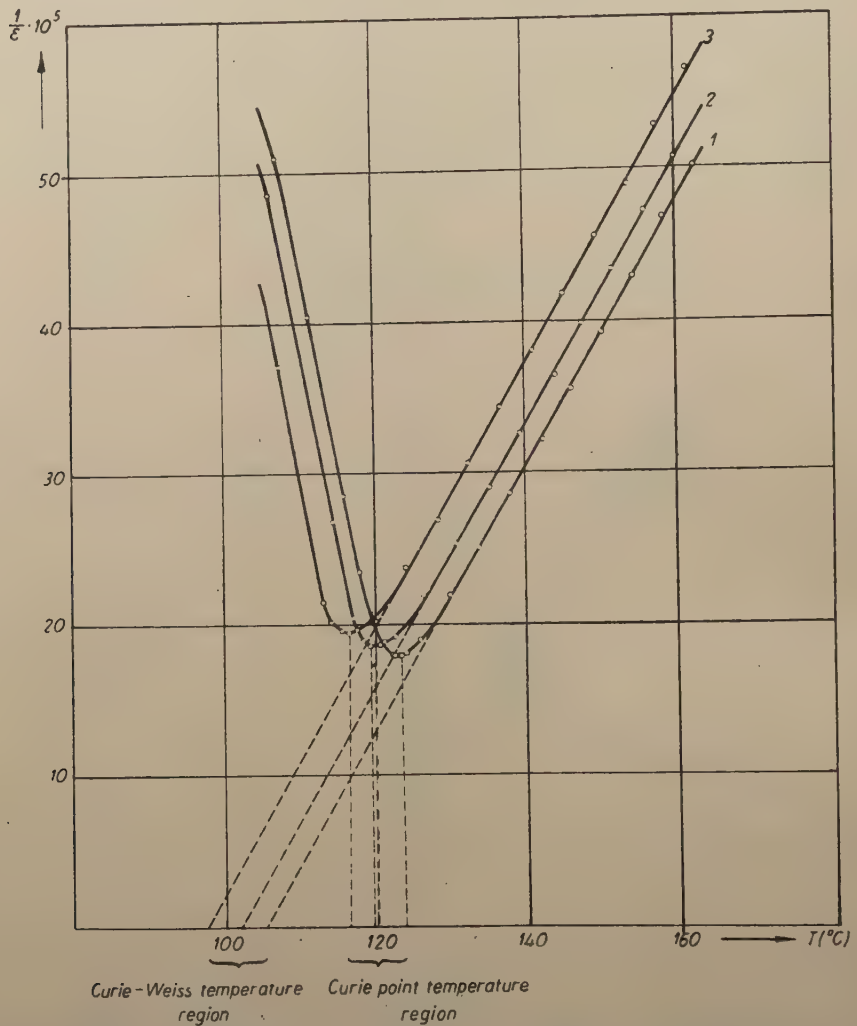

Fig. 7. Temperature dependance of $1/\varepsilon$ for ceramic, at the hydrostatic pressure values of Fig 6.

with ceramic manifests itself in the region of the Curie point: at higher hydrostatic pressures, the $\varepsilon(T)$ curve for ceramic exhibits a marked flattening at the transition, with a lowering of the dielectric premittivity.

The authors propose to explain the effect by the fact that ceramics are inhomo-

geneous systems consisting of crystallites; internal anisotropic stresses arise in the latter when hydrostatic pressure is applied.

In Fig. 8, the reciprocal value of the permittivity, $1/\varepsilon$, is plotted *versus* the hydrostatic pressure at fixed temperatures, for a monocrystal and ceramic. The reciprocal $1/\varepsilon$ is seen to be a linear function of the hydrostatic pressure. Below the Curie point, $1/\varepsilon$ diminishes linearly as the pressure rises, the steepness being temperature depen-

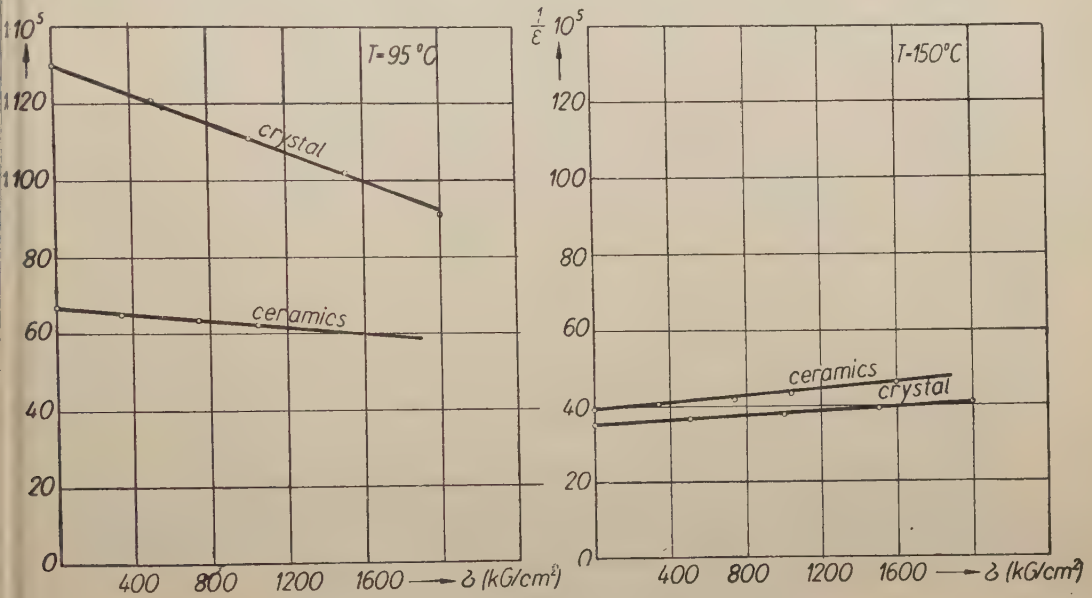

Fig. 8. Dependance of $1/\varepsilon$ on the hydrostatic pressure.

dent, whereas above the Curie point $1/\varepsilon$ increases linearly with the pressure and the steepness is constant and temperature-independent.

B. Pulse hydrostatic pressure was applied to and removed from $BaTiO_3$ single (*c* — domain) crystals and ceramics below and above the Curie point, the time variations of the capacity and temperature of the samples being measured simultaneously. Relaxation effects involving the dielectric permittivity were found to occur *only* in ceramic samples below the Curie point. Above the Curie point, variation in time of the dielectric permittivity of $BaTiO_3$ ceramic samples results only from the variation in time of the temperature.

When hydrostatic pressure is suddenly applied to the sample or suddenly removed therefrom (Fig. 9), the permittivity rises abruptly and, subsequently, decreases in time. At 20°C the variations of the permittivity are greater and require longer time for decay than at 70°C.

The effect observed greatly resembles the delay effects in an electric field below the Curie point as observed by Partington and co-workers (1949) and by Piekara and Pająk (1952).

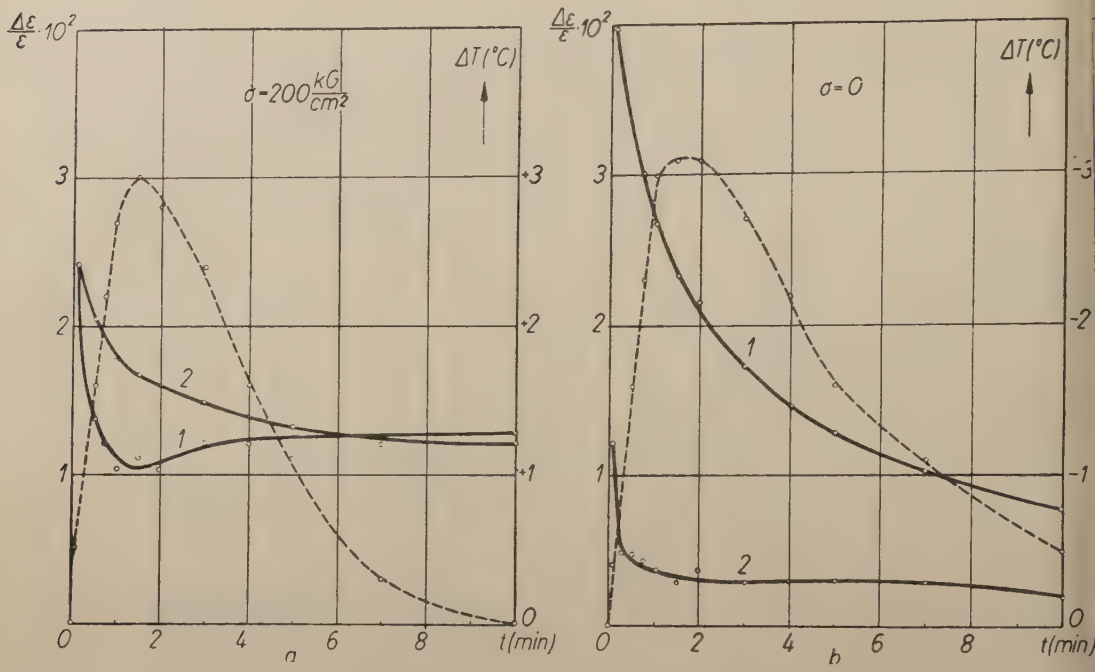

Fig. 9. Delayed variation of relative permittivity $\Delta\varepsilon/\varepsilon$ in a ceramic sample, as computed without accounting for changes in temperature, *a*) on applying suddenly, *b*) on removing suddenly hydrostatic pressure. Dashed line shows time variation of the temperature as arising from sudden change in pressure.
graph 1 — at 20°C,
graph 2 — at 70°C.

The authors propose to explain the delayed effects resulting from pressure or from an electric field by the complex domain structure of the ceramics (presenting domains with 90° and 180° walls).

3. Comparison of Theoretical and Experimental Results

Devonshire (1949) expressed the free energy of barium titanate as a function of the polarisation and strain. For the non-polarized cubic phase, the function is of the following form:

$$\begin{aligned} A(x, \ldots, P_x \ldots) = {} & \tfrac{1}{2} c_{11}(x_x^2 + y_y^2 + z_z^2) + c_{12}(y_y z_z + z_z x_x + x_x y_y) + \\ & + \tfrac{1}{2} c_{44}(x_y^2 + y_z^2 + z_x^2) + \tfrac{1}{2} \chi''(P_x^2 + P_y^2 + P_z^2) + \\ & + \tfrac{1}{4} \xi_{11}''(P_x^4 + P_y^4 + P_z^4) + \tfrac{1}{2} \xi_{12}''(P_x^2 P_z^2 + P_z^2 P_x^2 + P_x^2 P_y^2) + \\ & + g_{11}(x_x P_x^2 + y_y P_y^2 + z_z P_z^2) + g_{12}\{x_x(P_y^2 + P_z^2) + y_y(P_z^2 + P_x^2) + \\ & + z_z(P_x^2 + P_y^2)\} + g_{44}(y_z P_y P_z + z_x P_z P_x + x_y P_x P_y) + \\ & + \tfrac{1}{6} \zeta''(P_x^6 + P_y^6 + P_z^6) \end{aligned} \tag{1}$$

Let us now consider the free energy as dependent on the quantities x_x, y_y, z_z and P_z alone (for brevity, strain and polarization will be denoted by x, y, z and P, respectively) The remaining components of strain x_y, y_z, z_x and the polarisation components P_x and P_y will be assumed to vanish; this yields (Forsbergh, 1954)

$$A(x, \ldots, P) = \tfrac{1}{2} c_{11}(x^2 + y^2 + z^2) + c_{12}(yz + zx + xy) + g_{11} z P^2 + \\ + g_{12}(x + y) P^2 + \tfrac{1}{2} \chi'' P^2 + \tfrac{1}{4} \xi'' P^4 + \tfrac{1}{6} \zeta'' P^6 \qquad (2)$$

It will be assumed that positive stresses correspond to compression, and nagative ones — to stretching. Thr stress components are the following:

$$X = -\frac{\partial A}{\partial x}; \; Y = -\frac{\partial A}{\partial y}; \; Z = -\frac{\partial A}{\partial z} \qquad (3)$$

For hydrostatic pressure, eq. (2) yields the following expressions:

$$\begin{aligned} -\sigma &= c_{11} x + c_{12}(z + y) + g_{12} P^2 \\ -\sigma &= c_{11} y + c_{12}(z + x) + g_{12} P^2 \\ -\sigma &= c_{11} z + c_{12}(y + x) + g_{11} P^2, \end{aligned} \qquad (4)$$

σ denoting the pressure. The system is solved in x and z assuming that in an electric field applied along the z-direction there is transition of the cubic into the tetragonal phase; thus, the x and y strains are equal, and the system (4) reduces to two equations. The solutions are the following:

$$x = y = -\frac{1}{c_{11} + 2c_{12}} \sigma - \frac{c_{11} g_{12} - c_{12} g_{11}}{(c_{11} - c_{12})(c_{11} + 2c_{12})} P^2 \qquad (5)$$

$$z = -\frac{1}{c_{11} + 2c_{12}} \sigma + \frac{2c_{12} g_{12} - (c_{11} + c_{12}) g_{11}}{(c_{11} - c_{12})(c_{11} + 2c_{12})} P^2 \qquad (6)$$

The free energy $A(X, \ldots, P)$ can now be expressed as a function of the stresses and the polarisation by applying (Tisza, 1951) Legendre's transformation:

$$A(X, \ldots, P) = A(x, \ldots, P) - x \frac{\partial A}{\partial x} - y \frac{\partial A}{\partial y} - z \frac{\partial A}{\partial z} \qquad (7)$$

Substituting (5) and (6) in eq. (7) and ordering by growing powers of P yields

$$A(\sigma, P) = -\tfrac{1}{2} \varkappa \sigma^2 + \eta \sigma P^2 + \tfrac{1}{2} \chi' P^2 + \tfrac{1}{4} \xi'_{11} P^4 + \tfrac{1}{6} \zeta' P^6$$

or

$$A(\sigma, P) = -\tfrac{1}{2} \varkappa \sigma^2 + \eta \sigma P^2 + A(0, P) \qquad (8)$$

wherein $\varkappa = \dfrac{3}{c_{11} + 2c_{12}}$ is the coefficient of compressibility, $\eta = -\dfrac{g_{11} + 2g_{12}}{c_{11} + 2c_{12}}$ — the coefficient of volume electrostriction, and $A(0, P)$ — the free energy expressed as a function of the polarisation at zero stresses.

From eq. (8), the dielectric permittivity can be computed:

$$\frac{\partial^2 A(\sigma, P)}{\partial P^2} = \frac{4\pi}{\varepsilon_\sigma} = +2\eta\sigma + \frac{\partial^2 A(0, P)}{\partial P^2}$$

whence

$$\frac{1}{\varepsilon_\sigma} = \frac{\eta}{2\pi}\sigma + \frac{1}{\varepsilon} \tag{9}$$

wherein ε_σ is the permittivity under hydrostatic pressure, and ε — that at zero stresses. By eq. (9), it is seen that above Curie point $1/\varepsilon$ is a linear function of the hydrostatic pressure. This result is in agreement with experiment (cf. Fig. 8). It is now possible to compute η numerically, assuming $\frac{1}{\varepsilon_\sigma} - \frac{1}{\varepsilon} = 5.3 \times 10^{-5}$ (from the diagram of Fig. 5) at $\sigma = 2.000$ kG/cm^2, which yields a value of

$$\eta = 1.7 \times 10^{-13} \text{ cm}^2/\text{dyn}$$

On the other hand, η can also be computed from the relative variation of the volume and the variation of the spontaneous polarisation at the Curie point. Differentiating eq. (8) with respect to the perssure and assuming $\sigma = 0$ yields $\frac{\Delta V}{V} = \eta\ P^2$, whence, with $\frac{\Delta V}{V} = 4.9 \times 10^{-4}$ (Kay and Vousden, 1949) and $P = 18\ \mu$C/cm^2 (Merz, 1953), a value of $\eta = 1.7 \times 10^{-13}$ cm^2/dyn is obtained. The relation between the shift in the Curie-Weiss temperature and the hydrostatic pressure is obtained from eq. (9) and the hydrostatic pressure is obtained from eq. (9) and the Curie-Weiss law:

$$\Theta_\sigma = \Theta + k\sigma \tag{10}$$

wherein Θ_o is the Curie-Weiss temperature at pressure σ; Θ — the Curie-Weiss temperature at $\sigma = 0$; C — the Curie-Weiss constant, and $k = -2\eta C$. Substituting herein the values of η and C from the authors, measurements, a value of $k = -3.6 \times \times 10^{-3}$ °C · cm^2/kG is obtained, in good agreement with direct measurements of the shift in the Curie-Weiss temperature produced by hydrostatic pressure, which yield $k = -3.6 \times 10^{-3}$ °C · cm^2/kG.

4. Conclusion

Both in monocrystals and in ceramic, the reciprocal of the dielectric permittivity diminishes linearly below the Curie point and increases linearly above the Curie point with increasing hydrostatic pressure.

The Curie point and Curie Weiss temperature decrease linearly as the hydrostatic pressure increases; the steepness amounts to -4.1×10^{-3} °C/at and -3.6×10^{-3} °C/at

respectively, for a monocrystal, and to -4.5×10^{-3} °C/at in both cases for ceramic. The Curie-Weiss constant does not depend on the hydrostatic pressurre.

The peak of the dielectric permittivity at transition temperature rises with increasing hydrostatic pressure in the case of a crystal, whereas it diminishes and becomes diffluent in that of ceramic.

The results obtained above the Curie point are accounted for by Devonshire's phenomenological theory.

Sudden applying or removing of hydrostatic pressure produces delayed variation of the dielectric permittivity in $BaTiO_3$ ceramics only below the Curie point; a single c-domain crystal presents no such effect.

The authors wish to express their thanks to Professor Dr A. Piekara for directing the present investigation and for his constant advice and valuable discussions.

REFERENCES

Devonskire, A. F., *Phil. Mag.*, **40**, 1040 (1949).
Forsbergh, P. W., *Phys. Rev.*, **93**, 686 (1954).
Jaffe, H., Don Berlinecourt and McKee, J. M., *Phys. Rev.*, **105**, 37 (1957).
Kay, H. F. and Vousden, P., *Phil. Mag.*, **40**, 1019 (1949).
Koch, W., *Z. Naturforsch.*, **13a**, 303 (1958).
Merz, W. G., *Phys. Rev.*, **77**, 52 (1950); *Phys. Rev.*, **91**, 513 (1953).
Partington, I. R.. Planer, G. V., and Boswell, I. I., *Phil. Mag.* ,**40**, 301 (1949).
Piekara A., and Pająk, Z., *Acta phys. Polon.* **11**, 256 (1953).
Tisza, L., *Phase Transformation in Solids*, *Wiley*, *New York*, 1951.
Trzebiatowski, W., Wojciechowska, J., and Damm, J., *Roczn. Chem.* **26**, 12 (1952).
Vul, B. M., and Vereshtchagin, L. F., *DAN SSSR*, **48**, 662 (1945).

SOME REMARKS ON COLLECTIVE DESCRIPTION OF ELECTRON INTERACTIONS. THE PARTITION FUNCTION

By Jan Śledzik

Institute of Physics of the Polish Academy of Sciences, Department of Ferromagnetics, Poznań.

(Received December 8, 1959)

The nearly-Hermitian variant of collective description is formulated. The correct partition function is obtained. Thereby the exact proof is given that the subsidiary conditions proposed by Kanazawa lead to false results, whereas those of Bohm and Pines yield the exact statistical function, provided the renormalizing procedure proposed by the author in a former paper is applied to their theory.

1. Introduction

In a former paper (1958a) I have formulated a renormalizing method leading to elimination of divergences from the collective description. This has been achieved by a reformulation of the subsidiary conditions. They differ from the form given by Bohm and Pines (1953b) by the additional term $i\omega_\lambda(1-x_\lambda)/c(1+x_\lambda)$ (div $\vec{A}(\boldsymbol{r})$)$_\lambda$ where x_λ are renormalization parameters and their values are restrained to the interval $0 \leqslant x_\lambda < 1$, with ω_λ denoting the frequency of collective oscilations, c — the speed of light, $\vec{A}(\boldsymbol{r})$ — the longitudinal vector potential and λ — the Fourier expansion vector (reciprocal lattice vector).

The difficulties of the collective description are the same as in quantum field theory. In either case the state vectors (in the latter case for free fields) are not normalizable. Hence, in either case, renormalizing procedures are required. Renormalizing of the state vectors of the Bohm and Pines theory includes transition with dimensionless para- meters x_λ to their values near unity.

In one respect the collective description differs from the picture of two strong interacting fields in quantum theory. In facts we know the exact eigenfunction both of the Bohm and Pines Hamiltonian and of the subsidiary conditions. Such eigenvectors depend on x_λ. When x_λ is nearly unity (strongly coupled plasmon and electron fields, because of the divergence of the averaged interaction term (the plasmon part represents the infinite superposition of the boson creation operator pairs $(a^*_\lambda a^*_{-\lambda})^s$,

here s is a natural number, whereas with $x_\lambda = 0$ (weak coupling of electron and plasmon fields) the plasmon state vector is in reality the vacuum vector. This problem will be discussed subsequently and it will be pointed out that the form of the Kanazawa theory (1957) should be correct at high temperatures, that is when the linear formalism of the collective description ceases to be useful. Hence, it seems that the Kanazawa's subsidiary conditions are not correct.

The physical sense of the ground state function obtained in (1958a) is not the same as in Bohm and Pines paper (1953b). This results from the fact that Bohm and Pines use a function that does not satisfy the subsidiary conditions. Notwithstanting this, the ground state vector derived in (1958a) is physically correct. The reason for it is the following: in quantum field theory the ground state is the state of vacuum, provided the interaction of the fields is weak; in the case of strong coupling we do not know the exact state vector, hence we are unable to say anything whatsover about the ground state. On the contrary in collective description, notwithstanding strong interaction, this state is obtained with precision. The state thus obtained is indeed the ground state, although it differs from the common picture of the ground state, i. e. the vacuum vector.

2. Nearly-Hermitian collective description

Let us write the extended Hamiltonian and the subsidiary conditions according to Bohm and Pines (1953b):

$$\hat{H}_{\text{ext}} = \hat{H} + \frac{1}{2}\sum_{|\vec{k}|\leqslant k_c} p_k p_{-k} - \sum_{|\vec{k}|\leqslant k_c}\left(\frac{4\pi}{Vk^2}\right)^{1/2} \varrho_k p_k, \tag{2.1}$$

$$H = \sum_{i=1}^{n} \hat{\mathbf{p}}_i^2/2m + \frac{2\pi}{V}\sum_{\vec{k}(\neq 0)} \frac{\varrho_k \varrho_{-k} - n\varepsilon^2}{k^2}, \tag{2.2}$$

$$p_k \Phi = 0, \qquad |\vec{k}| \leqslant k_c, \tag{2.3}$$

wherein q_k, p_k are coordinates and momenta of the long-range Coulomb field, ϱ_k — the Fourier transform of the charge density, ε — the electron charge, n — the number of electrons and V — the box volume.

The quantities q_k, p_k and ϱ_k satisfy the relations

$$q_k^* = q_{-k},\ p_k^* = p_{-k},\ \varrho_k^* = \varrho_{-k}, \tag{2.4}$$

the longitudinal vector potential is

$$\vec{A}(\mathbf{r}) = i\left(\frac{4\pi c^2}{V}\right)^{1/2} \sum_{|\vec{k}|\leqslant k_c} q_k \frac{\vec{k}}{k} e^{i\vec{k}\cdot\vec{r}} \tag{2.5}$$

and, respectively

$$\vec{E}(\boldsymbol{r}) = -\frac{1}{c}\frac{\partial}{\partial t}\vec{A}(\boldsymbol{r}) = -i\left(\frac{4\pi}{V}\right)^{1/2}\sum_{|\vec{k}|\leqslant k_c} q_k \frac{\vec{k}}{k} e^{i\vec{k}\cdot\vec{r}} = -i\left(\frac{4\pi}{V}\right)^{1/2}\sum_{|\vec{k}|\leqslant k_c} p_{-k}\frac{\vec{k}}{k} e^{i\vec{k}\cdot\vec{r}}. \tag{2.6}$$

(The transition $q_k = p_{-k}$ requires exact investigations. It is admissible when the Hamiltonian is stricly oscillatory, or if the electron — plasmon interaction term is small, which is not the case in the Bohm — Pines theory).

It can be readily shown that the vector potential is not univocally defined. In order to prove this let us write the oscillator Hamiltonian in the form

$$\hat{H}_{\text{osc}} = \tfrac{1}{2}\sum_{|\vec{k}|\leqslant k_c}(p_k p_{-k} + \omega_k^2 q_k q_{-k}). \tag{2.7}$$

The operator (2.7) in invariant with respect to real and orthogonal rotations in the plane p_k, $\omega_k q_{-k}$,

$$\begin{aligned} p_k' &= \cos\alpha_k p_k + \omega_k \sin\alpha_k q_{-k}, \\ q_{-k}' &= -\frac{1}{\omega_k}\sin\alpha_k p_k + \cos\alpha_k q_{-k}, \end{aligned} \tag{2.8}$$

where α_k denotes the angle of rotation. Inversion of the equations (2.8) yields

$$\begin{aligned} p_k &= \cos\alpha_k p_k' - \omega_k \sin\alpha_k q_{-k}', \\ q_{-k} &= \frac{1}{\omega_k}\sin\alpha_k p_k' + \cos\alpha_k q_{-k}', \end{aligned} \tag{2.9}$$

hence, with respect to the relations

$$\begin{aligned} p_k' &= \left(\frac{\hbar\omega_k}{2}\right)^{1/2}(a_{-k} + a_k^*), \\ q_k' &= i\left(\frac{\hbar}{2\omega_k}\right)^{1/2}(a_k - a_{-k}^*), \end{aligned} \tag{2.10}$$

the subsidiary conditions (2.3) take the form

$$\left(\frac{\hbar\omega_k}{2}\right)^{1/2}[\cos\alpha_k(a_{-k} + a_k^*) - i\sin\alpha_k(a_{-k} - a_k^*)]\,\Phi = 0, \qquad |\vec{k}|\leqslant k_c \tag{2.11a}$$

or

$$(e^{-i\alpha_k} a_{-k} + e^{i\alpha_k} a_k^*)\,\Phi = 0, \qquad |\vec{k}|\leqslant k_c \tag{2.11b}$$

The equation (2.11b) is easily solved yielding

$$\Phi = \prod_{\substack{|\vec{k}|\leqslant k_c \\ k_z>0}} \Phi_k \cdot \chi(\boldsymbol{r}_1, \ldots, \boldsymbol{r}_n), \tag{2.12a}$$

wherein

$$\Phi_k = e^{-(\cos 2\alpha_k + i \sin 2\alpha_k) a_k^* a_{-k}^*} \Phi_0, \tag{2.12b}$$

$$\hat{H} \chi(\boldsymbol{r}_1, \ldots, \boldsymbol{r}_n) = E \chi(\boldsymbol{r}_1, \ldots, \boldsymbol{r}_n). \tag{2.12c}$$

The operator H is given by (2.2); a_k, a_k^* are the oscillator destruction and creation operators, ω_k — the oscillator frequency. The vacuum vector is defined by formulas

$$\Phi_0^* \Phi_0 = 1, \quad a_k \Phi_0 = 0, \quad \Phi_0^* a_k^* = 0. \tag{2.13}$$

By (2.12b) the orthogonal rotations do not affect the norm of the state vector, though they modify the form of the vector potential. Thereby the situation resembles gauge invariance in quantum field theory.

It is known, Kanazawa (1957), that the subsidiary conditions (2.3) or, with respect to (2.10),

$$(a_{-k} + a_k^*) \Phi_k = 0, \quad |\vec{k}| \leqslant k_c, \tag{2.14}$$

are satisfied by the non-normalizable vectors

$$\Phi_k = e^{-a_k^* a_{-k}^*} \Phi_0. \tag{2.15}$$

This difficulty can be avoided by a renormalizing method entirely different from that given in (1958a). For this purpose we retain the original form of the Bohm and Pines theory, but define the operators q_k and p_k in a somewhat different manner. We write

$$\hat{H}_{\text{ext}} = \hat{H} + \frac{1}{2} \sum_{|\vec{k}| \leqslant k_c} \hat{p}_k \hat{p}_{-k} - \sum_{|\vec{k}| \leqslant k_c} \left(\frac{4\pi}{V k^2} \right)^{1/2} \varrho_k \hat{p}_k, \tag{2.16}$$

$$\hat{p}_k \Phi = 0, \quad |\vec{k}| \leqslant k_c, \tag{2.17}$$

$$\hat{p}_k = \left(\frac{\hbar \omega_k}{2} \right)^{1/2} (\hat{a}_{-k} + \hat{a}_k^*), \tag{2.18}$$

$$\hat{q}_k = i \left(\frac{\hbar}{2\omega_k} \right)^{1/2} (\hat{a}_k - \hat{a}_{-k}^*), \tag{2.19}$$

wherein

$$\hat{a}_k = \frac{1}{1 - \nu_k a_k^* a_k} a_k, \quad \hat{a}_k^* = a_k^* (1 - \nu_k a_k^* a_k),$$

$$\nu_k = \nu_{-k}, \quad |\nu_k| < 1. \tag{2.20}$$

The newly defined operators are no longer Hermitian. The degree of their deviation from the Hermitian form depends on the number ν_k. As $\nu_k \to 0$ the deviation vanishes.

We have

$$\frac{1}{1-\nu_k a_k^* a_k} a_k = a_k \frac{1}{1-\nu_k(a_k^* a_k - 1)}, \quad \frac{1}{1-\nu_k a_k^* a_k} a_k^* = a_k^* \frac{1}{1-\nu_k(a_k^* a_k + 1)},$$

$$\frac{1}{1-\nu_k(a_k^* a_k + 1)} a_k = a_k \frac{1}{1-\nu_k a_k^* a_k}, \quad \frac{1}{1-\nu_k(a_k^* a_k - 1)} a_k^* = a_k^* \frac{1}{1-\nu_k a_k^* a_k}. \tag{2.21}$$

With eqs. (2.21) we obtain

$$[\hat{a}_k, \hat{a}_s] = 0, \quad [\hat{a}_k^*, \hat{a}_s^*] = 0, \quad [\hat{a}_k, \hat{a}_s^*] = \delta_{\vec{k},\vec{s}}, \tag{2.22}$$

hence

$$[\hat{q}_k, \hat{q}_s] = 0, \quad [\hat{p}_k, \hat{p}_s] = 0, \quad [\hat{p}_k, \hat{q}_s] = \frac{\hbar}{i} \delta_{\vec{k},\vec{s}}. \tag{2.23}$$

The subsidiary condition are now

$$(\hat{a}_{-k} + \hat{a}_k^*)\, \Phi = 0, \quad |\vec{k}| \leqslant k_c \tag{2.24a}$$

or

$$\left[\frac{1}{1-\nu_k a_{-k}^* a_{-k}} a_{-k} + a_k^*(1-\nu_k a_k^* a_k)\right] \Phi = 0, \quad |\vec{k}| \leqslant k_c \tag{2.24b}$$

and, finally,

$$[a_{-k} + (1-\nu_k a_{-k}^* a_{-k})\, a_k^*(1-\nu_k a_k^* a_k)]\, \Phi = 0, \quad |\vec{k}| \leqslant k_c. \tag{2.24c}$$

We put

$$\Phi = \prod_{\substack{|\vec{k}| \leqslant k_c \\ k_z > 0}} \Phi_k \cdot \chi(\mathbf{r}_1, \ldots, \mathbf{r}_n) \tag{2.25a}$$

and

$$\Phi_k = \sum_{\substack{l=0 \\ s=0}}^{+\infty} c_k(s, l)\, (a_k^*)^s\, (a_{-k}^*)^l\, \Phi. \tag{2.25b}$$

Simple computation yields

$$\Phi_k = c_k(0, 0) \sum_{s=0}^{+\infty} (-1)^s \frac{1}{(1-s\nu_k)^2\, s!} \prod_{l=0}^{s} (1-l\nu_k)^2\, (a_k^* a_{-k}^*)^s\, \Phi_0, \tag{2.25c}$$

with

$$\Phi_0^* \Phi_0 = 1, \quad a_k \Phi_0 = 0, \quad \Phi_0^* a_k^* = 0. \tag{2.25d}$$

We cut off the infinite sum in (2.25c) putting

$$\nu_k = \frac{1}{n_k}, \quad n_k \gg 1, \tag{2.25e}$$

wherein n_k is a natural number. Substituting (2.25e) yields

$$\Phi_k \equiv \Phi_k^{n_k} = c_k(0,0)\,(n_k!)^2 \sum_{s=0}^{n_k} (-1)^s \frac{1}{n_k^{2s}\,[(n_k-s)!]^2\,s!}\,(a_k^* a_{-k}^*)^s\,\Phi_0 \tag{2.26}$$

or, on normalization

$$\Phi_k^{n_k} = \frac{n_k^{2n_k}}{\left(\sum_{s=0}^{n_k} \frac{n_k^{4s}}{(s!)^4}\right)^{1/2}} \sum_{s=0}^{n_k} (-1)^s \frac{1}{n_k^{2s}\,[(n_k-s)!]^2\,s!}\,(a_k^* a_{-k}^*)^s\,\Phi_0 . \tag{2.27}$$

Thus it has been proved that the original formulation of the Bohm — Pines theory can be approximated to any degree of accuracy, provided the oscillator operators are replaced by their nearly-Hermitian analogues. The theory proposed differs from that given in (1958a), since the equivalence with Schrödinger' equation is now direct and not on average. This is made possible by (2.23).

3. The partition function

In order to derive the correct statistical function, we apply the identity, Dyson (1956),

$$e^{-\beta(\hat{H}_1+\hat{H}_2} = \sum_{m=0}^{+\infty} (-1)^m \int_0^{\beta} d\beta_1 \int_0^{\beta_1} d\beta_2 \ldots \int_0^{\beta_{m-1}} d\beta_m\, e^{-\beta\hat{H}_1} \cdot e^{\beta_1\hat{H}_1}\hat{H}_2\, e^{-\beta_1\hat{H}_1} \cdot e^{\beta_2\hat{H}_1}\hat{H}_2 e^{-\beta_2\hat{H}_1} \times$$

$$\times \ldots \times e^{\beta_m\hat{H}_1}\hat{H}_2\, e^{-\beta_m\hat{H}_1},\ [\hat{H}_1, \hat{H}_2] \neq 0. \tag{3.1}$$

The identity is proved in Appendix

We choose the extended Hamiltonian and the subsidiary conditions according to the author's paper (1958a):

$$\hat{\mathcal{H}}_{ext} = \hat{H} + \frac{1}{4} \sum_{|\vec{\lambda}| \leqslant \lambda_c} \hbar\omega_\lambda (a_\lambda^* a_\lambda + a_\lambda a_\lambda^* + a_\lambda a_{-\lambda} + a_\lambda^* a_{-\lambda}^*) -$$

$$- \sum_{|\vec{\lambda}| \leqslant \lambda_c} h_\lambda \hbar\omega_\lambda (a_{-\lambda} + a_\lambda^*)\,\varrho_\lambda - \frac{1}{4} \sum_{|\vec{\lambda}| \leqslant \lambda_c} \frac{1-x_\lambda}{1+x_\lambda}\,\hbar\omega_\lambda, \tag{3.2}$$

$$(a_{-\lambda} + x_\lambda a_\lambda^*)\,\Phi = 0, \quad |\vec{\lambda}| \leqslant \lambda_c, \tag{3.3}$$

where the x_λ are renormalizing parameters

$$0 \leqslant x_\lambda < 1, \tag{3.4}$$

and

$$h_\lambda = \left(\frac{2\pi}{V\hbar\omega_\lambda \lambda^2}\right)^{1/2}.$$

In the foregoing relations $\vec{\lambda}$ is the reciprocal lattice vector, ω_λ — the frequency of the collective oscillations,

$$\omega_\lambda^2 \approx \omega_p^2 = \frac{4\pi n\varepsilon^2}{\mu V}, \quad \frac{1}{\mu} = \frac{1}{m} + \frac{Z}{M}, \tag{3.5}$$

n — the number of electrons, Z — the number of valence electrons per atom, m and M — the masses of electron and ion-core respectively, ϱ_λ — the Fourier transform of charge density and $\hat{H}$ the energy operator of Schrödinger's equation

$$\hat{H} = \sum_{i=1}^{n} \frac{\hat{\boldsymbol{p}}_i^2}{2m} + \sum_{\alpha=1}^{N} \frac{\hat{\boldsymbol{p}}_\alpha^2}{2M} + \frac{2\pi}{V} \sum_{\vec{\lambda}(\neq 0)} \frac{\varrho_\lambda \varrho_{-\lambda} - (1+Z)\, n\varepsilon^2}{\lambda^2}. \tag{3.6}$$

The total charge of the system is assumed to be zero.

We have further

$$\Phi = \prod_{\substack{|\vec{\lambda}| \leqslant \lambda_c \\ \lambda_z > 0}} (1 - x_\lambda^2)^{1/2}\, e^{-x_\lambda a_\lambda^* a_{-\lambda}^*}\, \Phi_0 \cdot \chi(\ldots \boldsymbol{r}_i \ldots; \ldots \boldsymbol{r}_\alpha \ldots), \tag{3.7}$$

with

$$\hat{H}\chi(\ldots \boldsymbol{r}_i \ldots; \ldots \boldsymbol{r}_\alpha \ldots) = E\chi(\ldots \boldsymbol{r}_i \ldots; \ldots \boldsymbol{r}_\alpha \ldots). \tag{3.8}$$

Applying the subsidiary conditions (3.3) we now transform certain non-diagonal terms and the interaction member of the Hamiltonian (3,2). This yields

$$a_{-\lambda}\Phi = -x_\lambda a_\lambda^* \Phi, \quad a_\lambda a_{-\lambda}\Phi = -x_\lambda a_\lambda a_\lambda^* \Phi, \tag{3.9a}$$

$$a_{-\lambda}^* \Phi = -\frac{1}{x_\lambda} a_\lambda \Phi, \quad a_\lambda^* a_{-\lambda}^* \Phi = -\frac{1}{x_\lambda} a_\lambda^* a_\lambda \Phi_\lambda. \tag{3.9b}$$

The applied transtormation is permissible, when the difference $1-x_\lambda$ is sufficiently small, since the Hamiltonian (3.2) and the operator of subsidiary conditions (3.3) do not commute.

With the relations (3.9a), (3.9b), (3.9c) and replacing ω_λ by ω_p we have

$$\hat{\mathcal{H}}_{\text{ext}} = \hat{H} + \sum_{|\vec{\lambda}| \leqslant \lambda_c} \frac{\hbar\Omega_\lambda}{2} a_\lambda^* a_\lambda - \sum_{|\vec{\lambda}| \leqslant \lambda_c} h_\lambda \hbar\omega_p (1 - x_\lambda)\, a_\lambda^* \varrho_\lambda + \sum_{\substack{|\vec{\lambda}| \leqslant \lambda_c \\ \lambda_z > 0}} \frac{\hbar\omega_p}{2} \frac{x_\lambda (1 - x_\lambda)}{1 + x_\lambda}, \tag{3.10}$$

wherein

$$\Omega_\lambda = \omega_p \left(1 - \frac{1 + x_\lambda^2}{2x_\lambda}\right). \tag{3.11}$$

It is convenient to divide the Hamiltonian (3.10) into three parts

$$\hat{\mathscr{H}}_{\text{ext}} = \hat{H}_1 + \hat{H}_2 + C, \tag{3.12a}$$

with

$$\hat{H}_1 = \hat{H} + \hat{h}_1, \qquad h_1 = \sum_{|\vec{\lambda}| \leqslant \lambda_c} \frac{\hbar \Omega_\lambda}{2} a_\lambda^* a_\lambda, \tag{3.12b}$$

$$\hat{H}_2 = -\sum_{|\vec{\lambda}| \leqslant \lambda_c} h_\lambda \hbar \omega_p (1 - x_\lambda) a_\lambda^* \varrho_\lambda, \tag{3.12c}$$

$$C = \sum_{\substack{|\vec{\lambda}| \leqslant \lambda_c \\ \lambda_z > 0}} \frac{\hbar \omega_p}{2} \frac{x_\lambda (1 - x_\lambda)}{1 + x_\lambda}. \tag{3.12d}$$

We can now proceed to calculate the partition function, By (3.7) the trace of $exp\ (-\beta \hat{\mathscr{H}}_{\text{ext}})$ (where $\beta = 1/kT$, k — Boltzmann's constant, T — the absolute temperature) is computed by averaging the exponential over the plasmon part and taking the spur with help of the functions $\chi (\ldots \boldsymbol{r}_i \ldots; \ldots \boldsymbol{r}_\alpha \ldots)$. Thereby

$$Z = Tr < e^{-\beta \hat{\mathscr{H}}_{\text{ext}}} >, \tag{3.13}$$

where the mean $<\ldots>$ denotes

$$< \hat{A} > = \prod_{\substack{|\vec{\lambda}| \leqslant \lambda_c \\ \lambda_z > 0}} (1 - x_\lambda^2) \Phi_0^* \prod_{\substack{|\vec{\sigma}| \leqslant \lambda_c \\ \sigma_z > 0}} e^{-x_\sigma a_\sigma a_{-\sigma}} \hat{A} \prod_{\substack{|\vec{\varkappa}| \leqslant \lambda_c \\ \varkappa_z > 0}} e^{-x_\varkappa a_\varkappa^* a_{-\varkappa}^*} \Phi_0. \tag{3.14}$$

It is convenient to pass to the new representation of oscillators and charge Fourier transform:

$$a_\lambda (\beta) = e^{\beta \hat{H}_1} a_\lambda e^{-\beta \hat{H}_1} = e^{\beta \hat{H}_1} a_\lambda e^{-\beta \hat{H}_1}, \tag{3.15a}$$

$$a_\lambda^* (\beta) = e^{\beta \hat{H}_1} a_\lambda^* e^{-\beta \hat{H}_1}, \tag{3.15b}$$

$$\hat{\varrho} (\beta) = e^{\beta \hat{H}_1} \varrho_\lambda e^{-\beta \hat{H}_1} = e^{\beta \hat{H}_1} \varrho_\lambda e^{-\beta \hat{H}_1}. \tag{3.15c}$$

The representation introduced resembles the Tomonaga — Schwinger representation, at least with respect to the oscillator operators; the role of the time is played here by the parameter β.

We have then

$$<e^{-\beta\hat{\mathcal{H}}_{\text{ext}}}>=e^{-\beta C}<e^{-\beta(\hat{H}_1+\hat{H}_2)}>=e^{-\beta C}\sum_{m=0}^{+\infty}(-1)^m\int_0^{\beta}d\beta_1\cdots\int_0^{\beta_{m-1}}d\beta_m<e^{-\beta\hat{H}_1}\hat{H}_2(\beta_1)\times$$

$$\times\hat{H}_2(\beta)\ldots\hat{H}_2(\beta_m)>=e^{-\beta C}\{<e^{-\beta\hat{H}_1}>-\int_0^{\beta}d\beta_1<e^{-\beta\hat{H}_1}\hat{H}_2(\beta_1)>+$$

$$+\int_0^{\beta}d\beta_1\int_0^{\beta_1}d\beta_2<e^{-\beta\hat{H}_1}\hat{H}_2(\beta_1)\hat{H}_2(\beta_2)>-\int_0^{\beta}d\beta_1\int_0^{\beta_1}d\beta_1\int_0^{\beta_2}d\beta_3<e^{-\beta\hat{H}_1}\hat{H}_2(\beta_1)\hat{H}_2(\beta_2)\times$$

$$\times\hat{H}_2(\beta_3)>+\int_0^{\beta}d\beta_1\int_0^{\beta_1}d\beta_2\int_0^{\beta_2}d\beta_3\int_0^{\beta_3}d\beta_4<e^{-\beta\hat{H}_1}\hat{H}_2(\beta_1)\hat{H}_2(\beta_2)\hat{H}_2(\beta_3)\times$$

$$\times\hat{H}_2(\beta_4)>-\ldots\},\tag{3.16}$$

wherein

$$\hat{H}_2(\beta_i)=e^{\beta_i\hat{H}_1}\hat{H}_2\,e^{-\beta_i\hat{H}_1}.\tag{3.17}$$

The relation

$$\Phi_0^*\,a_{\vec{\lambda}}^*=0$$

yields

$$\Phi_0^*=e^{-\beta\hat{H}}\,\Phi_0^*\,e^{\beta\hat{H}_1},\tag{3.18a}$$

hence

$$<e^{-\beta\hat{H}_1}\hat{H}_2(\beta_1)\hat{H}_2(\beta_2)\ldots\hat{H}_2(\beta_m)>=e^{-\beta\hat{H}}\prod_{\substack{|\vec{\lambda}|\leqslant\lambda_c\\ \lambda_z>0}}(1-x_\lambda^2)\,\Phi_0^*\prod_{\substack{|\vec{\sigma}|\leqslant\lambda_c\\ \sigma_z>0}}e^{-x_\sigma a_\sigma(\beta)a_{-\sigma}(\beta)}\times$$

$$\times\hat{H}_2(\beta_1)\hat{H}_2(\beta_2)\ldots\hat{H}_2(\beta_m)\prod_{\substack{|\vec{\varkappa}|\leqslant\lambda_c\\ \varkappa_z>0}}e^{-x\varkappa a_{\varkappa}^*(0)a_{-\varkappa}^*(0)}\,\Phi_0,\tag{3.18b}$$

with

$$a_{\vec{\lambda}}^*(0)=e^{0\cdot\hat{H}_1}\,a_{\vec{\lambda}}^*\,e^{-0\cdot\hat{H}_1}\equiv a_{\vec{\lambda}}^*\tag{3.18c}$$

The following relations are readily proved:

$$[a_{\vec{\lambda}}(\beta_i),\,a_{\vec{\sigma}}^*(\beta_j)]=\delta_{\vec{\lambda},\vec{\sigma}}\,e^{(\beta_j-\beta_i)\hbar\Omega_\sigma/2}\tag{3.19a}$$

and, quite generally,

$$a_{\vec{\lambda}}^l(\beta_i)\,[a_{\vec{\lambda}}^*(\beta_j)]^s=\sum_{r=0}^{\min(l,s)}\binom{l}{r}\binom{s}{r}r!\,e^{(\beta_j-\beta_i)r\hbar\Omega_\lambda/2}\,[a_{\vec{\lambda}}^*(\beta_j)]^{s-r}\,a_{\vec{\lambda}}^{l-r}(\beta_i).\tag{3.19b}$$

The first term of the expansion (3.16) is now

$$<e^{-\beta\hat{H}_1}> =$$

$$=e^{-\beta H}\prod_{\substack{|\vec{\lambda}|\leqslant\lambda_c\\ \lambda_z>0}}(1-x_\lambda^2)\,\Phi_0^*\exp\Big[-\sum_{\substack{|\vec{\lambda}|\leqslant\lambda_c\\ \lambda_z>0}}x_\lambda a_\lambda(\beta)\,a_{-\lambda}(\beta)\Big]\cdot\exp\Big[-\sum_{\substack{|\vec{\lambda}|\leqslant\lambda_c\\ \lambda_z>0}}x_\lambda a_\lambda^*(0)\,a_{-\lambda}^*(0)\Big]\Phi_0=$$

$$=e^{-\beta H}\prod_{\substack{|\vec{\lambda}|\leqslant\lambda_c\\ \lambda_z>0}}(1-x_\lambda^2)\,\Phi_0^*\exp\left[-x_\lambda a_\lambda(\beta)\,a_{-\lambda}(\beta)\right]\cdot\exp\left[-x_\lambda a_\lambda^*(0)\,a_{-\lambda}^*(0)\right]\cdot\Phi_0=$$

$$=e^{-\beta\hat{H}}\prod_{\substack{|\vec{\lambda}|\leqslant\lambda_c\\ \lambda_z>0}}(1-x_\lambda^2)\sum_{\substack{l=0\\ s=0}}^{+\infty}\frac{(-x_\lambda)^{l+s}}{l!\,s!}\,\Phi_0^*\,a_\lambda^l(\beta)\,a_{-\lambda}^l(\beta)\,[a_\lambda^*(0)]^s\,[a_{-\lambda}^*(0)]^s\,\Phi_0=$$

$$=e^{-\beta\hat{H}}\prod_{\substack{|\vec{\lambda}|\leqslant\lambda_c\\ \lambda_z>0}}(1-x_\lambda^2)\sum_{\substack{l=0\\ s=0}}^{-\infty}\frac{(-x_\lambda)^{l+s}}{l!\,s!}\,l!\,s!\,\delta_{s,l}\,e^{-\beta S\hbar\Omega_\lambda}=e^{-\beta\hat{H}}\prod_{\substack{|\vec{\lambda}|\leqslant\lambda_c\\ \lambda_z>0}}\frac{1-x_\lambda^2}{1-x_\lambda^2\,e^{-\beta\hbar\Omega_\lambda}}\,. \tag{3.20}$$

The second term vanishes;

$$<e^{-\beta\hat{H}_1}\,\hat{H}_2(\beta_1)>=0, \tag{3.21}$$

as all matrix elements with odd products of $\hat{H}_2(\beta_i)$ vanish. This results from the fact that the plasmon part of the function (3.7) has the form of even products of creation and desctruction boson operators. Quite similarly the even products of a_λ^* vanish, provided the sum of index vectors $\vec{\lambda}$ is non-zero.

In order to compute the third term in eq. (3.16) we note that

$$\hat{H}_2(\beta_1)\,\hat{H}_2(\beta_2)=\sum_{\substack{|\vec{\lambda}|\leqslant\lambda_c\\ \lambda_z>0}}\sum_{\substack{|\vec{\sigma}|\leqslant\lambda_c\\ \sigma_z>0}}h_\lambda h_\sigma(1-x_\lambda)(1-x_\sigma)(\hbar\omega_p)^2\,[a_\lambda^*(\beta_1)\,\hat{}_\lambda(\beta_1)+a_{-\lambda}^*(\beta_1)\,\hat{\varsigma}_{-\lambda}(\beta_1)]\times$$

$$\times[a_\sigma^*(\beta_2)\,\hat{\varrho}_\sigma(\beta_2)+a_{-\sigma}^*(\beta_2)\,\varrho_{-\sigma}(\beta_2)]=\sum_{\substack{|\vec{\lambda}|\leqslant\lambda_c\\ \lambda_z>0}}h_\lambda^2(1-x_\lambda)^2\,(\hbar\omega_p)^2\,[a_\lambda^*(\beta_1)\,a_{-\lambda}^*(\beta_2)\times$$

$$\times\hat{\varrho}_\lambda(\beta_1)\,\hat{\varrho}_{-\lambda}(\beta_2)+a_{-\lambda}^*(\beta_1)\,a_\lambda^*(\beta_2)\,\hat{\varrho}_{-\lambda}(\beta_1)\,\hat{\varrho}_\lambda(\beta_2)]+\ldots \tag{3.22a}$$

The terms marked by dots vanish on averaging; hence

$$<e^{-\beta\hat{H}_1}\,\hat{H}_2(\beta_1)\,\hat{H}_2(\beta_2)>=e^{-\beta\hat{H}}(\hbar\omega_p)^2\sum_{\substack{|\vec{\sigma}|\leqslant\lambda_c\\ \sigma_z>0}}h_\sigma^2(1-x_\sigma^2)\,(1-x_\sigma)^2\,\Pi^{(\sigma)}_{\substack{|\vec{\lambda}|\leqslant\lambda_c\\ \lambda_z>0}}\frac{1-x_\lambda^2}{1-x_\lambda^2\,e^{-\beta\hbar\Omega_\lambda}}\times$$

$$\times\Phi_0^*\,e^{-x_\sigma a_\sigma(\beta)\,a_{-\sigma}(\beta)}\,a_\sigma^*(\beta_1)\,a_{-\sigma}^*(\beta_2)\,e^{-x_\sigma a_\sigma^*(0)\,a_{-\sigma}^*(0)}\,\Phi_0[\hat{\varrho}_\sigma(\beta_1)\,\hat{\varrho}_{-\sigma}(\beta_2)+\hat{\varrho}_{-\sigma}(\beta_1)\,\hat{\varrho}_\sigma(\beta_2)]=$$

$$=-e^{-\beta\hat{H}}(\hbar\omega_p)^2\sum_{\substack{|\vec{\sigma}|\leqslant\lambda_c\\ \sigma_z>0}}h_\sigma^2(1-x_\sigma^2)\,(1-x_\sigma)^2\,\Pi^{(\sigma)}_{\substack{|\vec{\lambda}|\leqslant\lambda_c\\ \lambda_z>0}}\frac{1-x_\lambda^2}{1-x_\lambda^2\,e^{-\beta\hbar\Omega_\lambda}}\,\frac{x_\sigma\,e^{(\beta_1+\beta_2-2\beta)\hbar\Omega_\sigma/2}}{(1-x_\sigma^2\,e^{-\beta\hbar\Omega_\sigma})^2}\times$$

$$\times[\hat{\varrho}_\sigma(\beta_1)\,\hat{\varrho}_{-\sigma}(\beta_2)+\hat{\varrho}_{-\sigma}(\beta_1)\,\hat{\varrho}_\sigma(\beta_2)]. \tag{3.22b}$$

Finally, we have

$$e^{-\beta\hat{H}_1}\hat{H}_2(\beta_1)\,\hat{H}_2(\beta_2) > = -\,e^{-\beta\hat{H}} \prod_{\substack{|\vec{\lambda}|\leqslant\lambda_c \\ \lambda_z>0}} \frac{1-x_\lambda^2}{1-x_\lambda^2\,e^{-\beta\hbar\Omega_\lambda}}\,(\hbar\omega_p)^2 \sum_{|\vec{\sigma}|\leqslant\lambda_c} \frac{h_\sigma^2\,x_\sigma(1-x_\sigma)^2}{1-x_\sigma^2\,e^{-\beta\hbar\Omega_\sigma}} \times$$

$$\times\, e^{(\beta_1+\beta_2-2\beta)\hbar\Omega_\sigma/2}\cdot\hat{\varrho}_\sigma(\beta_1)\,\hat{\varrho}_{-\sigma}(\beta_2). \tag{3.23}$$

The higher expansion terms, which are somewhat more involved. are of similar structure, and exact investigation proves that they are not necessary for the present computation.

We have now

$$<e^{-\beta\hat{\mathcal{H}}^{\mathrm{ext}}}> = e^{-\beta H}\left\{e^{-\beta C} \prod_{\substack{|\vec{\lambda}|\leqslant\lambda_c \\ \lambda_z>0}} \frac{1-x_\lambda^2}{1-x_\lambda^2\,e^{-\beta\hbar\Omega_\lambda}}\left[1-(\hbar\omega_p)^2 \sum_{|\vec{\sigma}|\leqslant\lambda_c} \frac{h_\sigma^2\,x_\sigma(1-x_\sigma)^2}{1-x_\sigma^2\,e^{-\beta\hbar\Omega_\sigma}} \times\right.\right.$$

$$\left.\left.\times\, e^{-\beta\hbar\Omega_\sigma}\int_0^\beta d\beta_1 \int_0^\beta d\beta_2\, e^{\beta_1\hbar\Omega_\sigma/2}\,\hat{\varrho}_\sigma(\beta_1)\,e^{\beta_1\hbar\Omega_\sigma/2}\,\hat{\varrho}_{-\sigma}(\beta_2)+\ldots\right]\right\}. \tag{3.24}$$

Let us investigate the form assumed by the equation (3.24) for the Bohm — Pines (1953b) subsidiary conditions. We have:

$$x_\lambda = 1-\delta_\lambda, \qquad 0\leqslant\delta_\lambda\ll 1, \tag{3.25}$$

$$C = \sum_{\substack{|\vec{\lambda}|\leqslant\lambda_c \\ \lambda_z>0}} \frac{\hbar\omega_p}{2}\,\frac{x_\lambda(1-x_\lambda)}{1+x_\lambda} = \sum_{\substack{|\vec{\lambda}|\leqslant\lambda_c \\ \lambda_z>0}} \frac{\hbar\omega_p}{2}\,\frac{\delta_\lambda(1-\delta_\lambda)}{2-\delta_\lambda}. \tag{3.26}$$

For sufficiently small δ_λ,

$$e^{-\beta C} = \prod_{\substack{|\vec{\lambda}|\leqslant\lambda_c \\ \lambda_z>0}} e^{-\beta\frac{\hbar\omega_p}{2}\frac{\delta_\lambda(1-\delta_\lambda F)}{2-\delta_\lambda}} \approx 1. \tag{3.27}$$

The quantity (3.11) in this case assumes the form

$$\Omega_\lambda = \omega_p\left(1-\frac{1+x_\lambda^2}{2x_\lambda}\right) = \omega_p\left[1-\frac{1}{2\,(1-\delta_\lambda)}-\frac{1-\delta_\lambda}{2}\right] =$$

$$= \omega_p\left[1-\frac{1}{2}\,(1+\delta_\lambda+\delta_\lambda^2+\ldots)-\frac{1}{2}+\frac{1}{2}\,\delta_\lambda\right] = -\,\frac{\omega_p}{2}\,\delta_\lambda^2. \tag{3.28}$$

The expression $1-x_\lambda^2/1-x_\lambda^2\,e^{-\beta\hbar\Omega_\lambda}$ transforms to

$$\frac{1-x_\lambda^2}{1-x_\lambda^2\,e^{-\beta\hbar\Omega_\lambda}} = \frac{1-(1-\delta_\lambda)^2}{1-(1-\delta_\lambda)^2\,e^{\beta\hbar\omega_p\,\delta_\lambda^2/2}} = \frac{2\,\delta_\lambda-\delta_\lambda^2}{2\,\delta_\lambda-(1+\beta\hbar\omega_p/2)\,\delta_\lambda^2} \approx 1+\beta\hbar\omega_p\,\delta_\lambda/4. \tag{3.29}$$

Finally

$$e^{-\beta\hbar\Omega_\sigma}\int_0^\beta d\beta_1\int_0^{\beta_1} d\beta_2\, e^{\beta_1\frac{\hbar\Omega_\sigma}{2}}\,\hat{\varrho}_\sigma(\beta_1)\,e^{\beta_2\frac{\hbar\Omega_\sigma}{2}}\,\hat{\varrho}_{-\sigma}(\beta_2)\approx\int_0^\beta d\beta_1\int_0^{\beta_1} d\beta_2\,\hat{\varrho}_\sigma(\beta_1)\,\hat{\varrho}_{-\sigma}(\beta_2) \tag{3.28e}$$

and

$$\frac{x_\sigma(1-x_\sigma)^2}{1-x_\sigma^2\,e^{-\beta\hbar\Omega_\sigma}}=\frac{\delta_\sigma^2(1-\delta_\sigma)}{2\delta_\sigma-(1+\beta\hbar\omega_\sigma/2)\,\delta_\sigma^2}\approx\frac{1}{2}\,\delta_\sigma. \tag{3.31}$$

We have now

$$<e^{-\beta\hat{\mathscr{H}}_{\rm ext}}>=e^{-\beta\hat{H}}\prod_{\substack{|\vec{\lambda}|\leqslant\lambda_c\\ \lambda_z>0}}e^{-\beta\frac{\hbar\omega_p}{2}\frac{\delta_\lambda(1-\delta_\lambda)}{2-\delta_\lambda}}\times(1+\beta\hbar\omega_p\,\delta_\lambda/2)\times$$

$$\times\left[1-(\hbar\omega_p)^2\sum_{|\vec{\sigma}|\leqslant\lambda_c}h_\sigma^2\delta_\sigma/2\int_0^\beta d\beta_1\int_0^{\beta_1}d\beta_2\,\hat{\varrho}_\sigma(\beta_1)\,\hat{\varrho}_{-\sigma}(\beta_2)+\ldots\right]=$$

$$=e^{-\beta\hat{H}}\prod_{\substack{|\vec{\lambda}|\leqslant\lambda_c\\ \lambda_z>0}}(1-\beta\hbar\omega_p\,\delta_\lambda/4)(1+\beta\hbar\omega_p\,\delta_\lambda/4)\left[1-(\hbar\omega_p)^2\sum_{|\vec{\sigma}|\leqslant\lambda_c}h_\sigma^2\delta_\sigma/2\cdot\int_0^\beta d\beta_1\int_0^{\beta_1}d\beta_2\,\hat{\varrho}_\sigma(\beta_1)\times\right.$$

$$\left.\times\,\hat{\varrho}_{-\sigma}(\beta_2)+\ldots\right]=e^{-\beta\hat{H}}\left[1-\frac{(\hbar\omega_p)^2}{2}\sum_{|\vec{\sigma}|\leqslant\lambda_c}h_\sigma^2\delta_\sigma\int_0^\beta d\beta_1\int_0^{\beta_1}d\beta_2\,\hat{\varrho}_\sigma(\beta_1)\,\hat{\varrho}_{-\sigma}(\beta_2)+\ldots\right] \tag{3.32}$$

For sufficiently small δ_0 one gets

$$Z=\mathrm{Tr}<e^{-\beta\hat{\mathscr{H}}_{\rm ext}}>=\mathrm{Tr}\,e^{-\beta\hat{H}} \tag{3.29}$$

The form of statistical function obtained is thus correct.

In the second extreme case, namely Kanazawa's case, x_λ is equal zero, hence the equations (3.2) and (3.3) assume the form

$$\hat{\mathscr{H}}_{\rm ext}=\hat{H}+\tfrac{1}{4}\sum_{|\vec{\lambda}|\leqslant\lambda_c}\hbar\omega_p\,(a_\lambda+a_\lambda^*)\,(a_{-\lambda}+a_\lambda^*)-$$

$$-\sum_{|\vec{\lambda}|\leqslant\lambda_c}h_\lambda\hbar\omega_\lambda\varrho_\lambda(a_{-\lambda}+a_\lambda^*)-\tfrac{1}{4}\sum_{|\vec{\lambda}|\leqslant\lambda_c}\hbar\omega_\lambda, \tag{3.34a}$$

$$a_\lambda\Phi=0,\qquad|\vec{\lambda}|\leqslant\lambda_c, \tag{3.34b}$$

$$\Phi=\Phi_0\cdot\chi(\ldots\boldsymbol{r}_i\ldots;\ldots\boldsymbol{r}_\alpha\ldots), \tag{3.34c}$$

where Φ_0 is plasmon vacuum vector.

We divide the Hamiltonian (3.34a) a gain into three parst ($\omega_\lambda = \omega_p$),

$$\hat{\mathscr{H}}_{\text{ext}} = \hat{H}_1 + \hat{H}_2 + C, \tag{3.35a}$$

$$\hat{H_1} = \hat{H} + \hat{h}_1, \quad h_1 = \tfrac{1}{4} \sum_{|\vec{\lambda}| \leqslant \lambda_c} \hbar\omega_p \, (a_\lambda + a^*_{-\lambda}) \, (a_{-\lambda} + a^*_\lambda), \tag{3.35b}$$

$$\hat{H}_2 = - \sum_{|\vec{\lambda}| \leqslant \lambda_c} h_\lambda \, \hbar\omega_p \, \varrho_\lambda \, (a_{-\lambda} + a^*_\lambda), \tag{3.35c}$$

$$C = - \sum_{|\vec{\lambda}| \leqslant \lambda_c} \frac{\hbar\omega_p}{4}. \tag{3.35d}$$

Since the plasmon part of the state vector is now the vacuum vector Φ_0 the averaging is very easy one giving

$$< e^{-\beta \hat{\mathscr{H}}_{\text{ext}}} > = e^{-\beta C} \, \Phi^*_0 \, e^{-\beta (\hat{H}_1 + H_2)} \, \Phi_0 = e^{-\beta C} \, \Phi^*_0 \, e^{-\beta \hat{H}_1} \times$$

$$\times \sum_{m=0}^{+\infty} (-1)^m \int_0^\beta d\beta_1 \ldots \int_0^{\beta_{m_1}} d\beta_m \, \hat{H}_2 \, (\beta_1) \ldots \hat{H}_2 \, (\beta_m) \, \Phi_0, \tag{3.36}$$

wherein

$$\hat{H}_2 \, (\beta_i) = e^{\beta_i \hat{H}_1} \, \hat{H}_2 \, e^{-\beta_i \hat{H}_1} = - \sum_{|\vec{\lambda}| \leqslant \lambda_c} h_\lambda \, \hbar\omega_p \, \hat{\varrho}_\lambda \, (\beta_i) \, (a_{-\lambda} + a^*_\lambda). \tag{3.37}$$

We have further

$$< e^{-\beta \hat{\mathscr{H}}_{\text{ext}}} > = e^{-\beta (C + \hat{H})} \, [\Phi^*_0 \, e^{-\beta \hat{h}_1} \Phi_0 + \sum_{|\vec{\lambda}| \leqslant \lambda_c} h_\lambda \, \hbar\omega_p \int_0^\beta d\beta_1 \, \hat{\varrho}_\lambda (\beta_1) \, \Phi^*_0 \, e^{-\beta \hat{h}_1} \times (a_{-\lambda} + a^*_\lambda) \, \Phi_0 +$$

$$+ \sum_{\substack{|\vec{\lambda}| \leqslant \lambda_c \\ |\vec{\sigma}| \leqslant \lambda_c}} h_\lambda \, h_\sigma \, (\hbar\omega_p)^2 \int_0^\beta d\beta_1 \int_0^{\beta_1} d\beta_2 \, \hat{\varrho}_\lambda (\beta_1) \, \varrho_\sigma (\beta_2) \, \Phi^*_0 \, e^{-\beta \hat{h}_1} (a_{-\lambda} + a^*_\lambda) \, (a_{-\sigma} + a^*_\sigma) \, \Phi_0 + \ldots]. \tag{3.38}$$

Let us compute the first term in the expansion (3.38).

$$\Phi^*_0 \, e^{-\beta \hat{h}_1} \, \Phi_0 = \prod_{\substack{|\vec{\lambda}| \leqslant \lambda_c \\ \lambda_z > 0}} \Phi^*_0 \, e^{-\beta \hbar\omega_p / 2 \cdot (a_{-\lambda} + a^*_\lambda)(a_\lambda + a^*_{-\lambda})} \, \Phi_0 = \prod_{\substack{|\vec{\lambda}| \leqslant \lambda_c \\ \lambda_z > 0}} \sum_{s=0}^{+\infty} \frac{(-\beta \hbar\omega_p/2)^s}{s!} \times$$

$$\times \Phi^*_0 \, (a_{-\lambda} + a^*_\lambda)^s \, (a_\lambda + a^*_{-\lambda})^s \, \Phi_0 = \prod_{\substack{|\vec{\lambda}| \leqslant \lambda_c \\ \lambda_z > 0}} \sum_{s=0}^{+\infty} \frac{(-\beta \hbar\omega_p/2)^s}{s!} \, \Phi^*_0 \, a^s_{-\lambda} \, (a^*_{-\lambda})^s \, \Phi_0 =$$

$$= \prod_{\substack{|\vec{\lambda}| \leqslant \lambda_c \\ \lambda_z > 0}} \sum_{s=0}^{+\infty} \frac{(-\beta \hbar\omega_p/2)^s}{s!} \, s! = \prod_{\substack{|\vec{\lambda}| \leqslant \lambda_c \\ \lambda_z > 0}} \frac{1}{1 + \beta \hbar\omega_p/2}, \tag{3.39a}$$

if

$$\beta\hbar\omega_p/2 < 1. \tag{3.39b}$$

We have used the equality 3.19b) ($\beta_i = \beta_j = 0$) and the relations

$$a_\lambda \Phi_0 = 0, \quad \Phi_0^* a_\lambda^* = 0.$$

The condition (3.39b) is not satisfied in low temperatures. The way to overcome this difficulty has been given by Dr A. Pawlikowski. The following computation belongs to him.

Let us write the destruction and creation boson operators as follows:

$$a_\lambda = \frac{1}{\sqrt{2}}(a_\lambda^r + ia_\lambda^i), \quad a_\lambda^+ = \frac{1}{\sqrt{2}}(a_\lambda^{r+} - ia_\lambda^{i+}), \tag{3.40a}$$

$$a_\lambda^r = a_{-\lambda}^r, \quad a_\lambda^i = -a_{-\lambda}^i, \tag{3.40b}$$

where a_λ^r, a_λ^i and a_λ^{r+}, a_λ^{i+} are the real and imaginary parts of destruction and creation operators.

Since, according to (3.40a, b),

$$[a_\lambda^r, a_\lambda^i] = 0, \quad [a_\lambda^{r+}, a_\lambda^{i+}] = 0, \quad [a_\lambda^r, a_\lambda^{i+}] = 0, \tag{3.40c}$$

$$[a_\lambda^r, a_\lambda^{r+}] = 1, \quad [a_\lambda^i, a_\lambda^{i+}] = 1, \tag{3.40d}$$

the Hamiltonian part (3.35b) may be written as

$$\hat{h}_1 = \frac{\hbar\omega_p}{4} \sum_{|\vec{\lambda}| \leqslant \lambda_c} (a_\lambda + a_{-\lambda}^+)(a_{-\lambda} + a_\lambda^+) = \frac{\hbar\omega_p}{4} \sum_{|\vec{\lambda}| \leqslant \lambda_c} (a_\lambda^r + a_\lambda^{r+})^2 (a_\lambda^i + a_\lambda^{i+})^2. \tag{3.41}$$

When we denote the plasmon vacuum vector as $|0>$, we obtain instead of (3.39a) the following expression:

$$<0|e^{-\beta\hat{\hbar}_1}|0> = \prod_{\substack{|\vec{\lambda}| \leqslant \lambda_c \\ \lambda_z > 0}} <0|e^{-\beta\hbar\omega_p/4 \cdot (a_\lambda^r + a_\lambda^{r+})^2 (a_\lambda^i + a_\lambda^{i+})^2} \cdot |0> =$$

$$= \prod_{\substack{|\vec{\lambda}| \leqslant \lambda_c \\ \lambda_z > 0}} <0|e^{-\sigma(a_\lambda^r + a_\lambda^{r+})^2}|0> <0|e^{-\sigma(a_\lambda^i + a_\lambda^{i+})^2}|0>, \tag{3.42}$$

with

$$\sigma = \frac{\beta\hbar\omega_p}{4}. \tag{3.43}$$

Each of the square terms in (3.42) may be brought into the linear form by means of the well known formula

$$e^{-\sigma u^2} = \frac{1}{\sqrt{\pi}} \int_{-\infty}^{+\infty} dx\, e^{-x^2 + 2i\sqrt{\sigma}\, xu}.$$

We have then,

$$< 0 | e^{-\sigma (a_\lambda^r + a_\lambda^{r+})^2} | 0 > = \frac{1}{\sqrt{\pi}} \int_{-\infty}^{+\infty} dx\, e^{-x^2} < 0 | e^{2i\sqrt{\sigma}\, x (a_\lambda^r + a_\lambda^{r+})} | 0 > . \tag{3.44}$$

On the other hand two boson operators satisfy the relation

$$e^{\alpha (a + a^+)} = e^{\alpha^2/2} \cdot e^{\alpha a^+} \cdot e^{\alpha a} . \tag{3.45}$$

In connection with the last formula we obtain finally

$$< | 0\, e^{-\sigma (a_\lambda^r + a_\lambda^{r+})^2} | 0 > = < 0 | e^{-\sigma (a_\lambda^t + a_\lambda^{t+})^2} | 0 > = \frac{1}{\sqrt{\pi}} \int_{-\infty}^{+\infty} dx \cdot e^{-(1+2\sigma)x^2} \times$$

$$\times < 0 | e^{2ix\sqrt{\sigma}\, a_\lambda^r} \cdot e^{2ix\sqrt{\sigma}\, a_\lambda^r} | 0 > = \frac{1}{\sqrt{\pi}} \int_{-\infty}^{+\infty} dx\, e^{-(1+2\sigma)x^2} = \frac{1}{(1+2\sigma)^{1/2}} . \tag{3.46}$$

Returning to the equation (3.42) we have

$$< 0 | e^{-\beta \hat{h}_1} | 0 > = \prod_{\substack{|\vec{\lambda}| \leqslant \lambda_c \\ \lambda_z > 0}} \left(\frac{1}{\sqrt{1+2\sigma}} \right)^2 = \prod_{\substack{|\vec{\lambda}| \leqslant \lambda_c \\ \lambda_z > 0}} \frac{1}{1+2\sigma} = \prod_{\substack{|\vec{\lambda}| \leqslant \lambda_c \\ \lambda_z > 0}} \frac{1}{1 + \beta\hbar\omega_p/2} . \tag{3.47}$$

We have then obtained the same result as in (3.39a), but without the supplementary condition

$$\frac{\beta\hbar\omega_p}{2} < 1 .$$

In the expansion (3.38) vanish all odd terms. The second non-vanishing term has the form

$$\sum_{|\lambda| \leqslant \lambda_c} h_\lambda^2 (\hbar\omega_p)^2 \int_0^\beta d\beta_1 \int_0^{\beta_1} d\beta_2\, \hat{\varrho}_\lambda (\beta_1)\, \hat{\varrho}_{-\lambda} (\beta_2)\, \Phi_0^* e^{-\beta \hat{h}_1} (a_{-\lambda} + a_\lambda^*) (a_\lambda + a_\lambda^*)\, \Phi_0 =$$

$$= \prod_{\substack{|\vec{\varkappa}| \leqslant \lambda_c \\ \varkappa_z > 0}} \sum_{|\lambda| \leqslant \lambda_c} h_\lambda^2 (\hbar\omega_p)^2 \int_0^\beta d\beta_1 \int_0^{\beta_1} d\beta_2\, \hat{\varrho}_\lambda (\beta_1)\, \hat{\varrho}_{-\lambda} (\beta_2)\, \Phi_0^* e^{-\beta\hbar\omega_p/2 \cdot (a_\varkappa + a_{-\varkappa}^*)(a_{-\varkappa} + a_\varkappa^*)} \cdot$$

$$\cdot (a_{-\lambda} + a_\lambda^*) (a_\lambda + a_\lambda^*)\, \Phi_0 =$$

$$= 2 \sum_{\substack{|\vec{\lambda}| \leqslant \lambda_c \\ \lambda_z > 0}} h_\lambda^2 (\hbar\omega_p)^2 \int_0^\beta d\beta_1 \int_0^{\beta_1} d\beta_2\, \hat{\varrho}_\lambda (\beta_1)\, \hat{\varrho}_{-\lambda} (\beta_2)\, \Phi_0^* e^{-\beta\hbar\omega_p/2) (a_{-\lambda} + a_\lambda^*)(a_\lambda + a_{-\lambda}^*)} \times$$

$$\times (a_{-\lambda} + a_{\lambda}^{*})(a_{\lambda} + a_{-\lambda}^{*}) \cdot \prod_{\substack{|\vec{\sigma}| \leqslant \lambda_c \\ \vec{\sigma} \neq \vec{\lambda} \\ \sigma_z > 0}} e^{-\beta \hbar \omega_p / 2 \cdot (a_{-\sigma} + a_{\sigma}^{*})(a_{\sigma} + a_{-\sigma}^{*})} \Phi_0 = \prod_{\substack{|\vec{\sigma}| \leqslant \lambda_c \\ \sigma_z > 0}} \frac{1}{1 + \beta \hbar \omega / 2} \times$$

$$\times \sum_{|\vec{\lambda}| \leqslant \lambda_c} \frac{h_{\lambda}^{2} (\hbar \omega_p)^2}{1 + \beta \hbar \omega_p / 2} \int_0^{\beta} d\beta_1 \int_0^{\beta_1} d\beta_2 \, \hat{\varrho}_{\lambda}(\beta_1) \, \hat{\varrho}_{-\lambda}(\beta_2). \tag{3.48}$$

From (3.38) and (3.48) we obtain

$$< e^{-\beta \hat{\mathcal{H}}^{\mathrm{ext}}} > = e^{-\beta (C + \hat{H})} \prod_{\substack{|\vec{\sigma}| \leqslant \lambda_c \\ \sigma_z > 0}} \frac{1}{1 + \beta \hbar \omega_p / 2} \left[1 + \sum_{|\vec{\lambda}| \leqslant \lambda_c} \frac{h (\hbar \omega)^2}{1 + \beta \hbar \omega / 2} \times \right.$$

$$\left. \times \int_0^{\beta} d\beta_1 \int_0^{\beta_1} d\beta_2 \, \hat{\varrho}_{\lambda}(\beta_1) \, \hat{\varrho}_{-\lambda}(\beta_2) + \ldots \right]. \tag{3.49}$$

The partition function assumes finally the form

$$Z = Tr < e^{-\beta \hat{\mathcal{H}}^{\mathrm{ext}}} > = e^{-\beta C} \, Tr \, e^{-\beta \hat{H}} \prod_{\substack{|\vec{\sigma}| \leqslant \lambda_c \\ \sigma_z > 0}} \frac{1}{1 + \beta \hbar \omega_p / 2} \left[1 + \right.$$

$$\left. + \sum_{|\vec{\lambda}| \leqslant \lambda_c} \frac{h_{\lambda}^{2} (\hbar \omega_p)^2}{1 + \beta \hbar \omega_p / 2} \int_0^{\beta} d\beta_1 \int_0^{\beta_1} d\beta_2 \, \hat{\varrho}_{\lambda}(\beta_1) \, \hat{\varrho}_{-\lambda}(\beta_2) + \ldots \right]. \tag{3.50}$$

We see that Kazanawa's theory (1957) leads to the false statistical function. Should we define the renormalization parameters as

$$x_{\lambda} = 1 - \frac{1}{\beta \hbar \omega_p} = 1 - \frac{kT}{\hbar \omega_p}, \tag{3.30}$$

this would suggest that the formulation of collective description given by Bohm and Pines (1953b) is valid for sufficiently low temperatures, whereas the approach of Kazanawa (1957) extends into range of temperatures wherein heat phenomena (electron collisions) play an important part; however in the latter circumstances the formalism of the theory becomes non-linear, Bohm and Pines (1952a).

4. *Conclusion*

In section 2 a new renormalizing procedure is formulated. The variant of collective description proposed by the author is nearly-Hermitan and approximates the Bohm and Pines theory to any desired degree of exactness. Equivalence with the many electron Schrädinger equation is direct.

In section 3 an exact statistical function is derived. In connection with the computations it was found that the Bohm — Pines subsidiary conditions, improved by

introducing a certain renormalizing term, yield the exact partition function, whereas the Kanazawa's supplementary conditions lead to false results. The possible interpretation of the renormalizing parameters as functions of absolute temperature is suggested.

The author wishes to express his best thanks to Professor R. Ingarden for his inspiration to enter upon the present investigation and his scientific coworker Dr A. Pawlikowski for the computation concerning the partition function in the case of Kanazawa's subsidiary conditions.

The author is also greatly indebted to Professor Dr S. Szczeniowski for his valuable help during the preparation of the present paper.

I thank also Mr R. Ferchmin for explaining some interpretational aspects of Dyson paper (1956).

Appendix

We prove the validity of (3.1). We have

$$(\hat{H}_1+\hat{H}_2)=\hat{H}_1^s+\sum_{l_1=0}^{s-1}\hat{H}_1^{l_1}\hat{H}_2\hat{H}_1^{s-1-l_1}+\sum_{l_1=0}^{s-2}\sum_{l_2=0}^{s-2-l_1}\hat{H}_1^{l_1}\hat{H}_2\hat{H}_1^{l_2}\hat{H}_2\hat{H}^{s-2-(l_1+l_2)}+$$

$$+\ldots+\sum_{l_1=0}^{s-k}\sum_{l_2=0}^{s-k-l_1}\ldots\sum_{l_k=0}^{s-k-(l_1+\ldots+l_{k-1})}\hat{H}_1^{l_1}\hat{H}_2\hat{H}_1^{l_2}\hat{H}_2\ldots\hat{H}_1^{l_k}\hat{H}_2\hat{H}^{s-k-(l_1+\ldots+l_k)}+\ldots+\hat{H}_2^s. \tag{A.1}$$

Further

$$e^{-\beta(\hat{H}_1+\hat{H}_2)}=\sum_{s=0}^{+\infty}\frac{(-1)^s\beta^s}{s!}\hat{H}_1^s+\sum_{s=1}^{+\infty}\frac{(-1)^s\beta^s}{s!}\sum_{l_1=0}^{s-1}\hat{H}_1^{l_1}\hat{H}_2\hat{H}_1^{s-2-l_1}+$$

$$+\sum_{s=2}^{+\infty}\frac{(-1)^s\beta^s}{s!}\sum_{l_1=0}^{s-2}\sum_{l_2=0}^{s-2-l_1}\hat{H}_1^{l_1}\hat{H}_2\hat{H}_1^{l_2}\hat{H}_2\hat{H}_1^{s-2-(l_1+l_2)}+\ldots+$$

$$+\sum_{s=k}^{+\infty}\frac{(-1)^s\beta^s}{s!}\sum_{l_1=0}^{s-k}\sum_{l_2=1}^{s-k-l_1}\ldots\sum_{l_k=0}^{s-k-(l_1+\ldots+l_{k-1})}\hat{H}_1^{l_1}\hat{H}_2\hat{H}_1^{l_2}\hat{H}_2\ldots\hat{H}_1^{l_k}\hat{H}_2\hat{H}^{s-k-(l_1+\ldots+l_k)}+$$

$$+\ldots=e^{-\beta\hat{H}_1}+\sum_{s=0}^{+\infty}\frac{(-1)^{s+1}\beta^{s+1}}{(s+1)!}\sum_{l_1=0}^{s}\hat{H}_1^{l_1}\hat{H}_2\hat{H}_1^{s-l_1}+$$

$$+\sum_{s=0}^{+\infty}\frac{(-1)^{s+2}\beta^{s+2}}{(s+2)!}\sum_{l_1=0}^{s}\sum_{l_2=0}^{s-l_1}\hat{H}_1^{l_1}\hat{H}_2\hat{H}_1^{l_2}\hat{H}_2\hat{H}^{s-l_1-l_2}+\ldots+$$

$$+\sum_{s=0}^{+\infty}\frac{(-1)^{s+k}\beta^{s+k}}{(s+k)!}\sum_{l_1=0}^{s}\sum_{l_2=0}^{s-l_1}\ldots\sum_{l_k=0}^{s-(l_1+\ldots+l_{k-1})}\hat{H}_1^{l_1}\hat{H}_2\hat{H}_1^{l_2}\hat{H}_2\ldots\hat{H}_1^{l_k}\hat{H}_2\hat{H}^{s-(l_1+\ldots+l_k)}+\ldots \tag{A.2}$$

On the other hand,

$$e^{-\beta(\hat{H}_1+\hat{H}_2)} = \sum_{m=0}^{+\infty}(-1)^m \int_0^{\beta} d\beta_1 \int_0^{\beta_1} d\beta_2 \dots \int_0^{\beta_{m-1}} d\beta_m \, e^{(\beta_1-\beta)\hat{H}_1}\hat{H}_2\, e^{(\beta_2-\beta_1)\hat{H}_1}\hat{H}_2 \times$$

$$\times e^{(\beta_m-\beta_{m-1})\hat{H}_1}\hat{H}_2\, e^{-\beta_m\hat{H}_1} = e^{-\beta\hat{H}_1} - \int_0^{\beta} d\beta_1\, e^{(\beta_1-\beta)\hat{H}_1}\hat{H}_2\, e^{-\beta_1\hat{H}_1} + \int_0^{\beta} d\beta_1 \int_0^{\beta_1} d\beta_2\, e^{(\beta_1-\beta)\hat{H}_1} \times$$

$$\times \hat{H}_2 e^{(\beta_2-\beta_1)\hat{H}_1}\hat{H}_2\, e^{-\beta_2\hat{H}_1} + \dots + (-1)^k \int_0^{\beta} d\beta_1 \dots \int_0^{\beta_{k-1}} d\beta_k e^{(\beta_1-\beta)\hat{H}_1}\hat{H}_2 \dots e^{(\beta_k-\beta_{k-1})\hat{H}_1}\hat{H}_2\, e^{-\beta_k\hat{H}_1} + \dots \tag{A.3}$$

The first terms in expansions (A.2) and (A.3) are the identical. Let us compute the second term in (A.3). For this purpose the following integral is required:

$$\int_0^{\beta_i} d\beta_{i+1}(\beta_{i+1}-\beta_i)\,\beta_{i+1}^l = (-1)^s \frac{s!\,l!}{(s+l+1)!}\beta_i^{s+l+1} \quad \text{for} \quad s \gtrless l. \tag{A.4}$$

Then

$$-\int_0^{\beta} d\beta_1\, e^{(\beta_1-\beta)\hat{H}_1}\hat{H}_2\, e^{-\beta_1\hat{H}_1} = \sum_{l=0}^{+\infty}\sum_{s=0}^{+\infty}\frac{(-1)^{l+1}}{l!\,s!}\int_0^{\beta} d\beta_1(\beta_1-\beta)^s\beta_1^l\,\hat{H}_1^s\,\hat{H}_2\,\hat{H}_1^l =$$

$$= \sum_{l=0}^{+\infty}\sum_{s=0}^{+\infty}\frac{(-1)^{s+l+1}}{(s+l+1)!}\beta^{s+l+1}\hat{H}_1^s\,\hat{H}_2\,\hat{H}_1^l = \sum_{n=0}^{+\infty}\frac{(-1)^{n+1}}{(n+1)!}\beta^{n+1}\sum_{s=0}^{n}\hat{H}_1^s\,\hat{H}_2\,\hat{H}_1^{n-s} =$$

$$= \sum_{s=0}^{+\infty}\frac{(-1)^{s+1}\beta^{s+1}}{(s+1)!}\sum_{l_1=0}^{s}\hat{H}_1^{l_1}\,\hat{H}_2\,\hat{H}_1^{s-l_1}. \tag{A.5}$$

The term derived is identical with the second term in expansion (A.2).

Quite generally,

$$\sum_{s=0}^{+\infty}\frac{(-1)^{s+k}\beta^{s+k}}{(s+k)!}\sum_{l_1=0}^{+\infty}\sum_{l_2=0}^{+\infty}\dots\sum_{l_k=0}^{s-(l_1+\dots+l_{k-1})}\hat{H}_1^{l_1}\,\hat{H}_2\,\hat{H}_1^{l_2}\,\hat{H}_2\dots\hat{H}_1^{l_k}\,\hat{H}_2\,\hat{H}^{s-(l_1+\dots+l_k)} =$$

$$= (-1)^k\int_0^{\beta} d\beta_1\int_0^{\beta_1} d\beta_2\dots\int_0^{\beta_{k-1}} d\beta_k\, e^{(\beta_1-\beta)\hat{H}_1}\hat{H}_2\, e^{(\beta_2-\beta_1)\hat{H}_1}\hat{H}_2\dots e^{(\beta_k-\beta_{k-1})\hat{H}_1}\hat{H}_2\, e^{-\beta\hat{H}_1}. \tag{A.6}$$

The equality is proved step by step. According to (A.4) and (A.5),

$$\int_0^{\beta_{k-1}} d\beta_k\, e^{(\beta_k-\beta_{k-1})\hat{H}_1}\hat{H}_2\, e^{-\beta_k\hat{H}_1} = \sum_{n=0}^{+\infty}\frac{(-1)^n\beta_{k-1}^{n+1}}{(n+1)!}\sum_{p=0}^{n}\hat{H}_1^p\,\hat{H}_2\,\hat{H}_1^{n-p}. \tag{A.7a}$$

Furthermore,

$$\int_0^{\beta_{k-2}} d\beta_{k-1} \int_0^{\beta_{k-1}} d\beta_k \, e^{(\beta_{k-1}-\beta_{k-2})\hat{H}_1} \hat{H}_2 \, e^{(\beta_k-\beta_{k-1})\hat{H}_1} \hat{H}_2 \, e^{-\beta_k \hat{H}_1} =$$

$$= \sum_{n=0}^{+\infty} \frac{(-1)^n}{(n+1)!} \int_0^{\beta_{k-2}} d\beta_{k-1} \, \beta_{k-1}^{n+1} \, e^{(\beta_{k-1}-\beta_{k-2})\hat{H}_1} \hat{H}_2 \sum_{p=0}^{n} \hat{H}_1^p \hat{H}_2 \hat{H}_1^{n-p} =$$

$$= \sum_{n=0}^{+\infty} \sum_{s=0}^{+\infty} \frac{(-1)^n}{s!\,(n+1)!} \int_0^{\beta_{k-2}} d\beta_{k-1} \, (\beta_{k-1}-\beta_{k-2})^s \, \beta_{k-1}^{n+1} \hat{H}_1^s \hat{H}_2 \sum_{p=0}^{+\infty} \hat{H}_1^p \hat{H}_2 \hat{H}_1^{n-p} =$$

$$= \sum_{n=0}^{+\infty} \sum_{s=0}^{+\infty} \sum_{p=0}^{n} \frac{(-1)^{n+s}}{s!\,(n+1)!} \frac{s!\,(n+1)!}{(s+n+2)!} \, \beta_{k-2}^{s+n+2} \hat{H}_1^s \hat{H}_2 \hat{H}_1^p \hat{H}_2 \hat{H}_1^{n-p}.$$

We put $n+s = l$, obtaining

$$\int_0^{\beta_{k-2}} d\beta_{k-1} \int_0^{\beta_{k-1}} d\beta_k \, e^{(\beta_{k-1}-\beta_{k-2})\hat{H}_1} \hat{H}_2 \, e^{(\beta_k-\beta_{k-1})\hat{H}_1} \hat{H}_2 \, e^{-\beta_k \hat{H}_1} =$$

$$= \sum_{l=0}^{+\infty} \sum_{s=0}^{l} \sum_{p=0}^{l-s} \frac{(-1)^l}{(l+2)!} \beta_{k-2}^{l+2} \hat{H}_1^s \hat{H}_2 \hat{H}_1^p \hat{H}_2 \hat{H}^{l-s-p}. \qquad \text{(A.7b)}$$

The third integration yields

$$\int_0^{\beta_{k-3}} d\beta_{k-2} \int_0^{\beta_{k-2}} d\beta_{k-1} \int_0^{\beta_{k-1}} d\beta_k \, e^{(\beta_{k-2}-\beta_{k-3})\hat{H}_1} \hat{H}_2 \, e^{(\beta_{k-1}-\beta_{k-2})\hat{H}_1} \hat{H}_2 \, e^{(\beta_k-\beta_{k-1})\hat{H}_1} \hat{H}_2 \, e^{-\beta_k \hat{H}_1} =$$

$$= \sum_{s=0}^{+\infty} \sum_{l_1=0}^{s} \sum_{l_2=0}^{s-l_1} \sum_{l_3=0}^{s-l_1-l_2} \frac{(-1)^s}{(s+3)!} \beta_{k-3}^{s+3} \hat{H}_1^{l_1} \hat{H}_2 \hat{H}_1^{l_2} \hat{H}_2 \hat{H}_1^{l_3} \hat{H}_2 \hat{H}^{s-(l_1+l_2+l_3)}. \qquad \text{(A.7c)}$$

The k-th step gives the identity (A.6).

Let us now investigate the form of the fourth term in (3.16) (the third term vanishes). For this purpose we select from $\hat{H}_2(\beta_1)\,\hat{H}_2(\beta_2)\,\hat{H}_2(\beta_3)\,\hat{H}_2(\beta_4)$ the terms, which do not vanish on averaging. Let us write them symbolically as follows:

$$\sum_{\vec{\lambda},\vec{\sigma}} \sum_{\vec{\varkappa}\,\vec{\varrho}} = \Big(\sum_{\vec{\lambda}=\vec{\sigma}} + \sum_{\vec{\lambda}=-\vec{\sigma}} + \sum_{\substack{\vec{\lambda},\vec{\sigma} \\ \vec{\lambda}\neq\pm\vec{\sigma}}}\Big)\Big(\sum_{\vec{\varkappa}=\vec{\varrho}} + \sum_{\vec{\varkappa}=-\vec{\varrho}} + \sum_{\substack{\vec{\varkappa},\vec{\varrho} \\ \vec{\varkappa}\neq\pm\vec{\varrho}}}\Big) =$$

$$= \sum_{\vec{\lambda}=\vec{\sigma}} \sum_{\vec{\varkappa}=\vec{\varrho}} + \sum_{\vec{\lambda}=\vec{\sigma}} \sum_{\vec{\varkappa}=-\vec{\varrho}} + \sum_{\substack{\vec{\lambda},\vec{\sigma} \\ \vec{\lambda}\neq\pm\vec{\sigma}}} \sum_{\substack{\vec{\varkappa},\vec{\varrho} \\ \vec{\varkappa}\neq\pm\vec{\varrho}}} + \cdots \qquad \text{(A.8)}$$

Hence, according to (3.12c)

$$\hat{H}_2(\beta_1)\hat{H}_2(\beta_2)\hat{H}_2(\beta_3)\hat{H}_2(\beta_4) = (\hbar\omega_p)^4\{\sum_{\substack{|\vec{\lambda}|\leqslant\lambda_c\\ |\vec{\varkappa}|\leqslant\lambda_c}} h_\lambda^2 h_\varkappa^2 (1-x_\lambda)^2(1-x_\varkappa)^2 [a_\lambda^*(\beta_1)\, a_\lambda^*(\beta_2)\, a_\varkappa^*(\beta_3)\times$$

$$\times a_\varkappa^*(\beta_4)\,\hat{\varrho}_\lambda(\beta_1)\,\hat{\varrho}_\lambda(\beta_2)\,\hat{\varrho}_\varkappa(\beta_3)\,\hat{\varrho}_\varkappa(\beta_4) + a_\lambda^*(\beta_1)\, a_{-\lambda}^*(\beta_2)\, a_\varkappa^*(\beta_3)\, a_{-\varkappa}^*(\beta_4)\,\hat{\varrho}_\lambda(\beta_1)\,\hat{\varrho}_{-\lambda}(\beta_2)\,\hat{\varrho}_\varkappa(\beta_3)\times$$

$$\times\hat{\varrho}_{-\varkappa}(\beta_4) + \sum_{\substack{|\vec{\lambda}|\leqslant\lambda_c\\ |\vec{\sigma}|\leqslant\lambda_c\\ \vec{\lambda}\neq\pm\vec{\sigma}}}\sum_{\substack{|\vec{\varkappa}|\leqslant\lambda_c\\ |\vec{\varrho}|\leqslant\lambda_c\\ \vec{\varkappa}\neq\pm\vec{\varrho}}} h_\lambda h_\sigma h_\varkappa h_\varrho (1-x_\lambda)(1-x_\sigma)(1-x_\varkappa)(1-x_\varrho)\, a_\lambda^*(\beta_1)\, a_\sigma^*(\beta_2)\, a_\varkappa^*(\beta_3)\, a_\varrho^*(\beta)\times$$

$$\times\hat{\varrho}_\lambda(\beta_1)\,\hat{\varrho}_\sigma(\beta_2)\,\hat{\varrho}_\varkappa(\beta_3)\,\hat{\varrho}_\varrho(\beta_4)\} + \ldots = (\hbar\omega_p)^4\{\sum_{|\vec{\lambda}|\leqslant\lambda_c} h_\lambda^4(1-x_\lambda)^4\,[a_\lambda^*(\beta_1)\, a_\lambda^*(\beta_2)\, a_{-\lambda}^*(\beta_3)\times$$

$$\times a_{-\lambda}^*(\beta_4)\,\hat{\varrho}_\lambda(\beta_1)\,\hat{\varrho}_\lambda(\beta_2)\,\hat{\varrho}_{-\lambda}(\beta_3)\,\hat{\varrho}_{-\lambda}(\beta_4) + a_\lambda^*(\beta_1)\, a_{-\lambda}^*(\beta_2) a_\lambda^*(\beta_3) a_{-\lambda}^*(\beta_4)\,\hat{\varrho}_\lambda(\beta_1)\hat{\varrho}_{-\lambda}(\beta_2)\hat{\varrho}_\lambda(\beta_3)\times$$

$$\times\hat{\varrho}_{-\lambda}(\beta_4) + a_\lambda^*(\beta_1)\, a_{-\lambda}^*(\beta_2)\, a_{-\lambda}^*(\beta_3)\, a_\lambda^*(\beta_4)\,\hat{\varrho}_\lambda(\beta_1)\,\hat{\varrho}_{-\lambda}(\beta_2)\,\hat{\varrho}_{\ \lambda}(\beta_3)\,\hat{\varrho}_\lambda(\beta_4)] +$$

$$+\sum_{\substack{|\vec{\lambda}|\leqslant\lambda_c\\ |\vec{\varkappa}|\leqslant\lambda_c\\ \vec{\lambda}\neq\pm\vec{\varkappa}}} h_\lambda^2 h_\varkappa^2 (1-x_\lambda)^2(1-x_\varkappa)^2\,[a_\lambda^*(\beta_1)\, a_{-\lambda}^*(\beta_2)\, a_\varkappa^*(\beta_3)\, a_{-\varkappa}^*(\beta_4)\,\hat{\varrho}_\lambda(\beta_1)\,\hat{\varrho}_{-\lambda}(\beta_2)\,\hat{\varrho}_\varkappa(\beta_3)\,\hat{\varrho}_{-\varkappa}(\beta_4) +$$

$$+ a_\lambda^*(\beta_1)\, a_\varkappa^*(\beta_2)\, a_{-\lambda}^*(\beta_3)\, a_{-\varkappa}^*(\beta_4)\,\hat{\varrho}_\lambda(\beta_1)\,\hat{\varrho}_\varkappa(\beta_2)\,\varrho_{-\lambda}(\beta_3)\,\hat{\varrho}_{-\varkappa}(\beta_4) +$$

$$+ a_\lambda^*(\beta_1)\, a_\varkappa^*(\beta_2)\, a_{-\varkappa}^*(\beta_3)\, a_{-\lambda}^*(\beta_4)\,\hat{\varrho}_\lambda(\beta_1)\,\hat{\varrho}_\varkappa(\beta_2)\,\hat{\varrho}_{-\varkappa}(\beta_3)\,\hat{\varrho}_{-\lambda}(\beta_4)]\} + \ldots \qquad \text{(A.9)}$$

The procedure of averaging is an easy one; we give the final result only:

$$\int_0^\beta d\beta_1\int_0^{\beta_1} d\beta_2\int_0^{\beta_2} d\beta_3\int_0^{\beta_3} d\beta_4 < e^{-\beta\hat{H}_1}\hat{H}_2(\beta_1)\hat{H}_2(\beta_2)\hat{H}_2(\beta_3)\hat{H}_2(\beta_4) > =$$

$$= e^{-\beta\hat{H}}\prod_{\substack{|\vec{\lambda}|\leqslant\lambda_c\\ \lambda_z>0}}\frac{1-x_\lambda^2}{1-x_\lambda^2 e^{-\beta\hbar\Omega_\lambda}}\Big\{2(\hbar\omega_p)^2\sum_{|\vec{\sigma}|\leqslant\lambda_c}\frac{h_\sigma^4 x_\sigma^2(1-x_\sigma)^4}{(1-x_\sigma^2 e^{-\beta\hbar\Omega_\sigma})^2}\int_0^\beta d\beta_1\int_0^{\beta_1} d\beta_2\int_0^{\beta_2} d\beta_3\int_0^{\beta_3} d\beta_4\times$$

$$\times e^{(\beta_1+\beta_2+\beta_3+\beta_4-4\beta)\hbar\Omega\sigma/2}[\hat{\varrho}_\sigma(\beta_1)\,\hat{\varrho}_\sigma(\beta_2)\,\hat{\varrho}_{-\sigma}(\beta_3)\,\hat{\varrho}_{-\sigma}(\beta_4) + \hat{\varrho}_\sigma(\beta_1)\,\hat{\varrho}_{-\sigma}(\beta_2)\,\hat{\varrho}_\sigma(\beta_3)\,\hat{\varrho}_{-\sigma}(\beta_4) +$$

$$+\hat{\varrho}_\sigma(\beta_1)\,\hat{\varrho}_{-\sigma}(\beta_2)\,\hat{\varrho}_{-\sigma}(\beta_3)\,\hat{\varrho}_\sigma(\beta_4)] + (\hbar\omega_p)^4\sum_{\substack{|\vec{\sigma}|\leqslant\lambda_c\\ |\vec{\varkappa}|\leqslant\lambda_c\\ \vec{\sigma}\neq\pm\vec{\varkappa}}}\frac{h_\sigma^2 h_\varkappa^2 x_\sigma x_\varkappa(1-x_\sigma)^2(1-x_\varkappa)^2}{(1-x_\sigma e^{-\beta\hbar\Omega_\sigma})(1-x_\varkappa e^{-\beta\hbar\Omega_\varkappa})}\times$$

$$\times\int_0^\beta d\beta_1\int_0^{\beta_1} d\beta_2\int_0^{\beta_2} d\beta_3\int_0^{\beta_3} d\beta_4\,[e^{(\beta_1+\beta_2-2\beta)\hbar\Omega\sigma/2}\cdot e^{(\beta_3+\beta_4-2\beta)\hbar\Omega\varkappa/2}\cdot\hat{\varrho}_\sigma(\beta_1)\,\hat{\varrho}_{-\sigma}(\beta_2)\,\hat{\varrho}_\varkappa(\beta_3)\,\hat{\varrho}_{-\varkappa}(\beta)+$$

$$+ e^{(\beta_1+\beta_3-2\beta)\hbar\Omega\sigma/2}\cdot e^{(\beta_2+\beta_4-2\beta)\hbar\Omega\varkappa/2}\,\hat{\varrho}_\sigma(\beta_1)\,\hat{\varrho}_\varkappa(\beta_2)\,\hat{\varrho}_{-\sigma}(\beta_3)\,\hat{\varrho}_{-\varkappa}(\beta_4) + e^{(\beta_1+\beta_4-2\beta)\hbar\Omega\sigma/2}\times$$

$$\times e^{(\beta_2+\beta_3-2\beta)\hbar\Omega\varkappa/2}\,\hat{\varrho}_\sigma(\beta_1)\,\hat{\varrho}_\varkappa(\beta_2)\,\hat{\varrho}_{-\varkappa}(\beta_3)\,\hat{\varrho}_{-\sigma}(\beta_4)]. \qquad \text{(A.10)}$$

By a procedure identical to the one of the text, the term (A.10) is proved: in the case of the Bohm — Pines subsidiary conditions to contribute but negligibly. The higher expansion terms in (3.16) behave quite similarly.

REFERENCES

Bohm, D. and Pines, D., *Phys. Rev.*, **85**, 338 (1952*a*), *Ibid.* **92**, 609 (1953*b*).
Dyson, F., *Phys. Rev.*, **102**, 1217 (1956).
Ingarden, R. and Ziętek, W. (private communication).
Kanazawa, H., *Prog. theor. Phys.*, **18**, 247 (1957).
Lipkin, H., *Phys. Rev. Letters* **2**, 159 (1959).
Pawlikowski, A. and Szczurówna, W., (private communication).
Śledzik, J., *Acta phys. Polon.*, **17**, 463 (1958a) *Ibid.* **18**, 57 (1959b), *Ibid.* **18**, 295 (1959c).

LETTERS TO THE EDITOR

EINFLUSS VON ÜBERNÄCHSTEN NACHBARN AUF DIE ÜBERSTRUKTURELLE ANISOTROPIE DER SPINWELLENDISPERSION

Von Henryk Cofta

Institut für Theoretische Physik, A. Mickiewicz Universität, Poznań und Abteilung für Ferromagnetismus des Physikalischen Instituts der Polnischen Akademie der Wissenschaften, Poznań

In einer früheren Note (Cofta 1957) haben wir auf das Problem der Abhängigkeit der Spinwellenausbreitung von der Überstruktur des antiferromagnetischen Raumgitters aufmerksam gemacht. An Hand der angenäherten Rechnungen haben wir dort gezeigt, dass für manche antiferromagnetische Überstrukturen eine ausgesprochene Anisotropie der Spinwellendispersion auftreten muss, hervorgerufen ausschliesslich durch die Überstruktur. Hier wollen wir einige Resultate der genauen Rechnungen vorstellen.

Wir können uns auf die Formel (25) von Cofta (1959) stützen. Ihre Anwendung auf die einzelnen Überstrukturen der kubischen antiferromagnetischen Gittern bestätigt unsere Vermutung, dass die überstrukturelle Anisotropie der Spinwellendispersion in allen Fällen auftritt, wo die parallele ferromagnetische Ebenen mit abwechselnd gerichteten Spins vorhanden sind. Der einzige Ausnahmefall betrifft „gewöhnliche" oder „natürliche" Spinordnung (d.h. alle nächste Nachbarn haben entgegengesetzte Spins). Die Rechnungen zeigen, dass das effektive Feld H_A der magnetischen Anisotropie fast keine Rolle in er unteruschten Erscheinung spielt.

Die Berücksichtigung von übernächsten Nachbarn führt zu sehr interessanten Folgerungen. Da die Wechselwirkungen zwischen den übernächsten Nachbarn im allgemeinen einen anderen Charakter haben als die zwischen den nächsten, hängen die Anisotropieparametern von dem Verhältniss $\eta = J_1/J_2$ ab, wo J_1 das Austauschintegral zwischen nächsten Nachbarn und J_2 — das zwischen den übernächsten bedeutet.

Diese letzte Frage wollen wir an einem ziemlich einfachen Beispiel verfolgen, nämlich an dem *FC*-Gitter mit (001) ferromagnetischen Ebenen. Aus der obengenann-

ten Formel erhalten wir in diesem Falle für die Kreisfrequenz der langen Spinwelle ($ak \ll 1$):

$$\omega = |\gamma| \{C + 2a^2 [H_A (H_1 + 2H_2) - 32 H_1 H_2] (k_x^2 + k_y^2) + 4a^2 [H_A H_2 + 16 H_1 (H_1 - H_2)] k_z^2\}^{1/2} \quad (1)$$

Das Symbol γ bedeutet hier den magnetomechanischen Faktor, a ist die Gitterkonstante und k_x, k_y, k_z sind die Komponenten des Wellenvektors. Ausserdem sind in (1) die Abkürzungen

$$H_1 = S^z J_1/\gamma\hbar \quad \text{und} \quad H_2 = S^z J_2/\gamma\hbar$$

sowie $C = H_A(H_A - 32H_1)$ eingeführt. Da das Feld H_A bekanntlich sehr schwach gegen das „Austauschfeld" H_1 oder H_2 ist, können wir H_A vernachlässigen und schreiben:

$$\omega = 8 |\gamma| a \{H_1 (H_1 - H_2) k_z^2 - H_1 H_2 (k_x^2 + k_y^2)\}^{1/2} \quad (2)$$

Für die Wechselwirkung zwischen nächsten Nachbarn ($J_2 = 0$) erhalten wir eine ausgeprägte Anisotropie:

$$\omega = |\gamma| \{C' + 2a^2 H_1 [H_A [(k_x^2 + k_y^2 (- 32 H_1 k_z^2]\}^{1/2} \quad (32)$$

die die Richtung [001] senkrecht zur ferromagnetischen Ebenen auszeichnet. Wenn wir dagegen nur die übernächste Nachbarn berücksichtigen ($J_1 = 0$), dann wird die Dispersionformel isotrop:

$$\omega = |\gamma| \{C'' + 4a^2 H_A H_2 k^2\}^{1/2} \quad (4)$$

was sich leicht auf Grund der geometrisch-physikalischen Betrachtungen erklären lässt (Cofta 1960a zund 1960b). Beide Effekte sind demnach sehr verschieden. Die isoenergetische Fläche E = const stellt für die wahrscheinlichste Werte (Cofta 1960a) $\eta < 0$ ein Rotationsellipsoid dar. Das Achsenverhältniss a:c hängt in der Näherung (2) nur vom η ab:

$$\frac{a}{c} = \sqrt{1 - \eta} \quad (5)$$

Die Abhängigkeit (5) schafft die Möglichkeit einer unmittelbaren Bestimmung von η durch die Messung des Parameters $a:c$ der überstrukturellen Anisotropie. Da wir bis jetzt fast nichts über das Verhältniss η in einzelnen antiferromagnetischen Stoffen wissen, wäre eine solche Auskunft sehr wertvoll. Die möglichen Messmethoden werden später bearbeitet.

Die analogischen Untersuchungen lassen sich für alle antiferromagnetische Überstrukturen mit ferromgnetischen Ebenen durchführen (Cofta 1960a). Als eine

sehr nützliche Hilfsmethode erwies sich dabei die Einführung einer geeigneter Klassifikation von Überstrukturen (Cofta 1960b).

Die Einzelheiten der genauen Rechnungen sowie volle Diskussion werden in Kürze in Acta phys. Polon. publiziert.

LITERATURHINWEISE

Cofta, H., *Acta phys. Polon.*, **16**, 481 (1957)
Cofta, H., *Acta phys. Polon.*, **18**, 215 (1959)
Cofta, H., Thesis, A. Mickiewicz Universität, Poznań, 1960 a
Cofta, H., *Acta phys. Polon.*, **19** (im Drucke, 1960 b)

NON-LINEAR EQUATIONS FOR SPINOR FIELDS

JERZY RAYSKI

Institute of Physics of the Jagellonian University, Kraków

and

Physical Institute of the Polish Academy of Science, Warszawa

A plausible form of a non-linear spinor equation, similar to the equation of Heisenberg, is derived by using the principle of correspondence with general relativity.

Several authors suggested that the exact equations for spinor fields should be non-linear. In particular, Heisenberg[1] investigated two versions of such equations, based on the Lagrangians

$$\bar{\psi}\gamma_\mu \partial_\mu \psi + \frac{l^2}{2}(\bar{\psi}\psi)^2 \quad \text{or} \quad \bar{\psi}\gamma_\mu \partial_\mu \psi + \frac{l^2}{2}(\bar{\psi}\gamma_\mu\gamma^5 \psi)^2. \tag{1}$$

Such assumptions are usually believed to be merely examples of the simplest kinds of non-linearity, whereas the exact form of non-linear terms is not known and may finally turn out to be rather complicated. However, criteria for discriminating a particular type of non-linearity are not yet known. The present note is devoted to the problem of determining a plausible type of non-linearity by advocating the principle of correspondence with general relativity.

At the present stage of development of theoretical physics gravitation plays a distinguished role. Being completely amalgamated with geometry, the theory of gravitation is free of arbitrary and simplifying assumptions to a degree surpassing by far the other theories of fields. And just the equations of gravitation are non-linear and the form of their non-linearity is well determined (except for the disputable question of existence of the cosmical term). This fact constitutes a strong argument in favour of the opinion that — similarly as in the theory of gravitation — linear equations constitute only the first approximation valid in the limit of weak fields. At the same time it constitutes a hint as regards the problem of determination of the proper form of non-linear field equations since there may exist an analogy between the type of non-linearity encountered in the equations of gravitation and in the equations of other fields.

Since (covariant) lagrangians for different fields have to be added to the lagrangian

of gravitation, there should exist some relationship, some analogy between these lagrangians and the curvature, otherwise their union into a common lagrangian could be regarded as an artificial "cementing of quite different pieces".

In the unitary theory of a gravito-electromagnetic field ([2]) there exists indeed a close relationship between the lagrangian of gravitation and that of the electromagnetic field: both appear to be parts of a common lagrangian being the curvature of a six-dimensional space. However, one must not hope that by a further extension of the number of dimensions of the underlying manifold it will be possible to include all the fields playing a role in Nature. In particular, a lagrangian with the simple geometrical meaning of curvature cannot account automatically for the existence of spinor fields. Therefore the relationship between spinor field and gravitational field lagrangians must be of a different character from the relationship between the electromagnetic field and gravitational field lagrangians.

Since the curvature is expressible in terms of Christoffel symbols and their first derivatives, the analogy between the lagrangian of spinor field and the curvature may consist in the fact that there exist some analogues of these symbols (let us call them $\Gamma^{\nu}_{\lambda\mu}[\psi]$) and their first derivatives (let us call them $\partial_{\varrho}\Gamma^{\nu}_{\lambda\mu}[\psi]$) and that the lagrangian for the spinor field ψ is the same function of these analogues as the curvature is of Christoffel symbols,

$$L(\psi) = Cg^{\lambda\mu}\left(\partial_{\mu}\Gamma^{\sigma}_{\lambda\sigma}[\psi] - \partial_{\sigma}\Gamma^{\sigma}_{\lambda\mu}[\psi] + \Gamma^{\tau}_{\lambda\sigma}[\psi]\,\Gamma^{\sigma}_{\mu\tau}[\psi] - \Gamma^{\tau}_{\lambda\mu}[\psi]\,\Gamma^{\sigma}_{\tau\sigma}[\psi]\right). \tag{2}$$

The fact that the lagrangian for a spinor field is to be obtained (up to the factor C) from the expression for the curvature by mere substitutions of the Christoffel symbols by their analogues, explains their relationship and the necessity of fusing them into a common lagrangian describing gravitation together with its sources in a more or less uniform way.

Since particles with half-integral spin admit two concepts of velocity given by the operators

$$\vec{\alpha} = i\gamma^4\vec{\gamma} \quad \text{and} \quad \frac{1}{im}\frac{\partial}{\partial\vec{x}} \tag{3}$$

(to be generalized in a straightforward way for four dimensions), the expressions

$$\gamma^{\nu}_{\lambda\mu} = -\frac{m}{2}\,g^{\nu\sigma}\,\gamma^4\left(\gamma_{\lambda}\,g_{\mu\sigma} + \gamma_{\mu}\,g_{\lambda\sigma} - \gamma_{\sigma}\,g_{\lambda\mu}\right) \tag{4}$$

constitute some analogues of the Christoffel symbols. More exactly, the analogues of the Christoffel symbols we are looking for should be proportional to the densities of the above expressions

$$\Gamma^{\nu}_{\lambda\mu}[\psi] = k\psi^{*}\gamma^{\nu}_{\lambda\mu}\psi \quad \text{and} \quad \partial_{\varrho}\Gamma^{\nu}_{\lambda\mu}[\psi] = k\psi^{*}\partial_{\varrho}\gamma^{\nu}_{\lambda\mu}\psi \tag{5}$$

where ∂_{ϱ} operates upon everything to the right, and k is again a factor of proportionality.

In contradistinction to the usual Christoffel symbols and their derivatives, their analogues (5) do not vanish even in the limit of flat space and in inertial coordinate systems. Thus, for reasons of simplicity, let us neglect the curvature of space-time and consider the expressions (5) in an inertial coordinate system, introducing an imaginary time coordinate and the usual (hermitian) Dirac matrices. Under these assumptions (5) assume the form

$$\Gamma^{\nu}_{\lambda\mu}[\psi] = \varkappa\,\bar{\psi}\,(\gamma_\lambda\,\delta_{\mu\nu} + \gamma_\mu\,\delta_{\lambda\nu} - \gamma_\nu\,\delta_{\lambda\mu})\,\psi \tag{6'}$$

$$\partial_\varrho\,\Gamma^{\nu}_{\lambda\mu}[\psi] = \varkappa\,\bar{\psi}\,(\gamma_\lambda\,\delta_{\mu\nu} + \gamma_\mu\,\delta_{\lambda\nu} - \gamma_\nu\,\delta_{\lambda\mu})\,\partial_\varrho\,\psi. \tag{6''}$$

where $\bar{\psi} = \psi^*\,\gamma^4$ and $\varkappa$ is again a proportionality factor. Introducing (6) into (2) we find the plausible non-linear form of the spinor field lagrangian

$$L(\psi) = 6C\varkappa\,[(\bar{\psi}\,\gamma_\mu\,\partial_\mu\,\psi) + \varkappa\,(\bar{\psi}\,\gamma_\mu\,\psi)\,(\bar{\psi}\,\gamma_\mu\,\psi)] \tag{7}$$

where $6C\varkappa$ is the coupling constant of gravitation and k is another constant with dimension [cm^2[in natural units $h = c = 1$.

Thus, we got a lagrangian resembling closely that of Heisenberg except for the factor γ^5 in the non-linear term.

It is easily seen that the possibility of supplementing this lagrangian with a term of the form $m\bar{\psi}\psi$ corresponds exactly to the possibility of supplementing the curvature-lagrangian with a cosmical term.

The essential step in our procedure was the replacement of the derivatives ∂_μ in the Christoffel symbols by $-\,m\gamma^4\,\gamma_\mu$ according to the two concepts of velocity for spinor particles, and a subsequent transition to the densities $\gamma^\nu \to \psi^*\,\gamma^\nu_{\lambda\mu}\,\psi$. Such a procedure can be understood intuitively in the following way: there are two aspects of the motion of the spinning particles. One of them, connected with the Zitterbewegung, does not agree with the classical requirement of the geodesic motion of a free particle. But any departure from uniform motion of a free particle can be understood as an encroachment upon geometry. The expressions (5) determine a sort of "affine connection" accounting for the "geomtery" where Zitterbewegung replaces the uniform motion along a straight line.

---

(1) Heisenberg, W., *Rev. Modern Phys.*, **29** 269 (1957)
(2) Rayski, J., *Nuclear Physics*, **16**, (1960)

Volumen XIX — Fasciculus 3

Letters to the Editor